## INFORMATION TO USERS

This reproduction was made from a copy of a document sent to us for microfilming. While the most advanced technology has been used to photograph and reproduce this document, the quality of the reproduction is heavily dependent upon the quality of the material submitted.

The following explanation of techniques is provided to help clarify markings or notations which may appear on this reproduction.

1. The sign or "target" for pages apparently lacking from the document photographed is "Missing Page(s)". If it was possible to obtain the missing page(s) or section, they are spliced into the film along with adjacent pages. This may have necessitated cutting through an image and duplicating adjacent pages to assure complete continuity.

2. When an image on the film is obliterated with a round black mark, it is an indication of either blurred copy because of movement during exposure, duplicate copy, or copyrighted materials that should not have been filmed. For blurred pages, a good image of the page can be found in the adjacent frame. If copyrighted materials were deleted, a target note will appear listing the pages in the adjacent frame.

3. When a map, drawing or chart, etc., is part of the material being photographed, a definite method of "sectioning" the material has been followed. It is customary to begin filming at the upper left hand corner of a large sheet and to continue from left to right in equal sections with small overlaps. If necessary, sectioning is continued again beginning below the first row and continuing on until complete.

4. For illustrations that cannot be satisfactorily reproduced by xerographic means, photographic prints can be purchased at additional cost and inserted into your xerographic copy. These prints are available upon request from the Dissertations Customer Services Department.

5. Some pages in any document may have indistinct print. In all cases the best available copy has been filmed.

University Microfilms International
300 N. Zeeb Road
Ann Arbor, MI 48106

Som, Dilip Kumar

COMPUTER MODELING OF CRACKS

*City University of New York* PH.D. 1982

# COMPUTER MODELING OF CRACKS

by

DILIP K. SOM

A dissertation submitted to the Graduate Faculty in Physics in partial fulfillment of the requirements for the degree of Doctor of philosophy, The City University of New York

1982

The manuscript has been read and accepted for the Graduate Faculty in Physics in satisfaction of the dissertation requirement for the degree of Doctor of Philosophy.

7/15/82
date

Arthur Kosowsky
Chairman of Examining Committee

7/15/82
date

Frank A. Harkins
Executive Officer

Ralph J. Harrison

G. J. Devaney

C. R. Finden

Supervisory Committee

The City University of New York

ABSTRACT

COMPUTER MODELING OF CRACKS
by
Dilip K. Som

Advisor: Professor Arthur Paskin

Brittle fracture is one of the most important properties of solids and yet there is little direct experimental confirmation of the basic models of the underlying atomic mechanisms. In brittle fracture, while there have been some notable experimental confirmations of the basic Griffith approach to fracture, controlled microscopic experiments have not been possible to test these ideas. It is only with the advent of modern computers that theoretical investigations of the pertinent atomic processes have been possible.

The results of a recent molecular dynamic study of a two-dimensional triangular Lennard-Jones system of about 10,000 atoms will be described. Static calculations on this system show very little lattice trapping in contrast to the often quoted results of lattice statics models. It is shown that when lattice statics calculations and hybrid lattice statics calculations are performed using realistic, long-range potentials, lattice trapping is small. Using molecular dynamics, the properties of the system, with and without a crack, are understood sufficiently quantitatively to allow extrpolation to infinite size. With 10,000 atoms size effects are small enough to render the simulation highly reliable.

Dynamic simulations at constant applied load show an intricate interplay between brittle crack propagation and the tendency to form dislocations. At low stresses the behavior is brittle, while disloction generation and crack blunting are observed at elevated stress.

The velocity of crack propagation was also studied by simulating fracture under constant external displacement. A constant terminal velocity was attained relatively soon after the crack began to propagate. While the constant terminal velocity is in accord with theoretical prediction, the velocity is smaller than expected. Estimates indicate that the finite size of the sample is responsible for the lower value of the terminal velocity.

Brittle fracture is known to occur in normally ductile metals under the influence of certain specific external environments. This effect is commonly termed stress corrosion cracking and/or hydrogen embrittlement. Simulating a crack coated with an elastically hard film, brittle fracture was observed in various computer simulations. A model was developed for how the environment can trigger such a brittle behavior in a material that is inherently ductile.

Dedicated

to my wife and my parents

for their constant encouragement

I would like to take this opportunity to thank Professor Arthur Paskin of Queens College of C.U.N.Y. for his constant encouragement and advice. I would also like to thank Dr. George J. Dienes of Brookhaven National Laboratory for many valuable discussions and Ms. Marilyn McKeown for her constant help in computer programming.

TABLE OF CONTENTS

PART I

HOMOGENOUS MATERIAL

PART II

INHOMOGENOUS MATERIAL

## NOTATION

| | |
|---|---|
| $A$ | Area of two dimensional sample |
| $d$ | Equilibrium bond length at zero temperature |
| $d_i$ | Inflection point of the L-J potential vs. distance curve |
| $d_{c-1}$ | Length of second unbroken bond at the crack tip |
| $d_c$ | Length of first unbroken bond at the crack tip |
| $d_{c+1}$ | Length of first broken bond at the crack tip |
| $e$ | Strain |
| $e_{ext}$ | External fixed strain |
| $e_c$ | Critical strain |
| $e_+$ | Upper bound of lattice trapping strain |
| $e_-$ | Lower bound of lattice trapping strain |
| $E$ | Total energy |
| $E_{el}$ | Elastic strain energy |
| $E_k$ | Kinetic energy |
| $E_s$ | Surface energy |
| $F$ | Stress concentration factor |
| FF | strength of film-film bond (in units of $\epsilon/d^2$) |
| FS | Strength of film-substrate bond (in units of $\epsilon/d^2$) |
| $F_{max}$ | Maximum force exerted by the L-J potential at its inflection point (in units of $\epsilon/d$) |
| $F_T$ | Tensile force (in units of $\epsilon/d$) |
| $K$ | Stress intensity factor |
| $l$ | Crack, half length |
| $l_o$ | Initial crack, half length |

| | |
|---|---|
| $m$ | Mass of atoms |
| $M$ | Young's modulus of perfect sample under external loading |
| $M_o$ | Young's modulus of perfect sample under no external loading |
| $M'$ | Young's modulus of a sample with a crack under some external loading |
| $M'_o$ | Young's modulus of a sample with a crack under no external loading |
| $N_R$ | Number of rows of the 2-D lattice |
| $NTM_{even}$ | Number of atoms in the even rows of the 2-D lattice |
| $NTM_{odd}$ | Number of atoms in the odd rows of the 2-D lattice = $NTM_{even} - 1$ |
| NBB | Number of broken bonds in half sample |
| $r_c^L$ | Position of the crack tip atom on the lower surface of the crack |
| $r_c^U$ | Position of the crack tip atom on the upper surface of the crack |
| R | Range of influence of the L-J potential in the present calculation |
| $R_T$ | Lattice trapping ratio |
| SS | Strength of substrate bonds (in units of $\epsilon/d^2$) |
| t | Time |
| $v_c$ | Crack tip velocity |
| $V_L$ | Longitudinal velocity of sound |
| $V_S$ | Surface wave velocity |
| $V_T$ | Crack terminal velocity |

| | |
|---|---|
| $\alpha$ | Width of thecore region of a crack tip |
| $\beta$ | Damping parameter |
| $\delta$ | $2\pi l_o^2/A$ |
| $\epsilon$ | Depth of the L-J potentential |
| $\eta, \eta'$ | Slopes of the straight lines (modulus M & M' vs. strain e) |
| $\gamma$ | Surface energy per unit area ( unit length in 2-D) |
| $\lambda, \mu$ | Lame constants |
| $\nu$ | Poisson's ratio |
| $\phi_{ij}$ | L-J potential energy of an atom pair (ij) |
| $\sigma$ | Stress |
| $\sigma_c$ | Critical stress |
| $\sigma_{max}$ | Maximun stress the lattice can withstand |
| $\sigma_+$ | upper bound of the lattice trapping stress |
| $\sigma_-$ | Lower bound of the lattice trapping stress |
| $\sigma_{ext}$ | Fixed external load |
| $\sigma_{true}$ | True external stress after equilibrium is reached |
| $\sigma_{max}^U$ | Maximum force on an atom on the upper surface of the crack |
| $\sigma_{max}^L$ | Maximum force on an atom on the lower surface of the crack |
| $\sigma_c^L$ | Force on an atom at the crack tip(lower surface) |
| $\sigma_c^U$ | Force on an atom at the crack tip( upper surface) |
| $\sigma_{c\pm i}^L$ | Force on ± i-th atom from the crack tip (lower surface) |
| $\sigma_{c\pm i}^U$ | Force on ± i-th atom from the crack tip (upper surface) |

LIST OF TABLES

LIST OF FIGURES

# INTRODUCTION

In this thesis an atomistic study of brittle fracture was conducted. The study was performed on a two dimensional triangular lattice whose atoms interact via a two body central (Lennard-Jones) potential. A high speed CDC 7600 computer was used for simulations. The effect of cracks on the mechanical strength of a material, the criterion for crack propagation and the behavior of crack propagation are the main topics which were investigated.

Real materials usually do not have a perfect crystalline structure. Almost always there are present some vacancies, interstitials, dislocations and different sizes of thin cracks. Since the local stress near a sharp notch may rise to a level several times that of applied stress, thin cracks in solids reduce the theoretical strength of materials by several orders of magnitude and thus cause materials to fracture at low stress levels. Griffith, applying a simple energy balance concept, arrived at a quantitative criterion for equilibrium condition for the fracture. Despite some discrepancies with experimental results, the Griffith theory was considered quite a triumph.

The brittle fracture of solids is essentially an atomic process, in which the force-separation relationships for the cohesive bonds at the crack tip are non-linear. To obtain the above mentioned fracture criterion, Griffith had to use some results from continuum mechanics which is based on linear elasticity theory. Thus, the validity of the Griffith critical criterion and most of the work done in this field based on continuum mechanics are questionable, particularly because the predictions from these theories have proved to be inadequate to explain many macroscopic experimental data in complete detail.

Although there have been some notable macroscopic confirmations of the Griffith approach to fracture, it has not been possible to perform controlled microscopic experiments to clarify the fundamental atomistic picture of the equilibrium (static) and dynamic behavior of crack propagation. It is only with the advent of modern computers that it has been possible to investigate the microscopic behavior during fracture. While computer simulations are not really the desired microscopically controlled experiments, they can serve as a first step in investigating the atomic role in fracture.

In the earlier computer simulations unrealistic simple potentials as well as small samples (except in the case of a small atomic region embedded in an infinite elastic continuum used in some simulations) were usually used. The effect of the size of the sample on the results was not evaluated quantitatively in any of those simulations. Thus, it is not known whether some of the results of those simulations may be artifacts of the unrealistic potential and/or finite sample size.

One of the important aspects of the present investigation was the study of the effect of sample size on the material properties, such as the modulus of elasticity and the elastic strain energy. By simulating samples of different sizes with a thin crack of the same length under the same external displacement, it was possible to assess quantitatively the error contained in the simulation results due to the finite size of the sample used. It was found that the change in strain energy (due to the introduction of crack) for our largest sample (about 11000 atoms) was about 12% lower than that for an infinite sample.

An unexpected consequence of atomistic or lattice calculations of brittle fracture is the phenomenon known as "Lattice trapping". In contrast to the Griffith stress concept, Thomson et al found that

for a discrete lattice a crack could have a range of applied stresses for which it would be stable or "trapped", i.e., the crack would neither propagate nor heal. The ratio of the upper to lower stresses is a measure of the order of lattice trapping. Different calculations have yielded a range of values of this ratio from 1.13 to 7.3. Calculations using unrealistic simple potentials usually gave large values of the trapping ratio. In addition, the problem of using small sample sizes, is also present in these calculations. Accordingly, after understanding the effect of sample size on the results of our simulations, the phenomenon of latticeM trapping was studied using our more realistic (L-J) potential. A negligible trapping ratio (1.03) was observed

Recently Eringen and co-workers have reformulated continuum mechanics to include the effects of non-locality in space and time. They obtained some stress profiles around a stable crack tip under external load. Stress profiles around crack tip along different directions of interest in the lattice were calculated in our simulations and compared with those obtained by the Eringen nonlocal theory. They are in reasonable agreement with that obtained by non-local theory.

If the external stress or strain is increased slightly from the Griffith critical strain, according to Mott, the crack velocity is expected to increase slowly and finally attain a terminal value. It had been also predicted that the terminal velocity is independent of the external load provided it is close to the critical value. Substances like glass have been observed to behave in this manner for a wide range of stress levels and application rates, but the terminal velocity was attained much earlier than predicted by Mott. Our simulations yielded a somewhat lower value of the terminal velocity and it was attained much earlier, confirming experimental results. Thus, although Mott's analysis explains the basic character of crack propagation, it is not a complete description. A

quantitive analysis of the attainment of terminal velocity was made by analyzing the change in strain and in kinetic energies as the crack propagates.

In all the simulations, the atomic positions, atomic velocities, the forces acting on all the atoms, Young's modulus, Poisson's ratio and all the energies (potential, kinetic and surface) were monitored to obtain the static, dynamic and most of the thermodynmic properties of the system. The goal of this thesis was to test the existing assumptions widely used in investigating crack propagation with the help of quantitative data generated by the time evolution of the above parameters.

The basic results of static continuum theory, from the classical Griffith approach to the more recent non-local theory put forward by Eringen and co-workers, are summarized in chapter 1. A lattice theory of fracture formulated by Thomson et al is outlined in chapter 2. The phenomenon of lattice trapping is also disucssed in some detail. Chapter 3 deals with the dynamical continuum theories of Mott with emphasis on the effect of sample size on the behavior of crack propagation.

The importance of atomistic models of fracture processes is indicated in chapter 4. Atomistic calculations made earlier by Weiner and Pear, Ashurst and Hoover, Sinclair et al and Paskin et al are described emphasizing the specific restrictions and idealizations used in those models and their effects on the calculations. The motivation for performing the present computer simulations is then given.

The present atomistic model, the calculations and the results are presented in chapters 5 through 8. The properties of crack propagation both in homogenous and inhomogenous materials were studied. Part I ( chapters 5 and 6) deals with homogenous material

and Part II (chapter 7) deals with inhomogenous material. Molecular dynamic techniques pertinent to the statics of fracture are outlined in chapter 5 with details of the computer program used in the calculations. The mechanical properties of the two dimensional triangular lattice are discussed. A quantitative assessment is made of the error contained in our simulation results due to the finite size of the sample used. Static continuum theories are then reviewed in the light of the present simulations. The phenomenon of lattice trapping is analyzed critically. Molecular dynamic techniques pertinent to the dynamic calculations is outlined in chapter 6. The Mott theory is analyzed with proper consideration of the finite size of the sample used. The propagation of crack under fixed stress is analyzed in section 6.4. The propagation of cracks coated with an elastically hard film is studied extensively. A small sample under fixed load was used to gain an understanding of the embrittlement of our inherently ductile material. Concluding remarks are to be found in chapter 8.

# CHAPTER 1
# STATIC CONTINUUM THEORY

## 1.1 Crack as a Stress Concentrator

Numerous laboratory tests indicate that microcracks (which are common in almost all real materials) reduce the mechanical strength of materials by several orders of magnitudes. It has also been observed that in real materials under external load, propagation of cracks is essentially due to the increase in length of pre-existing microcracks. In other words, microcracks inside real materials are potentially the weakest points. It is important, therefore, to look at the stress and the displacement fields near the tip of the microcracks under some external loading conditions. The full mathematical analyses of the stress and the displacement fields for anything but simple crack geometries are extremely complex. The calculations of the stress fields at the tip of a thin crack as pictured by Griffith (1920) will be discussed here briefly.

Griffith pictured a thin crack as an infinitesimally narrow elliptic hole. He then used the Inglis (1913) solutions for the stress fields of an elliptical hole in an uniformly stressed material to calculate the stress field at the crack tip. The case of interest here is the so-called Mode-I configuration in which the loading is uniaxial with the major axis of the elliptical hole perpendicular to the axis of tension (as shown in figure 1.1.1.). If it is assumed that Hook's law is valid everywhere, that the surface of the hole is free of traction and that the axes 2b and 2l are small compared to the dimensions of the plate, it is quite straightforward to calculate the stress fields using linear elasticity theory. It is at the points L and L' that the greatest concentrations of stress occur. The stresses $\sigma_{yy}$ at the points L and L' are given by

$$\sigma_{yy}(\pm l, 0) = \sigma[1 + 2l/b] \qquad 1.1.1$$

$$= \sigma[1 + 2(l/\rho)^{1/2}] \qquad 1.1.2$$

where $\rho (= b^2/l)$ is the radius of curvature at the points L and L'. Thus for a thin crack ( $b/l << 1$)

$$\frac{\sigma_{yy}(\pm l, 0)}{\sigma} \approx \frac{2l}{b} \approx 2\left(\frac{l}{\rho}\right)^{1/2} \qquad 1.1.3$$

Figure 1.1.2 shows the dependence of $\sigma_{yy}$ and $\sigma_{xx}$ as a function of distance from the crack tip (for an elliptic hole with l = 3b), where r is the distance along the major axis.

The above ratio of the stress at the crack tip along the y axis to the external stress is called the stress intensity factor F. For a thin crack the value of F can be quite large if the radius of curvature of the crack tip is small. As a result the bonds near the crack tip are more susceptible to rupture than bonds elsewhere. Thus, one can see that the crack tip acts as a stress concentrator and is potentially the weakest point of a material. Although this picture due to Griffith and Inglis throws some light on the fact that materials with inherent microcracks are susceptible to fracture at relatively low stress level, one still needs a better quantitative criterion for fracture mechanism.

## 1.2 The Griffith Approach To The Crack Problem

The Griffith approach to the crack problem is based on the first and second laws of thermodynamics. The basic idea is that as a crack advances, energy is released from the external loading system (in case of constant loading) or from the strain field (in case of constant strain) to the crack tip. At the same time energy is consumed to create the new crack surfaces. For a given crack length and external load if the rate of energy supplied to the crack tip is greater than the rate of energy consumption in creating the surface, then the crack extends otherwise it closes. For a material with a crack under some external loading, one can write, as the crack advances by an infinitesimal amount

$$\delta E_{ext} + \delta \Delta E_{el} + \delta E_S = 0 \qquad 1.2.1$$

where $\delta E_{ext}$ = change in potential energy of the loading mechanism
$\delta \Delta E_{el}$ = change in elastic strain energy of the material
$\delta E_S$ = change in surface energy of the material due to the formation of new surfaces at the crack tips
$\Delta E_{el}$ = Difference in elastic energy due to the crack.

The above equation is valid if there is no plastic deformation at the crack tip and the kinetic effects are negligible. Thus the thermodynamical equilibrium is attained by balancing the total energy of the system over a virtual crack extension as shown in figure 1.2.1.

$$\frac{\delta}{\delta l}(E_{ext} + \Delta E_{el} + E_S) = 0 \qquad 1.2.2$$

This is the Griffith criterion for predicting the fracture behavior of a material. An example of the fracture behavior of a crack in a thin plate under uniaxial tension as seen from Griffith's point of view will be discussed next.

Crack in a Thin Plate Under Uniaxial Tension

To confirm the energy balance concept, Griffith applied it to a real situation. The situation is shown in figure 1.2.2, where a crack of length 2l in an infinite material is under the influence of an uniform external tensile stress. Now as the crack extends by an infinitesimal amount, one can write, assuming that a linear relation holds between stress and strain

$$\delta E_{ext} = -2\,\delta(\Delta E_{el}) \qquad 1.2.3$$

The change in strain energy could be written as

$$\delta(\Delta E_{el}) = \frac{2\pi\sigma^2 l}{M_0}\,\delta l \qquad 1.2.4$$

and, for unit width of crack, the change in surface energy due to the formation of four new surfaces at the two crack tips

$$\delta E_S = 4\gamma\,\delta l \qquad 1.2.5$$

where $\gamma$ = surface energy per unit area, $M_o$ = Young's modulus at infinitesimal stress. Thus, the criterion for equilibrium, using equations 1.2.2 through 1.2.5 is

$$l_c = 2M_o\gamma/\pi\sigma_c^2 \qquad 1.2.6$$

$$\sigma_c = (2M_o\gamma/\pi l_c)^{1/2} \qquad 1.2.7$$

where $l_c$ and $\sigma_c$ are the critical length and stress.

If the energies are plotted against l, as shown in figure 1.2.3, it is seen that the energy of the system is a maximum at equilibrium, so that the system is in unstable equilibrium. This implies that, for a given stress $\sigma$ if l is greater than $l_c$, the crack will propagate spontaneously without limit, and if l is less than $l_c$ the crack will close. Similarly, for a given crack length if is greater than $\sigma_c$ the crack will propagate otherwise it will heal.

Griffith tested his criterion (equation 1.2.6) by introducing cracks of known length in bulbs made of very brittle glass. He burst these bulbs (cylindrical and spherical) by exerting an internal pressure via an inserted fluid. The glass specimens were annealed prior to testing and then cracks of lengths 4 mm to 23 mm were introduced on the surface by a glass cutter. Griffith found, as predicted, that only the stress component normal to the crack plane was important in extending the crack. He also observed a linear relation between $\sigma_c$ and $(1/l)^{1/2}$, as expected. The constant of proportionality agreed with theory to an order of magnitude. Despite this discrepancy the theory was considered quite a triumph. This is because it explained the large difference between the experimentally measured strength for a crack free sample, which is of the order of $10^8$ psi for this glass, and the observed strength for glass with a crack which is of the order of $10^3$ psi. Thus, the Griffith approach not only establishes the fact that the microcracks found inside real materials are responsible for the drastic reduction of their theoretical strength by several orders of

magnitudes but has also established a criterion for crack propagation.

## 1.3 Stress Intensity Approach

Another approach to the crack problem is the stress intensity approach which is based solely on linear elasticity theory. The basic idea is to investigate the manner in which a crack modifies the stress and the displacement fields in an ideal elastic solid. As the mathematical analysis for a complicated crack configuration is intractable it has been necessary to use a simple crack geometry. The simplifying assumption made in this analytical approach is the so called "sharp slit approximation".

It is assumed that the crack tip in the unstressed state is perfectly sharp which is not obviously true in reality. Real crack tips usually have radii of curvature of the order of atomic bonds. It is also assumed that the crack walls are free of tractions at all stages of loading. The difference between this continuum model and the earlier one ( section 1.1) based on a very thin elliptic hole is more mathematical than physical. The stress and the displacement fields near the crack tip are calculated following Westergaard (1939) (for review see Irwin 1958). In case of uniaxial loading (which is the case of interest in this thesis) the stress and the displacement fields at a point (x,y) taking the crack tip as the origin (as shown in figure 1.3.1) are given by

$$\begin{Bmatrix} \sigma_{xx} \\ \sigma_{yy} \\ \sigma_{xy} \end{Bmatrix} = \frac{K_I}{(2\pi r)^{1/2}} \begin{Bmatrix} \cos(\theta/2)[1 - \sin(\theta/2)\sin(3\theta/2)] \\ \cos(\theta/2)[1 + \sin(\theta/2)\sin(3\theta/2)] \\ \sin(\theta/2)\cos(\theta/2)\cos(3\theta/2) \end{Bmatrix}$$

$$\begin{Bmatrix} \sigma_{rr} \\ \sigma_{\theta\theta} \\ \sigma_{r\theta} \end{Bmatrix} = \frac{K_I}{(2\pi r)^{1/2}} \begin{Bmatrix} \cos(\theta/2)[1 + \sin^2(\theta/2)] \\ \cos^3(\theta/2) \\ \sin(\theta/2)\cos^2(\theta/2) \end{Bmatrix} \qquad 1.3.1$$

$$\begin{Bmatrix} u_x \\ u_y \end{Bmatrix} = \frac{K_I}{2\mu}\left(\frac{r}{2\pi}\right)^{1/2} \begin{Bmatrix} (1+\nu)[(2\kappa - 1)\cos(\theta/2) - \cos(3\theta/2)] \\ (1+\nu)[(2\kappa + 1)\sin(\theta/2) - \sin(3\theta/2)] \end{Bmatrix} \qquad 1.3.2$$

$$\begin{Bmatrix} u_r \\ u_\theta \end{Bmatrix} = \frac{K_I}{2M_o}\left(\frac{r}{2\pi}\right)^{1/2} \begin{Bmatrix} (1+\nu)[(2\kappa-1)\cos(\theta/2) - \cos(3\theta/2)] \\ (1+\nu)[-(2\kappa+1)\sin(\theta/2) + \sin(3\theta/2)] \end{Bmatrix} \qquad 1.3.2$$

where $K_I$ is the stress intensity factor for mode I given by

$K_I = \sigma(\pi \ell)^{1/2}$ for a sharp slit crack

$M_o$ is the Young's modulus, $\nu$ is the Poisson's ratio and

$$\kappa = \frac{3-\nu}{1+\nu} \quad : \text{plane stress}$$

$$= 3-4\nu \quad : \text{plane strain}$$

The stress intensity factor $K_I$ depends on the applied load and the crack geometry and consequently determines the local field intensity.

It should be noted that the above results are not valid for r too small or too large. Higher order terms have been neglected in the derivation. If the field is to match with the outer boundary those higher order terms need to be included. Also, because of the sharp slit approximation, the singularity in the stress field at the crack tip is unavoidable.

Despite the above anomaly the paramter $K_I$ might reasonably be expected to be associated intimately with the conditions of crack extension. It is Irwin and his associates who developed a new formulation (for reference see Irwin 1958) of fracture mechanics based on the concept of stress intensity factor. Their idea had been to calculate the strain energy release when a crack of length 2l is extended to a length $2(\ell+\delta\ell)$ under constant external loading and express it in terms of some function of $K_I$ .

Let us consider, following Irwin, a crack tip region (as shown in figure 1.3.2) which is small compared to the dimensions of the whole sample but sufficiently large with respect to the atomic

dimensions. As a special case, let us assume that the crack is in a thin plate under constant strain. The distribution of the stress ($\sigma_{yy}$) and the displacement ($u_y$) fields near the crack tip are also shown. It was argued by Irwin that the strain energy release for an extension of the crack from L to L' would be the same in magnitude as the work done by the surface forces across the length LL' when the crack is closed from L' to L because the processes are reversible. The energy change $\delta E_{el}$ could be expressed as

$$\delta E_{el} = \int_0^{\delta l} \sigma_{yy} \cdot u_y \cdot dr \qquad 1.3.3$$

From equation 1.3.1, taking L as the origin, the stress at a point R in the region LL' is given by

$$\sigma_{yy}(r, \theta = 0) = \frac{K_I}{\sqrt{2\pi r}} \qquad 1.3.4$$

and from equations 1.3.2, taking L' as the origin, the displacement field at a point R in the region LL' is given by

$$u_y(\delta l - r, \theta = \pi) = \frac{K_I}{M_0} \cdot \frac{2\sqrt{2}}{\pi} (\delta l - r) \qquad 1.3.5$$

Therefore, $$\delta E_{el} = \frac{2K_I^2}{\pi M_0} \int_0^{\delta l} \frac{(\delta l - r)^{1/2}}{r^{1/2}} dr \qquad 1.3.6$$

Substituting $r = \delta l \sin\theta$, this integral can be evaluated to give

$$\delta E_{el} = \frac{K_I^2}{M_0} \delta l$$

$$\frac{\delta E_{el}}{\delta l} = \frac{K_I^2}{M_0} \qquad 1.3.7$$

The above ratio is the so called strain energy release rate G. Under fixed strain condition (where the external work done on the system is zero and the only driving force for the extension crack comes from the release of strain energy) the elastic strain energy release per unit increment in crack length (per unit width of the crack front) is given by

$$G = \frac{K_I^2}{M_0} \qquad 1.3.8$$

The strong point of this method of determining energy release rate is the fact that G can be expressed in terms of standard stress intensity values (just as equation 1.3.8 for a sharp slit crack) which are usually available to the structural engineers for a wide variety of crack geometries and loading systems.

So far there has been no mention of a fracture criterion. For a brittle material, whether a particular value of G or $K_I$ would cause a catastrophic fracture or not depends on whether the strain energy release rate is sufficient to exceed the energy needed, $2\gamma$, to separate the two surfaces for unit increment of crack length. Here $\gamma$ is the surface energy per unit area of the material. Thus, one can derive a fracture criterion by equating the above two energies as

$$\frac{K_{IC}^2}{M_o} = 2\gamma$$

$$\frac{\pi l_c \sigma_c^2}{M_o} = 2\gamma$$

$$\sigma_c = \left(\frac{2 M_o \gamma}{\pi l_c}\right)^{1/2} \qquad 1.3.10$$

where $K_{IC}$, $l_c$ and $\sigma_c$ are the critical values of $K_I$, $l$ and $\sigma$ at which brittle fracture occurs. Equation 1.3.10 is the Griffith criterion (equation 1.2.7) for brittle fracture.

## 1.4 Eringen Non-Local Theory

It was indicated in the previous section that a very sharp crack gives rise to a singularity in the stress field at the crack tip. In reality no crack is sharp compared to atomic dimensions and there is no stress singularity at any real crack tip. The crack tip singularity is nothing but the outcome of the mathematical idealization of infinitesimally thin crack.

Numerous attempts have been made over the years to overcome this singularity problem but with little success. Except for the recent attempt made by Eringen and co-workers (1977 a & b) using non-local elastic theory, all other attempts suffer from serious criticisms. The bulk of the recent literature follows from the idea of introducing compressional cohesive stress in a small region near the crack tip put forward by Barenblatt (1962) and Dugdale (1960). By determining the distribution of this superficial stress, Barenblatt closed the tip in a cusp as shown in figure 1.4.1 and Dugdale accomplished the same result by assuming that a constant compressive stress is distributed over an unknown length s beyond the geometrical tip of the crack so that the tip is closed for a particular value of s, as shown in figure 1.4.2. While such attempts removes the stress singularity, the physical justification of the compressive stresses acting at the free surfaces of the crack tip unless they are applied externally is questionable. Instead of going into the details of these patched-up theories, which only bring up new objections to remove old ones, we will study the non-local theory put forward by Eringen et al in some detail.

In the local elasticity theory the stress at a point depends only on the strain at that point.

$$\sigma_{kl}(\mathbf{x}') \equiv \sigma'_{kl} = \lambda e'_{rr}(\mathbf{x}')\,\delta_{kl} + 2\mu e'_{kl}(\mathbf{x}') \qquad 1.4.1$$

where $\sigma_{kl}(\mathbf{x}')$ is the stress at the point $\mathbf{x}'$
$e_{kl}(\mathbf{x}')$ is the strain at the point $\mathbf{x}'$
$\lambda$ and $\mu$ are the Lame constants

In the non-local theory, the stress at a point is not only a function of the strain at that point but also depends on the strains at other points in the vicinity. Following Eringen one may write

$$t_{kl} = \int_{\tau} [\lambda'(|\mathbf{x}'-\mathbf{x}|)e_{rr}(\mathbf{x}')\delta_{kl} + 2\mu'(|\mathbf{x}-\mathbf{x}'|)e_{kl}(\mathbf{x}')]\, d\iota(\mathbf{x}'), \qquad 1.4.2$$

where $t_{kl}(x)$ is the stress at a point x,

$e_{kl}(x')$ is the strain at a point x',

$\lambda'$ and $\mu'$ are functions of the distance ( $|x' - x|$ ).

For an isotropic non-local elastic solid

$$(\lambda', \mu') = (\lambda, \mu)\alpha(|x'-x|), \qquad 1.4.3$$

$$\alpha(|x'-x|) = \begin{cases} K(a-|x'-x|), & |x-x'| \le a, \\ 0, & |x-x'| \ge a, \end{cases} \qquad 1.4.4$$

where K is the material constant, a is the atomic bond length.

In the limit $a \to 0$,

$$(\lambda', \mu') \to (\lambda, \mu)$$

Combining equations 1.4.1. and 1.4.2., one gets

$$t_{kl} = \int_V \alpha(|x'-x|)\sigma_{kl}(x')\, dv(x') \qquad 1.4.5$$

The equations of equilibrium of non-local elasticity, with vanishing body force, are Cauchy's relations

$$t_{kl,k} = 0 \qquad 1.4.6$$

where, 'k' is the partial derivative with respect to the k-th space component. Thus,

$$\int_V \alpha(|x'-x|)\sigma_{kl,k}(x')\, dv(x') = 0 \qquad 1.4.7$$

It can be proved that (see Eringen 1976) when $\alpha(x')$ is a continuous function of x' with a bounded support where $\alpha > 0$, equ. 1.4.7. is satisfied if and only if

$$\sigma_{kl,k} = 0 \qquad 1.4.8$$

Equation 1.4.8 is the fundamental equation of elastostatics for any well posed boundary value problem. The solutions of this equation in two dimension has been given by Sneddon (1951) in the general form

$$\left.\begin{aligned} u &= (2\pi)^{-\frac{1}{2}} \int_{-\infty}^{\infty} \frac{i}{k} [|k| A(k) + (|k| y - (\lambda+3\mu)/(\lambda+\mu)) B(k)] \exp(-|k| y - ikx)\, dk, \\ v &= (2\pi)^{-\frac{1}{2}} \int_{-\infty}^{\infty} [A(k) + yB(k)] \exp(-|k| y - ikx)\, dk, \end{aligned}\right\} \qquad 1.4.9$$

where A(k) and B(k) are to be determined from the boundary conditions.

For the crack geometry shown in figure 1.2.2 and for a stress $\sigma$ applied on the crack surfaces the boundary conditions are given by

$$\left.\begin{aligned} &t_{yx}(x, 0) = 0, \quad t_{yy}(x, 0) = -t_0(x), \quad |x| < l, \\ &\frac{\partial u}{\partial y}(x, 0) = 0, \quad v(x, 0) = 0, \quad |x| \geq l, \\ &(u, v) \to 0 \quad \text{as } r \to \infty, \quad r \equiv (x^2 + y^2)^{\frac{1}{2}}. \end{aligned}\right\} \qquad 1.4.10$$

The stress field in accordance with equ. 1.5.2 for the two dimensional case has the form

$$\left.\begin{aligned} t_{xx} &= \iint_R \alpha(|x' - x|)[\lambda(u'_{,x'} + v'_{,y'}) + 2\mu u'_{,x'}]\, dx'\, dy', \\ t_{yx} &= \iint_R \alpha(|x' - x|)\mu(u'_{,y'} + v'_{,x'})\, dx'\, dy', \\ t_{yy} &= \iint_R \alpha(|x' - x|)[\lambda(u'_{,x'} + v'_{,y'}) + 2\mu v'_{,y'}]\, dx'\, dy', \end{aligned}\right\} \qquad 1.4.11$$

$$|x' - x| = [(x' - x)^2 + (y' - y)^2]^{\frac{1}{2}}.$$

When these stresses $t_{kl}$ (equ. 1.4.11) are used with the boundary conditions (equ. 1.4.10) a set of integral equations for A(k) and B(k) is obtained. Eringen et al solved this set of equations numerically to obtain A(k) and B(k).

Finally, to obtain the stress field for the case of $t_{yy} = \sigma$ (x) applied at y = $\infty$ with traction free crack surfaces, they superposed the solution of the above problem on that for an uncut plate subject to $t_{yy} = \sigma(x)$ at y = $\infty$. For constant $\sigma$, this simply gives $t_{yy} = \sigma$ at all points occupied by the material. The results of the Eringen calculation can be summarized as follows.

For a thin crack in an infinite two dimensional material subjected to an uniaxial constant stress acting on the boundary surfaces, as shown in figure 1.2.2.

(1) The stress concentration factor is

$$F = \frac{t_{yy}(l,0)}{\sigma} = C\sqrt{\frac{2l}{a}} \qquad 1.4\ 12$$

where C is a function of l/a. With the increase of l/a the value of C decreaes and converges to .73 (with some small oscillations) when $l/a > 50$. Thus, the stress at the crack tip is finite and it could be infinite only if the atomic distance 'a' is zero. The stress distribution curves obtained by Eringen for different values of 2l/a are shown in figure 1.4.3.

(2) When $t_{yy}(1,0) = t_c$ =cohesive stress, the crack starts to propagate. In that case

$$\sigma^2 l = \frac{a\, t_c^2}{2\, C^2} \qquad 1.4.13$$

This is basically the Griffith criterion for brittle fracture, where the right hand side is a material constant.

(3) The stress intensity factor for mode I

$$K_I = \sigma (\pi l)^{1/2}$$

could be expressed in a more fundamental way

$$K_I = 1.72\, t_{yy}(l,0)\, a^{1/2} \qquad 1.4.14$$

when $t_{yy}(1,0) = t_c$ , this gives the fracture toughness $K_{Ic}$

$$K_{Ic} = 1.72\, t_c\, a^{1/2} \qquad 1.4.15$$

This is independent of $l$ and clearly a material property. This fact is well known in engineering fracture and has been verified many times through experiments.

# CHAPTER 2
# LATTICE STATICS THEORY OF FRACTURE

## 2.1 Lattice Statics Approach

It is clear that to obtain a good understanding of the criterion of fracture and of the properties of crack propagation, as in any thermodynamic process, one must look at the problem at the atomic or molecular level, especially since it is the nature of the cohesive bonding between the atoms of a solid which ultimately determines the resistance to crack propagation. Keeping this in mind, attempts have been made over the last decade in this direction. The lattice statics method put forward by Thomson et al (1971) is one such attempt. Thomson et al have done some further work in the following years by extending the original calculation for one dimension to two dimensions. Among other calculations, the work done be Esterling (1976) on three-dimensional crack is to be noted (also see Fuller & Thomson, 1978 and Esterling, 1979 for full review).

The main feature of lattice statics calculations has been to treat an infinite sample with discrete atoms, arranged in a lattice, interacting via some central two body potential. To make the calculations mathematically tractable the following approximations are usually made:

(1) Only near neighbor interactions play the dominant role
(2) The interatomic force is linear up to some critical value of displacement at which it is truncated discontinuously and set to zero for larger displacements as shown in figure 2.1.1.

The original one-dimensional model of Thomson et al will be described here briefly. They used a semi-infinite double chain of

atoms bonded together horizontally by bendable bonds and vertically by stretchable bonds as shown in figure 2.1.2. The zeroth atoms are stretched apart vertically by the forces $\sigma$ and the first n vertical bonds are streched beyond their limit and are broken forming a crack of finite length. The main idea of the detailed calculations is to calculate the total energy. To obtain a fracture criterion, they minimized the total energy with respect to the displacements. Figure 2.1.3 is a schematic diagram showing the bending of the horizontal bonds and the stretching of the vertical bonds.

The energy $E_j^B$ of the horizontal bond connecting j th and (j - 1) th atoms is

$$E_j^B = \tfrac{1}{2}\gamma(\theta_j - \theta_{j-1})^2 \qquad j = 1, 2, 3\cdots \qquad 2.1.1$$

where $\gamma$ is the spring constant of the bendable bonds.
For small angle bending $\theta_j$ can be written as

$$\theta_j = \tan\theta_j = y_{j+1} - y_j$$

$$E_j^B = \tfrac{1}{2}\gamma(y_{j+1} - 2y_j + y_{j-1})^2 \qquad j = 1, 2, 3\cdots \qquad 2.1.2$$

The energy of the stretchable bonds can be written as

$$E_j^S = \tfrac{1}{2}\gamma'(2y_j) \qquad j = n, n+1, n+2\cdots \qquad 2.1.3$$

and the total energy of the system is

$$E = -2\sigma y_0 + \sum_{j=1}^{\infty} E_j^B + \sum_{j=n}^{\infty} E_j^S \qquad 2.1.4$$

Inserting the equations of stability

$$\frac{\partial E}{\partial y_j} = 0 \qquad 2.1.5$$

one can obtain a set of equations which, when used with the obvious boundary condition,

$$\lim_{j \to 0} y_j = 0$$

yields the stability condition.

## 2.2 Lattice Trapping

When the calculations are done for the one dimensional model described in the previous section a totally unexpected phenomenon evolves. Unlike one critical stress as predicted in the Griffith theory two critical stresses ($\sigma_+$ & $\sigma_-$) are obtained. The crack is stable when the stress is of any value between the two critical stresses. The crack is expected to propagate for stresses higher than the higher value, $\sigma_+$ and to heal for stresses lower than the lower value $\sigma_-$ of the critical stresses. Explicit calculations give the ratio of the two stresses as

$$\frac{\sigma_+}{\sigma_-} = \begin{cases} 1+2k & \text{for } k \ll 1 \\ 4.3 & = 1 \\ k+9 & \gg 1 \end{cases} \qquad 2.2.1$$

where $k = 2\gamma'/\gamma$ is a measure of the relative stiffness of the stretchable and bendable bonds. Thus, unless k is very small the crack is stable (as if trapped) between two values of stresses which could differ widely.. This phenomenon is known as lattice trapping. It was believed by Thomson et al (1971) that k 1 is a reasonable guess giving $\sigma_+/\sigma_- \simeq 4$ ( a significant amount of lattice trapping). In the same paper they developed another independent model calculation to get confirmation of the above result. In that model the surface energy of the atoms on the crack plane was calculated as the crack tip advanced from one position of the lattice to the other as shown in figure 2.1.4.

In the energy calculation the form of the energy for the n - th bond was taken as

$$E(n) = \tfrac{1}{2} E_0 \left[ 1 - \frac{2}{\pi} \tan^{-1} \frac{n}{\alpha} \right] \qquad 2.2\,2$$

where the adjustable paramter $\alpha$ allows one to fit the results to the actual shape of the crack. $\alpha$ can be thought of as the width of a "core region" of a crack and is also responsible for the variation of energy in the vicinity of the crack tip. Initially the crack tip bond is at n = 0 and $E(0) = \frac{1}{2} E_o$, where $E_o$ is the cohesive bond strength of an atom pair. The justification of the choice of the energy function (equ. 2.1.7) that it has an analytic form of the correct physical shape.

$$E(+\infty) = 0 \qquad E(-\infty) = E_o \qquad 2.2.3$$

To move the crack tip a wedge was considered to push the atoms of the crack tip apart. When the tip of the crack is at the n th bond the surface energy is given by

$$\sum_{n=-\infty}^{\infty} E(n)$$

As the wedge is pushed rigidly from its initial position by an amount x the surface energy could be written as $\sum_{n=-\infty}^{\infty} E(n-x)$. These surface energy terms are divergent for a semi-infinite crystal but the quantity of interest, the difference of the two energies, is a convergent series

$$S(x) = \sum_{n=-\infty}^{\infty} E(n-x) - \sum_{n=-\infty}^{\infty} E(n) \qquad 2.2.4$$

$$x = 1, 2, 3 \cdots$$

In the continuum approximation S(x) is simply a linear function of x, but in the discrete case S(x) is periodic in x. The force, $\sigma$, to move the crack is then equal to -dS(x)/dx. Plots of the variation of S(x) and -dS(x)/dx versus x are shown in figure 2.1.5.

It is found that $\sigma$ has a maximum and a minimum value, and the ratio of the maximum $\sigma(\sigma_+)$ to the minimum $\sigma(\sigma_-)$ is given by

$$\frac{\sigma_+}{\sigma_-} = \frac{1 + 2e^{-2\pi\alpha} + e^{-4\pi\alpha}}{1 - 2e^{-2\pi\alpha} + e^{-4\pi\alpha}}$$

$$\approx 1 + 4e^{-2\pi\alpha} \qquad \text{if, } 2\pi\alpha > 1 \qquad 2.2.5$$

Thomson et al performed one of the most important steps in establishing the reliability of any quantitative, unexpected result for a model, since they did the calculation for a very different model in order to see how the results compare. They estimated $\alpha$ in a particular case from the computer calculations of Gehlen and Kanninen (1972) using a typical force law as proposed by Johnson (1966). Choosing the point of inflection of the potential at the atom pair n = 0 they calculated the displacement of the atom pair n = 0 and n = 1. Then they calculated the energy of the atom pair for n = 1 from Johnson's force law and, substituting that into their energy expression 2.2.2 they found $\alpha$ = .524 and $R_T = \sigma_+ / \sigma_-$ = 2.14, which led them to conclude that lattice trapping is significantly large. A numerical error in this calculation will be discussed in section 5.7 Their two dimensional calculations (1973) also showed significant lattice trapping for small value of the core width $\alpha$. In the two dimensional calculation, using the same energy expression (equation 2.2.2) for a square lattice they obtained a trpping ratio (for large cracks)

$$R_T = \frac{\sigma_+}{\sigma_-} = \coth(\pi\alpha) \qquad 2.2.6$$

Esterling (1976) analyzed the stability of three dimensional cracks in the same way as done by Thomson et al. Instead of using a bond snapping force law, as used by Thomson et al, he investigated the consequences of introducing a jog at the crack surface as well as the effects of various non-linear force laws. He observed that crack healing is sensitive to the long range portion of the cohesive force. It occurs when an applied load leads to a pair of atoms, whose bonds had been broken, acquiring a net displacement such that the cohesive force is non-negligible and increasing with decreasing displacement. He also obtained two values for the critical stresses in terms of stress intensity factors and crack lengths

$$\sigma_\pm = K_\pm / \sqrt{\ell} \qquad 2.2.7$$

For large cracks, $K_{\pm}$ was observed to be independent of the crack length 2l and to be characteristic of the material which serves to define its resistance to fracture.

# 3. DYNAMIC CONTINUUM THEORY

## 3.1 The Mott Theory

When the external stress or strain is slightly higher than the critical value a crack reaches a point of instability in its length due to the unbalanced force acting near the crack tip and the system acquires kinetic energy from the rapidly This mechanism of crack propagation separating crack surfaces. is of interest in this thesis.

Mott (1948) studied this type of crack propagation by including kinetic energy in the Griffith energy balance equation. He made some assumptions in order to derive a quantitative result relating crack velocity to crack length. He assumed:

(1) the stress and strain fields around a slowly moving crack are adequately defined by the equations of staic elasticity theory (quasi-static elastic approximation)

(2) the kinetic energy comes from the volume element of a dimension of the order of the crack length surrounding the crack.

(3) the fracture surface energy remains independent of the crack velocity.

Inclusion of the kinetic energy into the Griffith equation (equation 1.2.1) gives

$$\delta E_{ext} + \delta E_{el} + \delta E_s + \delta E_k = 0 \qquad 3.1.1$$

The kinetic energy of a two dimensional continuum containing a crack can be written as

$$E_k = \iint_R \tfrac{1}{2} \rho \, dx \, dy \left[ \left( \frac{du_x}{dt} \right)^2 + \left( \frac{du_y}{dt} \right)^2 \right] \qquad 3.1.2$$

Where $u_x$ and $u_y$ are the components of displacement and $\rho dxdy$ is the mass of an element at (x,y). R is a domain of the order of the crack length surrounding the crack.

Replacing du/dt by $(du/dl)_t.(dl/dt)$ i.e., by $(du/dl)_t \cdot v_c$, where $v_c$ is the velocity of the crack, we obtain from equation 3.1.2.

$$E_k = \frac{1}{2}\rho v_c^2 \iint_R \left[\left(\frac{\partial u_x}{\partial l}\right)^2 + \left(\frac{\partial u_y}{\partial l}\right)^2\right] dx\,dy \qquad 3.1.3$$

Following assumption (1), $u_x$ and $u_y$ can be written as the displacement fields in the static situations.

$$u_x = \frac{\sigma l}{M_0} f(\nu, x, y)$$
$$u_y = \frac{\sigma l}{M_0} g(\nu, x, y) \qquad 3.1.4$$

Here $\nu$ is Poisson's ratio and f and g are two dimensionless functions.

Finally $E_k$ can be written as

$$E_k = \frac{1}{2}\rho v_c^2 \frac{\sigma^2}{M_0^2} \iint_R h(\nu, x, y)\,dx\,dy \qquad 3.1.5$$

$$h(x, y, \nu) = f^2(\nu, x, y) + g^2(\nu, x, y)$$

Following assumption (2), if the above integral is replaced by some constant k times $l^2$, equation 3.1.5 reduces to

$$E_k = \frac{1}{2} k \rho v_c^2 \cdot \frac{\sigma^2 l^2}{M_0^2} \qquad 3.1.6$$

To calculate the crack velocity let us consider two different loading mechanisms separately.

External Fixed load

Under the influence of an external fixed load, equation 3.1.1 (using equation 1.2.3 through 1.2.5) reduces to

$$\delta E_k = \delta\left(\frac{\pi \sigma^2 l^2}{M_0} - 4\gamma l\right) \qquad 3.1.7$$

Using the Griffith condition (equation 1.2.7) we obtain the surface energy

$$\gamma = \frac{\pi l_o \sigma_c^2}{2 M_o}$$

and equation 3.1.7 reduces to

$$\delta E_k = \delta\left[\frac{\pi\sigma^2}{M_o}(l^2 - 2 l l_o)\right] \qquad 3.1.8$$

Using the boundary conditions: at $l=l_o$ i.e., when the crack is at rest, E = 0, the integration of equation 3.1.8 gives

$$E_k = \frac{\pi l_o^2 \sigma_c^2}{M_o}\left(1 - \frac{l_o}{l}\right)^2 \qquad 3.1.9$$

The crack velocity now follows by equating (3.1.6) an (3.1.9), i.e.,

$$v_c = \left(\frac{2\pi M_o k}{\rho}\right)^{1/2}\left(1 - \frac{l_o}{l}\right) \qquad 3.1.10$$

Thus, the crack asymptotically approaches a terminal velocity $[V_T = (\frac{2\pi M_o k}{\rho})^{1/2}]$ at large $l >> l_o$.

Fixed External Displacement

Suppose the sample is loaded just beyond the Griffith equilibrium as before, but this time the outer boundaries are held at constant displacement (i.e.fixed strain). Berry (1960) showed that this case could be treated as a modification of the external fixed load case. The elastic (strain) energy, E of a plate of area A under external stress $\sigma$ is $\frac{A\sigma^2}{2M_o}$. Now, if a crack of length l is created, the total elastic energy $E_{el}$ of the cracked plate is given by

$$E_{el} = \frac{A\sigma^2}{2M_o} + \frac{\pi\sigma^2 l^2}{M_o} \qquad 3.1.11$$

$$= A\left(1 + \frac{2\pi l^2}{A}\right)\frac{\sigma^2}{2M_o}$$

where

$$= \frac{A\sigma^2}{2M'} \qquad 3.1.12$$

$$M' = \frac{M_o}{1 + \frac{2\pi l^2}{A}} \qquad 3.1.13$$

M' may be called the effective elastic modulus in the presence of a crack. Thus, the response of a cracked sample is described by the stress-strain relation.

$$\sigma = \frac{M_0 e}{1 + \frac{2\pi l^2}{A}} \qquad 3.1.14$$

where e is the external strain.

It is clear that as $A \rightarrow \infty$ (for an infinite sample) $\sigma = M_0 e$, i.e. for an infinite sample fixed load and fixed strain gives identical result.

Lawn and Wilshaw (1975) using Berry's sample size criterion, modified Mott's result for a finite sample. To obtain an expression for velocity under fixed strain, $\sigma$ in equation 3.1.7 is replaced by the right hand side of equation 3.1.14. Calculation similar to the case of fixed load gives an expression for the kinetic energy analogous to equation 3.1.9 in terms of strain

$$E_k = \pi M_0 e^2 l^2 \left\{ 1/\left[ 1 + \delta \frac{l^2}{l_0^2} \right] - \frac{l_0}{l}\left(2 - \frac{l_0}{l}\right)/\left[1+\delta\right]^2 \right\} \qquad 3.1.15$$

where, $\delta = \frac{2\pi l_0^2}{A}$

In the same way equation 3.1.6 could be written as

$$E_k = \tfrac{1}{2} k' \rho v_c^2 e^2 l^2 / \left[ 1 + \delta \frac{l^2}{l_0^2} \right] \qquad 3.1.16$$

where k' might be different from the analogous k for a fixed load. (As $A \rightarrow \infty$, $k' \rightarrow k$)

Equating equations 3.1.5 and 3.1.1 gives

$$v_c = \left(\frac{2\pi M_0}{k'\rho}\right)^{1/2} \left\{ 1 - \frac{l_0}{l}\left(2 - \frac{l_0}{l}\right)\left[\left(1 + \delta\frac{l_0}{l}\right)/\left(1+\delta\right)\right]^2 \right\}^{1/2} \qquad 3.1.17$$

Limiting Crack Velocity and Size Effect

The equation for the velocity of a crack under the above two loading systems can be written as

$$v_c = V_T f\left(\frac{l}{l_0}, \delta\right) \qquad f \leq 1 \qquad 3\ 1.18$$

where, $$V_T = \left(\frac{2\pi}{k}\right)^{1/2} V_L \qquad 3\ 1.19$$

and $V_L$ ( $= (M/\rho)^{1/2}$) is the longitudinal velocity of sound. (ignoring differences between k and k').

The plot of $v_c$ vs. $1/l_0$ is shown in figure 3.1.1 for different values of $\delta$. As mentioned earlier, the two loading mechanisms become identical as $A \rightarrow \infty$ i.e., as $\delta \rightarrow 0$ which is again confirmed when we observe that $\delta = 0$ reduces equation 3.1.1 to equation 3.1.10. In these situations the velocity attains a terminal value $V_T$ .

For a non zero value of $\delta$ under fixed strain condition the velocity rises to a maximum value and then decreases until the crack comes to rest. The smaller the size of the samples, the earlier is the crack arrested. For example, when $\delta = .05$ the crack comes to rest when the length of the crack is little over twice the critical length.

Robert and Wells (1954) estimated the value of the terminal velocity ($V_T$) by following the second assumption of Mott i.e., that there exists a limit to the size of the domain R beyond which the material is undistributed by the fast moving crack. Taking R as a circle of radius r and estimating $r \simeq V_L \cdot t$, the distance travelled by the elastic wave in time t taken for the crack to extend through 1 V t at terminal velocity, one obtains $r/l \simeq V_L / V_T = (k/2\pi)^{1/2}$ . They obtained a second condition for k by evaluating the integral in 3.1.5 numerically as a function of r/l and arrived at a unique value of k which simultaneously satisfies $r/l = (k/2\pi)^{1/2}$ and the integral for k for a domain R of radius r giving

$$V_T = 0.38\, V_L \qquad 3.1.20$$

## 3.2 BRITTLENESS VS. DUCTILITY

Certain solids, those with strong covalent or ionic bonding and a relatively immobile defect population, fracture readily at low stress levels (compared with the theoretically attainable levels). These solids are designated brittle or highly brittle if the resistance to fracture is determined largely by the intrinsic bond strength. In brittle fracture the atomically sharp crack is maintained throughout the process, while in a ductile fracture the crack losses the initial sharp appearance, the tip becomes blunted, and the solid fractures through shear (slip) motionwith a large component of force perpendicular to the crack surface. Non glassy polymers, f.c.c. metals and some b.c.c. metals are ductile in nature. Between these two extremes lie a large number of solids exhibiting an intermediate behavior. Temperature also plays an important role in the modes of fracture. With the increase of temperature brittle materials show a tendency toward ductility.

It has been realized that a solid will be brittle or ductile depending on the ratio of tensile strength to the shear strength of the solid, or on the relative ease of bond rupture and atomic slip or glide. Kelly, Tyson and Cottrell (1967) studied the problem and postulated a criterion for ductility. According to these authors, tip blunting will occur and a shear instability will result if the maximum shear stress in the tip region exceeds the theoretical shear strength of the solid. Rice and Thomson (1974) on the other hand showed that the Kelly - Tyson - Cottrell criterion cannot be sufficient. This is because the shear stress fields around the tip are highly localized. The fact that these fields exceed a maximum at one point of the shear plane (shear line in 2D) does not guarantee that the slipping (or gliding) condition will be satisified on all points of the shear plane. Thus, the picture of

tip blunting via uniform shear motion had to be abandoned. Rice and Thomson reasoned that the matching of the highly sheared medium near the tip with the non-sheared medium at greater distances defines a dislocation. They worked out a criterion for brittleness versus ductility. They found some property of the general interaction between a crack tip and a dislocation. This interaction is attractive for small distances (from tip to dislocation core) and repulsive at larger distances. If a dislocation is present at a distance greater than the critical distance $r_c$ then it will be driven away to infinity. If it is at a smaller distace it will be attracted to the tip and be annihilated. The situation of interest is not that of an already existing dislocation but of one which is created at the tip. In the Rice-Thomson theory one considers the dislocation just after its creation. A comparison is made between the core cutoff $r_o$ and the critical distance $r_c$ . If $r_c > r_o$ then the newly created dislocation will find itself in the attractive part of the interaction and will not be free to leave the tip. Thus, for solids satisfying this condition, tip blunting will not occur and brittle behviour will result. This will continue to be the case until sufficient energy is supplied to the dislocation to overcome the attractive barrier and cause a brittle-ductile transition. Actually, even when such energy is made available to the region (e.g. by thermal fluctuations) the solid might prefer to use it in bond tearing rather than for slip processes. This means that substances satisfying the condition $r_c > r_o$ will be very good candidates for brittle behavior.

On the other hand $r_c \sim r_o$ or $r_c < r_o$ will give rise to ductile behaviour. The continuum analysis is not quantitatively valid for this situation but it still reveals the behaviour of the system. In this case the newly created dislocation finds itself in the repulsive part of the action and is driven away. In the Rice-Thomson theory, one writes

$$f_{dislocation-crack} = f = f_i + f_\ell + f_\sigma \qquad 3.2.1$$

where $f_i$ = the attractive image force between the dislocation and its image.

$f_\ell$ = the attractive force due to the dislocation ledge which is created when the dislocation is emitted.

$f_\sigma$ = the repulsive force exerted by the shear fields of the tip trying to drive the dislocation away.

The authors evaluated the total force when the applied load is of the order of the Griffith critical stress. The critical distance ($r_c$) is the value which makes $f = 0$.

$$f(r_c) = 0$$

Referring to figure 3.2.1 and following Rice-Thomson (1974) one can write

$$\mu b\left[-\frac{1}{4\pi\xi_c(1-\nu)} - \frac{2}{\pi\eta^2\beta'}\cdot\frac{\alpha}{\xi_c^2+\alpha^2} - \frac{1}{\eta\beta}\cdot\frac{1}{\sqrt{2\pi(1-\nu)\xi_c}}\right]=0 \qquad 3.2.2$$

where, b = Burger's vector, $\xi_c = r_c/b$

$$\alpha = e^{3/2}\xi_0/2\,,\quad \eta^2 = \mu b/\gamma\,,\quad \xi_0 = r_0/b$$

$$\frac{1}{\beta} = \sin\phi\cos(\phi/2)\,,\quad \frac{1}{\beta'} = \sin\phi$$

$\gamma$ = Surface energy per unit area

$\mu$ = Shear modulus

Neglecting the ledge interaction (middle term) one gets

$$r_c = \frac{1}{8\pi(1-\nu)}\cdot\beta^2\cdot\frac{\mu b^2}{\gamma} \qquad 3.2.3$$

Applying this equation to the two dimensional triangular lattice and for the first neighbour L-J potential, equation 3.2.3 reduces to gives

$$r_c = \frac{1+\nu_{2D}}{8\pi}\beta^2\cdot\frac{\mu b^2}{\gamma} \qquad 3.2.4$$

where is the depth of the potential and d is the nearest neighbour distance. In writing (3.2.4) the correspondence

$$\frac{1}{1-\nu_{3D}} \longrightarrow 1+\nu_{2D} \qquad 3.2.5$$

has been used (Dally and Riley 1965). $\nu_{2D}$ is the Poisson ratio in two dimensions. For an isotropic medium

$$\nu_{2D} = \frac{1}{3}$$

For a slip system making an angle of 60° with a <10> crack and a Burger's vector b = d , $r_c$ will be

$$r_c = \frac{4\sqrt{3}}{\pi} = 1.8\,d \qquad 3.2.6$$

From Esbjorn and Jensen (1976)

$$r_o = (1.7 \pm 0.2)\,d \qquad 3.2.7$$

The ductility criterion $r_c < r_o$ is satisfied. One expects the probability of dislocation emission to be quite high, although brittle behaviour can also result because the criterion is only barely satisfied.

If the ledge term is included it will increase the value of $r_c$ and might cause the system to stop satisfying the ductility criterion.

Thus according to the Rice-Thomson theory this system is expected to show a behaviour in between the two extremes, or it might show only one of the two types of behaviour in different situations depending on the dynamic details of the loading process.

# 4. ATOMISTIC CALCULATIONS

## 4.1 Motivation For The Atomistic Calculation

Fracture is essentially an atomic phenomenon. To develop a satisfactory theory one therefore should study the atomic processes near the crack tip. Although continuum mechanics gives an approximate description of fracture, it does not offer any insight of fracture at the microscopic level. Since the mechanisms of bond rupture and the mobility of the atoms at the crack tip ultimately determine the strength and brittleness (or ductility) of a cracked solid, the need for (1) the construction of an atomistic model by incorporating the key features of the system and (2) for the calculation, analytically or by computer techniques , of the physical characteristics of interest becomes essential. If step (2) is carried out to high accuracy, which can now be done with the availability of modern computers, then the limitations of the results are those of the model itself. Modeling can lead to very significant insights, but it is essential to try to determine which parts of the results are (or may be) artifacts of the model and which parts are general and relevant to the real physical system being modeled. There are always simplifying assumptions and constraints in a model which need careful scrutiny.

The description of a crack in a solid with an applied external load or displacement is rather simple to envision. One has a semi-infinite periodic three-dimensional array of atoms interacting with one another via an interatomic potential. A crack is inserted in the solid and a load is applied externally to appropriate surfaces. If the load is sufficiently large, the crack grows and the solid ultimately fractures. Why is this phenomenon so much more difficult to treat than other problems encountered in solid state physics? In most fundamental phenomena in solids, the periodicity of the solid is used to reduce the problem to an examination of a

simple representative cell or region. Hence, the infinite number of atoms is not a serious problem. In the case of a crack, with its finite extension and the resulting long-range strain field, such reductions are not possible. Hence, one must resort to simplified models to try and gain insight into the role of cracks in brittle fracture.

The various approaches are illustrated in the block diagram of Fig. 4.1.1. In each case, some trade off has been made between giving up some aspect of the phenomenon in nature for some simplification that enables one to carry out a quantitative study. The lattice statics method has already been described in chapter 2. Here the different kinds of trade-offs made in each type of model and the physical significance of the simplifying approximations will be described.

In the various approaches illustated in Fig. 4.1.1 different facets of the real phenomena are emphasized. If the semi-infinite periodic nature of the system is the major concern then one is led to the lattice statics method. Cracks in such lattices can be handled by these methods but only for very simple unrealistic interatomic potentials. In the so-called hybrid models (Sinclair et al, 1972, Gehlen, 1973 and Sinclair , 1975) a very small crystalline region, where the calculations are done with realistic potentials, is imbedded in a simplified elastic region. The boundary matching, the above simplification, and the appropriateness of the size of the imbedded region are the important approximations in this technique. If the nature of the atomic forces and of the atomic motions is the main concern one is led to the molecular dynamic approach which can be used on an unconstrained system of a "large" number of atoms interacting with a realistic interatomic potentil. Here, of course the question is how "large" is large enough to simulate the behavior of the corresponding infinite systems.

## 4.2 Previous Atomistic Calculations

### Hybrid Lattice Statics Calculations (Sinclair & Lawn)

Atomistic studies done by Sinclair et al (1972 & 1975) will be described here. The hybrid approach involves separating the infinite solid into two regions. In region I, near the crack tip, both the atomic structure and the atomic interaction are treated explicitly. In region II, the outside region, the force law and also the atomic structure are simplified. In an early Sinclair and Lawn [1972] calculation, region II is treated by the continuum approximation and the boundary between regions I and II is fixed. In a later calculation by Sinclair [1975] the I-II boundary is flexible and higher order terms are included in the elastic field equations. In the Sinclair and Lawn hybrid calculations, a suitable semiempirical potential for the diamond-structure crystals was constructed. The atoms were then relaxed within region I in such a way that the total potential energy tended to a minimum. This was systematically done on a computer with the boundary between I and II kept rigid. The boundary was obtained by solutions of the continuum field equations. While the results seem to be reasonable, it is difficult to determine their reliability.

Sinclair [1975] thought that the rigid boundary introduced some error in the hybrid calculations that made them not suitable for a study of the critical conditions for crack extension or closure. The reason is that, if the solutions of the inner region are not compatible or consistent with the solutions of the outer region in the rigid boundary method, no adjustment can be made for this mismatch in forces. The rigid boundary forces a state of stability in the system that may be inconsistent with the local stress fields. If the crack in region I would like to expand (or

contract) the rigid boundary prevents this relaxation. The flexible boundry model allows some relaxation of the boundary so as to prevent forces building up at the boundary. Sinclair did this by including higher order terms in the elastic crack-field equations for region II; by suitably adjusting the coefficients of these terms a configuration free of residual forces may be obtained for a given applied stress. The approximation in this procedure is that the forces are calculated correctly in region I but approximately in region II.

Major Results

a. Rigid Boundary.

The results for the rigid boundary model were mostly qualitative and reasonable. Sinclair and Lawn found that except for very near the crack tip the continuum and atomic relaxation calculations show close agreement, despite the fact that the elastic nonlinearity and the atomicity render continuum theory strictly invalid throughout the core region. It is not clear how much of this result depends on the use of rigid boundaries matched to continuum solutions. In Fig. 4.2.1 the bonds in the vicinity of the crack tip are shown. As illustrated in Fig. 4.2.2 the relaxation varies with the size of the atomic region. It is apparent that the continuum solutions are forcing a larger crack to exist than the atomic solutions yield. Thus, in this case the "true" crack is smaller than the "continuum" crack. Unfortunately, it is difficult to estimate the qutantitative errors introduced by this procedure.

b. Flexible Boundary

The main results of the flexible boundary hybrid treatment were directed towards examining the effect of various potentials on lattice trapping. In Fig. 4.2.3 the radial components of the force laws are shown. The important point to note is that potentials I,

II and III are quite long range compared to IV, which has the bond snapping character usually used in lattice statics. In the following table the lattice trapping ratios for these potentials are given. It should be noted that the long-range potentials yield $R_T$ ranging from 1.13 - 1.45 but the bond snapping force gives $R_T = 7.3$. Thus, the hybrid model clearly demonstrates that bond snapping severely exaggerates lattice trapping, while the long-range potentials yield much more modest lattice trapping.

Lattice-trapping ratios for straight [011] edge cracks.

| | Pot I | Pot II | Pot III | Pot IV |
|---|---|---|---|---|
| R | 1.13 | 1.45 | 1.41 | 7.3 |

Discussion

The fact that the hybrid lattice statics are in relatively good qualitative agreement with our molecular dynamic calculations (as discussed in section 5.7) shows that both models are reasonable. What is more difficult to assess is the accuracy of the hybrid model using flexible boundary conditions. There must be some artificial mismatch at the boundary as the force laws in regions I and II are not the same. A systematic variation of region I and the resulting variation of the thermodynamic properties to enable an extrapolation to the infinite atomic solid, would lend more credibility to the quantitative results. It is difficult to compare the lattice trapping results for the long-range potentials in the hybrid model with those of the molecular dynamic calculations. The potentials used by Sinclair are non-central whereas the molecular dynamic potentials are central. The non-central nature of the forces may allow nonbrittle distortions not contained in the central force treatment. In any event, hybrid lattice static calculations using semi-empirical potentials predict negligible to little lattice trapping, as opposed to the bond snapping force models which yield large ($R > 2$) lattice trapping.

Computer Simulation
Weiner-Pear (1975)

Weiner and Pear (1975) used a 2-D square lattice (figure 4.2.4) interacting via a force law (figure 4.2.5) which allows plastic flow and dislocation generation at the crack tip, to study the dynamic behavior of crack motion. Crack motion was allowed only in the direction perpendicular to the crack plane. The reason for the choice of this particular model was to make a direct comparison between their results and the results of an analytic calculation performed by Sanders (1960). Sander's potential could be obtained from the above one by letting $\delta_T = \delta_S = 0$ in figure 4.2.5.

Results

(1) For model parameters ( $\delta_T = 0 = \delta_S$ ) the system behaves in a brittle manner in which a pre- existing crack extends under an applied stress, while for other parameters ($\delta_T = \delta_S \neq 0$) ductile behavior was obseved. Temperature was restricted to zero in these studies.

(2) When plastic flow was allo ed, steady subsonic crack velocity was observed (as opposed to Sander's elastic model) and this terminal velocity was found to be stress dependent but temperature insensitive. Supersonic crack speed was observed at very high stress even when plastic flow occurred.

Discussion

The results of Weiner and Pear are quite valuable since they established the role of the decreasing part of the force law in causing crystal plasticity. When a possible energy dissipation mechanism is prohibited by an artificial aspect of the simulation,

the energy which would have been dissipated in such a mechanism, is forced to be dissipated by another mechanism. The rate at which this other mechanism proceeds would thus be higher than if the available energy is shared between the two mechanisms. Thus Sanders prohibited plasticity by letting $\delta_T = \delta_S = 0$. All the energy released from the load and the strain field at the tip, was forced to be dissipated in surface creation by crack propagation rather than being split between surface creation and dislocation formation. This forced the velocity to be unrealistically high (supersonic). When the sharing was allowed, the velocity was found to be subsonic.

This type of reasoning can be used to obtain an understanding of the supersonic velocities observed by Weiner-Pear in their high stress runs. The one dimensionality of their model prohibits crack branching (and bending). The propagation of the two new branches would necessarily involve bond tearing motions which have a horizontal component and, since these motions are forbidden in this model, branching cannot occur. According to the continuum models an accelerating crack will branch at a maximum velocity of about 0.6 $V_S$ ($V_S$ =surface wave velocity) and the two new branches will split the energy available for acceleration between them and start accelerating from zero. If the branching is prohibited then all the acceleration energy is retained by the original crack, which would thus unrealistically be accelerated to supersonic speeds.

Ashurst-Hoover (1976)

This study was carried out on a two dimensional triangular lattice (figure 4.2.6) using central pair potentials of the parabola, parabola-linear, and double parabola types (figure 4.2.7). This lattice is the simplest two dimensional lattice possessing shear stability in a first neighbour approximation. The simpler square lattice has shear stability only when second neighbours are included, and even then the shear modulus is still quite low.

This lattice has the advantage that it is elasticlly isotropic, and thus comparisons between its properties and those of isotropic continuum theories are valid. For other lattices comparisons must be made with anisotropic elastic theories. The two dimensional triangular lattice has the same strain energy as a two dimensional continuum when first neighbour Hookian springs connect the atoms. The energy of the continuum is computed by a finite element analysis in which the finite elements are triangles whose sides are Hookian springs (Hernikoff 1941). Fixed loading with periodic boundary condition in the x-direction was used for the static studies. For the dynamic studies Ashurst and Hoover switched to the fixed strain condition and with the x-periodicity removed replaced by fixed vertical boundaries.

The dynamic calculations were done in three stages, initialization, relaxation, and propagation. In the first stage the appropriate bonds were cut. In the second, the atomic motions were critically damped for a hundred steps. In the third, the widths of the potentials were adjusted so that the critical bond just broke. The results, therefore, do not represent experiments done on the same solid, but rather on a set of different solids having the same elastic properties but different mechanical strengths.

Major Results

(1) An appreciable amount of lattice trapping ($R_T = \sigma_+/\sigma_- = 3.7$) was observed.

(2) Using potential type (1) they obtained terminal crack velocities varying from $.34\, V_L$ to $.47\, V_L$ for different parameters of potential (1). ($V$ = longitudinal sound velocity). For larger width $\omega$ the terminal velocity was found to be larger. Type (2) potential gave somewhat lower terminal velocity due to the extra attractive energy offered by the type (2) potential.

(3) The terminal velocity was found to be dependent on the external strain. This is in contradiction to Mott's prediction.

(4) Introducing cracks into a prestrained sample they obtained supersonic terminal velocities up to a value of 2.50 $V_L$.

(5) No dislocations were observed in these studies.

Discussion

Simple potentials and the small number of atoms used in these simulations give rise to the question of the validity of the observed results. It is not known whether some of the results of this study are artifacts of the unrealistic potential and/or finite sample size.

The snapping mechanism by which the propagations were initiated can help in understanding the absence of dislocations in the double parabola runs. The double parabola gives rise to a force law similar to the Weiner et al plastic potentials, and should have given dislocations. In the Ashurst-Hoover study the bonds were broken and then the crystal was only partially relaxed (with critical damping) for a hundred steps. At the end of the hundred steps was reduced so that propagation started. This process does not allow the lattice to perform all the deformation it wants to perform (in order to minimize the free energy). First, the way in which the damping affects dislocation formation is not understood (it could oppose it because the rate of deformation is reduced). Second, as this dynamic study was performed under fixed displacement, i.e., the upper and lower boundaries are fixed, the crack can not grow wide enough to allow dislocation formation at the crack tip, particularly if the number of rows of the sample is small. Under a large external displacement, even if the distortion at the crack tip allows dislocation formation, the fixed boundaries prohibit the dislocation from proceeding to the surface. A-H used a

sample of only 10 row for the dynamic study. This explains why they did not observe any dislocations. The present dynamic simulation under fixed displacement does not show any tendency of dislocation formation either (cf. section 6.3) Third, even if the system, in spite of the damping, is proceeding towards a dislocation formation, the hundred steps of partial relaxation might not be sufficient for the dislocation to be formed completely. When is adjusted at the end of hundred steps, surface creation (by propagation) is given an artificial preference over plastic deformation. The sample was thus forced to possess more brittleness than it would have shown if it had been left to evolve by itself under a fixed potential.

The reason for the occurrence of supersonic velocities with the linear potential can be understood in the light of the Sanders and Weiner-Pear studies. As mentioned before in the discussion of these papers, the linear potential was found to prohibit plastic deformation. Thus, all the energy released from the strain field was forced to go into propagation, rather than being split between propagation and plastic deformation. This results in acceleration to supersonic velocities.

Finally, the fixed vertical boundaries could have prohibited motion parallel to the crack (resulting from the non-negligible shear fields). This is because these boundary conditions fix the density in the x - direction and would thus resist any motion which tends to alter this density.

Paskin et al (1977 - 1979)

Paskin, Gohar and Dienes (1980), used a sample which resembled the A-H two dimensional triangular lattice with the more realistic Lennard-Jones potential. They removed all restrictions on the atoms and allowed them to perform any preferred motion. The studies were restricted to the static and dynamic properties of fracture under

constant external load. The objectives of these simulations were to check the assumptions which go into the Griffith and the Mott theories, and to study the time evolution of the different parameters (energies, modulus etc.) as the crack propagates (Gohar, 1979).

Major Results

(1) Simulating cracks of different lengths under different constant load they found that for a large crack (NBB = 39) under a small load( $\sigma = .5 \epsilon/d$) the change in the strain energy during the time of early crack motion is almost zero suggesting a rigid tearing mode (figure 4.2.8a ) This fracture exhibited no dislocation formation or bifurcation - a clean example of brittle fracture. The critical stress was found to be of the same functional form as the Griffith stress, but is lower by a fctor of $\sqrt{2}$ .

(2) At a higher load ($\sigma = 1.3 \epsilon/d$) a crack propagated with large directional distortions near the tip (fig. 4.2.8b ). These distortions which may be considered incipient dislocations, are generated and absorbed as the crack propagates. At a load still higher than 1.3 /d, ($\sigma = 3.0 \epsilon/d$) immediate formation of dislocation, and the subsequent blunting of the tip was observed, indicating a ductile behvior of the model under high load. For a large initial crack (NBB = 39) with $\sigma = 1.3 \epsilon/d$, the crack propagated to the configuration shown in figure 4.2.8c. A dislocation can be seen at the lower end of the crack tip. This dislocation later on propagated to the surface and bifurcation occured.

(3) The static and dynamic stress profiles at or below the critical stress were found to be similar to those obtained by Sinclair (1975) and Eringen (1977).

Discussion

These results can be related to the Rice-Thompson (1970) treatment of crack-dislocation interaction. They consider a material to be brittle if a dislocation generated in the neighborhood of the crack tip cannot escape from the tip region. If the critical distance, $r_c$ , at which a straight dislocation is in unstable equilibrium (see section 3.2), is larger than the dislocation core cutoff, $r_o$ , then the material is brittle. For the present two-dimensional system, application of the Rice-Thomson equations yields $r_c = 1.8d$. From Esbjorn and Jensen (1976) $r_o$ for this system is 1.7d. Consequently, this two-dimensional Lennard-Jones system is barely brittle according to the Rice-Thomson criterion. As indicated above, crack propagation in this system varies from brittle to ductile depending on the applied stress and the detailed dynamics. This suggests that the Rice-Thomson formulation has considerable quantitative validity.

A more detailed examination of the Rice-Thomson treatment indicates that, as the applied load is increased above critical, the stress at a distance from the crack tip increases. Including this stress dependence in the Rice-Thomson formulation, it is found that $r_c$ is approximately proportional to $(\sigma_c/\sigma)^2$ and thus high applied loads, $\sigma$ , should reduce $r_c$ and produce a tendency towards dislocation emission. Since the model system is barely brittle at low stresses and low crack velocities, it is not surprising to find dislocation formation and ductility at high applied loads and large crack velocities.

The studies done by the above authors are of considerable importance in understanding the material behavior (brittle/ductile) of the 2-D triangular lattice interacting via the L-J potential.

## 4.3 Motivation For The Present Calculations

As discussed previously, the W-P and A-H models have given some results in contradiction with the continuum predictions. It is of interest to know whether these contradictions are artifacts of the idealization of the simulations or are the true cosequences of the atomic discreteness of the lattice. W-P used a quasi one-dimensional geometry and a piecewise linear tensile force law for atoms in the same column. A-H used a two-dimensional triangular lattice constrained so that Poisson's ratio is zero. They used, for the most part, bond snapping force laws similar to the Thomson et al. and Esterling lattice statics calculations. It is difficult to assess the quantitative aspects of their results both because of the simplification in the interatomic potential and the constraints against motion transverse to the applied stresses. For example, Weiner and Pear observed supersonic crack velocities at high stress values and A-H found a lattice trapping ratio of $R_T = 3.7$.

On the other hand, Paskin et al., using a long range potential and no artificial constraint on a moderately large sample, obtained some results supporting the Rice-Thomson calculations regarding the brittle and ductile properties of materials. However they too did not assess quantitatively the error contained in the simulation results due to the finite size of the sample.

Motivation for the present calculations is to continue the simulation studies started by Paskin et al. The present study was made on the 2-d triangular lattice interacting via the L-J potential. As the boundary condition of fixed displacement is theoretically advantageous because no external work is done on the sample leading to a much simpler energy analysis, fixed displacement boundary condition was used in most of the studies. Some studies using a fixed load boundary condition have also been conducted in order to understand the behavior of the sample under both types of

boundary conditions. The details of the motivation of the present calculations are summarized below

Summary

In section 4.1 an account has been given why atomistic calculations are of interest. In section 4.2 some details of the hybrid lattice statics model and previous molecular dynamic calculations have been described. Section 4.3 gives an account of the motivation of the present molecular dynamic calculation. The goals of the present calculation are summarized here.

(1) Studying the time evolution of the atomic positions, atomic velocities, forces acting on all the atoms, Young's modulus, Poisson's ratio and all energies (potential,kinetic and surface) to obtain the static, dynamic and most of the thermodynamic properties of the system with and without a crack.

(2) Understanding the mechanical properties of the two-dimen- sional triangular lattice interacting via the L-J potential.

(3) Checking the validity of the continuum expression for the change in elastic energy ($\Delta E_{el}$) upon the introduction of a crack.

(4) Studying the effect of the finite size of the sample on the material properties and the behavior of crack propagation.

(5) Examination of the Griffith theory.

(6) Calculation of the stress profiles arounds the crack tip and comparing them to the Eringen non-local profiles.

(7) Studying the phenomenon of lattice trapping.

(8) Examination of different assumptions which go into the Mott theory and studying the crack propagation under fixed displacement.

(9) Studying the role of the application of an external load on crack propagation. crack propagation under fixed stress.

(10) Constructing a model for the prpagation, under fixed load, of a crack coated with a hard film.

Molecular dynamic technique was used in all the simulations. These simulations do not correspond to any real material. It is believed that studies of such idealized models can still give valuable understanding of fracture before proceeding to more realistic three dimensional models.

# PART I

# HOMOGENOUS MATERIAL

# CHAPTER 5
# PRESENT CALCULATION: STATICS

## 5.1 Molecular Dynamic Technique

As the technique of molecular dynamics has become very well known, no detailed description of it will be given here (for various applications of molecular dynamics see Paskin et al, 1968-1982). Instead some of the limitations of the technique and details pertinent to our static calculations will be discussed here.

The basic limitation of the technique is the small duration in time of events which can be handled by this technique ( $10^{-10}$ sec.). i.e., only those phenomena for which the characteristic times are of this order of magnitude can be studied by this technique.

Another limitation is the small number of atoms which can be handled. This is actually not due to limitations in the technique but due to the constraints imposed by the use of computers to implement the technique. The limitation of computer memory capacity and the high cost of calculations for a large number of atoms, limit one in practice to a reasonably finite number of atoms. This limitation forced us to stay in two dimensions instead of simulating a more realistic three dimensional sample. In many situations a large enough two dimensional model can lead to a clearer and more realistic understanding of the basic principles of a phenomenon than the use of a much smaller three dimensional model. In other words, a finite three dimensional model is not necessarily more realistic than a two dimensional one. The Kanninen et al (1972 ) model is an example of this. Their whole sample is effectively a crack tip and the proximity of the boundaries produces unnecessary complications in the problem. However, the size limitation can cause a serious size dependence in the results of a simulation. This point will be discussed in great detail in sections 5.4, 5.7 and 6.3.

Crack propagation in a crystal was simulated by calculating the motion of atoms in a plane interacting through a pair potential. The atoms were arranged in a triangular array with each atom initially surrounded by six near neighbors (except in the case of surface atoms) as shown in figure 5.1.1. The external forces were applied perpendicular to the upper and lower surfaces, as shown, for the fixed load calculations. The external forces were kept constant throughout any given simulation. For fixed displacement calculations the upper and lower surfaces were pulled apart by a fixed distance and the y coordinates of the surface atoms were kept rigidly fixed throughout any particular simulation. The x coordinates of the surface atoms were allowed to move freely. Several sample sizes were used: our smallest sample consists of 39 rows with 67 atoms in odd rows and 68 atoms in even rows and the largest sample consists of 79 rows with 135 atoms in odd rows and 136 atoms in even rows. These arrangements were chosen to have a symmetry such that the external forces on the sample produce no net torque. The crack was introduced between rows in the sample in such a way that accidental equilibrium could not occur and a row of atoms be left at the center as the crack propagated (as observed by Ashurst and Hoover, 1976). The crack was then always introduced one row off the geometric center of the sample. The surfaces parallel to the applied stress or displacement were free to deform, or change in density, and thus for the non-zero value of Poisson's ratio.

The basic procedure used in the molecular dynamic simulation consisted of solving Newton's equations of motion in a difference form for a finite number of atoms. There are a number of different ways of solving Newton's differential equations of motion:

$$m \frac{d^2 r_i}{dt^2} = F_i \qquad 5.1.1$$

where m is the atomic mass, r is the position of the i-th atom and $F_i$ is the net force acting on the i-th atom by the neighboring atoms $[\sum_{i \neq j} f_i(r_{ij})]$ and also due to the external force, $F_{ext}$, if there is any acting on that atom.

$$F_i = \sum_{i \neq j} f(r_{ij}) + F_{ext} \qquad 5.1.2$$

In these calculations forces between atoms were derived from the Lennard-Jones potential as shown in figure 5.1.2a

$$\phi_{ij} = \epsilon \left[ \left(\frac{d}{r_{ij}}\right)^{12} - 2\left(\frac{d}{r_{ij}}\right)^{6} \right] \qquad 5.1.3$$

where $\epsilon$ is the depth of the potential energy and d is the nearest neighbor distance of the lattice at zero temperature with no applied load. The computer results are expressed in terms of the natural units of the system (m, $\epsilon$ ,d = 1 ). The Verlet central difference method was used to integrate the equations of motion (equation 5.1.1).

$$r_i(t+\delta t) = -r_i(t-\delta t) + 2r_i(t) + \frac{F_i}{m}(\delta t)^2 \qquad 5.1.4$$

In using eq. 5.1.4, the forces were calculated for atoms in the range R = 1.6d (see figure 5.1.2b). Equation 5.1.4 calculates the position of the i-th atom at time t + $\delta$ t from the positions of atoms acting at time t and t - $\delta$ t and the forces at time t. For static calculations a value of $\delta t = .08d\sqrt{m/\epsilon}$ was used throughout. This value was found to conserve energy to one part in $10^6$ in studies on a conservative system with the same lattice. Further reducing the time step resulted in no noticeable differences in the results of the crack simulations. The choice of the central difference method over the generalised predictor-corrector method or the Nordsiek-Gear method was a matter of practicability. The main difference between these methods is in the number of previous positions, or equivalently the number of higher order time derivatives, used to predict the new positions. More memory can be used to obtain a higher precision per time step or can be exchanged for a longer time interval for the same accuracy. The choice of a method depends on the computer and the accounting system (i.e., how it pro rates cost as a function of memory and calculating time and the time required to obtain the results because of the operating priority system). In the CDC 7600 computer at Brookhaven National

Laboratory, it was found that using the Nordsiek-Gear method of order seven, of comparable accuracy to the central difference method and of our choice of $\delta t$, time intervals of 4-6 times as large could be used for the same precision and a cost reduction of about a factor of two resulted for our medium sample simulations. However, the large memory requirement in the Nordsiek-Gear method made the time required to actually obtain data from the computer so long that the method was abandoned and the central difference method was found to be preferable.

In all simulations only the first nearest neighbor interaction was taken into calculations. One important difference in our potential compared to those used in earlier molecular dynamic simulations is that our potential is "long range" in the sense that the atoms behind and near the crack tip, still "feel" the potential even though the bonds at the crack tip have been stretched beyond the distance $d_i$ where there is an inflection in the potential energy versus distance curve and the pairwise interatomic force is a maximum. The range R was chosen to be 1.6d, slightly less than the second nearest neighbor distance $\sqrt{3}d$ but considerably larger than $d_i = (13/7)^{1/6} d = 1.11d$

The crack was introduced into the perfect sample by removing the forces between the atoms forming the crack: the 19-th and 20-th rows of the smallest or the 39-th and 40-th rows of the largest sample. This is the computational analog of inserting a very thin knife near the center of these samples and cutting the bonds between the two adjacent layers. Crack propagation simulations consisted of studying the behavior of the atoms subsequent to the insertion of the knife. If the atoms near the crack tip continuously increased their bond separation and this behavior spreads to neighboring atoms, the crack was said to propagate. If any crack tip separation comes to equilibrium, then the crack did not propagate and the equilibrium process could be studied albeit these are equilibrium

studies of a crack with a knife inserted to maintain the crack. To study the crack healing process the knife could be removed by restoring the forces between the rows of the atoms forming the crack.

The system with a crack under some external loading (stress or displacement) was allowed to come to equilibrium by introducing critical damping either at the same time as the time of the application of the external load or at some time after the load was applied. The damping removes a given amount of the kinetic energy at each time step to expedite the sample reaching its equilibrium state at zero temperature. A variety of damping parameters and damping techniques were examined. The method that was found most efficacious was continuous damping achieved by replacing equation 5.1.4 by

$$r_i(t+\delta t) - r_i(t) = \beta[\, r_i(t) - r_i(t-\delta t)] + \frac{F_i}{m}(\delta t)^2 \qquad 5.1.5$$

with $\beta = .895$, the optimum value found in our simulations for time step $\delta t = .08d(m/\epsilon)^{1/2}$. The smaller the value of $\beta$, the more energy is extracted per step but the slower the average speed of atomic motion and the longer it takes to obtain the equilibrium configuration.

In the static simulations the crack and the damping were introduced simultaneously from the very beginning and then the sample was allowed to evolve in time. Depending on the value of the external stress and displacement the sample could come to equilibrium or the crack could propagate. A number of mechanical and thermodynamical properties were monitored such as: Young's modulus M, the average strain e, Poisson's ratio $\nu$, the total kinetic energy $E_k$, the total potential energy of the system, local atomic positions, local interatomic forces, atomic velocities and the speed of crack propagation. In order to obtain the change in strain energy for crack formation, equilibrium values of the

potential energy are needed to a high precision. Such values were obtained directly in runs that were carried out for a few thousand time steps, in which energy did not vary in one part in $10^6$ over the last 100 time steps. In shorter runs an exponential extrapolation was used to obtain an accuracy in the equilibrium potential energy of about one part in $10^5$.

In the static calculations, obtaining the forces on each atom is a step in the numerical procedures. It is therefore convenient to give the forces on atoms rather than stresses which would involve some arbitrary element of area or length in these two dimensional calculations. For the small changes in length perpendicular to the applied load, the forces and certain stresses are simply related by a dimensional constant (see Appendix A). In order to analyze the present results in a conventional manner, the applied external load and the local forces on specified atoms were monitored. In the figures the forces above the reference row are described as $\sigma^{up}$ and below as $\sigma^{down}$.

About a fifty percent saving in computer time was obtained by using the left-right symmetry of the sample. This requires a special treatment of the atoms near the central vertical symmetry axis. One half of the sample plus two columns of atoms mirrored into the neglected half of the sample were used. The positions of the mirrored columns are found by reflecting the columns of the atoms, adjoining the central column, around the central column. Figure 5.1.3 shows the mirrored columns (m + 1) and (m + 2) by reflecting columns (m - 1) and (m - 2), respectively, about the column m which is the central column of the full sample. Thus, for example, our largest sample of 79 rows with 135 atoms in the odd rows and 136 atoms in the even rows, was simulated by using a sample of 79 rows with 70 atoms in each row, where the last two columns passing through the 69-th and 70-th atoms of the odd rows are the mirror images of the columns passing through the 67-th and 66-th

atoms of the odd rows, respectively, about the column passing through the 68-th atoms of the odd rows. Figure 5.1.4 shows the half of the largest sample used. The bonds and the atoms around the crack tip are designated by $d_{c\pm i}$ and $r_{c\pm i}$ respectively as shown in figure 5.1.5.

## 5.2 Mechanical Properties Of The Two Dimensional Triangular Lattice

Ashurst and Hoover (1976), as well as Esjborn and Jenson (1976) realized that the application of 3-D elasticity results to 2-D leads to some inconsistencies. The conclusion of Esjborn and Jenson is that for 2-D, the elasticity results of 3-D plane stress are correct. Detailed analysis leads to the conclusion that the Lame parameters $\lambda$ and $\mu$ (Born and Huang 1965) are equal for this lattice with a central pair potential interaction. The system is elastically isotropic. In 2-D it is found that

$$M_o = \frac{4\mu(\lambda+\mu)}{\lambda+2\mu} \quad , \quad \nu = \frac{\lambda}{\lambda+2\mu} \qquad 5.2.1$$

where $M_o$ is Young's modulus at small strain and $\nu$ is Poisson's ratio giving

$$M_o = \frac{8}{3}\mu \quad \& \quad \nu = \frac{1}{3} \qquad 5.2.2$$

For the Lennard-Jones potential, this gives

$$\mu = 18\sqrt{3}\ [\epsilon/d^2] \qquad 5.2.3$$

$$M_o = 83.14\ [\epsilon/d^2] \qquad 5.2.4$$

This value of $M_o$ does not take care of the non-linear nature of the potential. Thus, only for small value of stress or strain are these ones expected to be close to the measured values. The results from our simulations are in close agreement with these values.

It is also of interest to calculate the maximum local stress a triangular lattice can sustain in tension. Figure 5.2.1 shows a triangle made of three atoms interacting with each other. The maximum local tensile stress ($\sigma_{max}$) the lattice can withstand in the y direction is

$$\sigma_{max} = 2f_i \cos 30^\circ/d = 4.66\,\epsilon/d^2 \qquad 5.2.5$$

where $f_i$ is the maximum force exerted by the L-J bond at its inflection point ($d_i = (13/7)^{1/6} d = 1.11d$). In this estimate the decrease in the length of the lateral bond (AC)has not been taken into account.

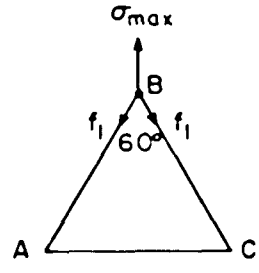


Figure 5.2.1 Undeformed elementary triangle. Calculation of maximum local force acting on crack tip.

In section 5.6 it will be shown how the lateral contraction of the bond (AC) and the local deformation of the crack tip bonds modify by a small factor the value of the maximum local stress the lattice can withstand.

## 5.3 Results

A small sample containing 13 rows with 19 atoms in the odd rows and 20 atoms in the even rows was simulated both under constant external load and constant external displacement to gain some familiarity with the system, i.e., to check the critical damping parameter $\beta$, the time step which could be used to minimize the cost of simulation without loss of the desired accuracy of the results and to get a feeling of the qualitative behavior of a crack under external load and displacement. As the details of these simulations would make this thesis unnecessarily bulky they are not described here. Instead, the basic results obtained from these simulations are given in table 5.3.1. For static calculations the time step $\delta t = .08d\sqrt{m/\epsilon}$ was found to be the largest time step which could be used to conserve energy to one part in $10^6$ (which is our desired accuracy) in studies of a conservative system under fixed external displacement. A damping parameter $\beta = .895$ was found to damp the system critically towards equilibrium for the above time step. Values of $\beta$ larger or smaller than .895 delay the attainment of equilibrium.

The experience gained from simulating a small sample led us to simulate large sample in order to obtain quantitative results. Summary of all the static simulations on various samples are tabulated in tables 5.3.2 through 5.3.8. Tables 5.3.2 through 5.3.4 summarize the results of fixed external loading and tables 5.3.5 through 5.3.8 deal with fixed external displacements.

### Fixed External Load

Fixed external load simulations to study crack statics (equilibrium) are designated by SFL. To cut down the cost by a significant amount of bringing a perfect sample under a fixed

external load to equilibrium the following procedure was adopted. Atoms of each sample were first placed in positions appropriate to the required value of the strain corresponding to the particular value of the external load. Knowledge of Young's modulus and Poisson's ratio corresponding to the particular load is necessary to obtain the value of the strain corresponding to the load. As for example, for run SFL-4 the external load is 1.3. From figure 5.4.4 and 5.4.2 and table 5.4.1, it is seen that the strain and Poisson ratio corresponding to stress 1.3 are .017 and .285 respectively. When equilibrium is reached after application of an external load there will, of course, some lateral contraction which will increase the external stress by a small amount. Thus, after the atoms were placed in positions which are very cloase to their equilibrium ones, it takes very little time to attain equilibrium.

When a sample with a crack is under a fixed small external load the strain in the whole sample, except near the crack region, is almost the same as the strain in the perfect sample under the same external load. In all the simulations (SFL-1 to SFL-3 and SFL-6 to SFL-8) the atoms of the sample, with or withouta crack, were positioned near equilibrium configuration and then allowed to evolve to equilibrium under a load of $\sigma$ = 0.5 and under critical damping $\beta$ = 0.895 from the very beginning. To simulate samples with cracks at the hiegher stresses, the atomic distances between the rows were scaled linearly from that of the samples at the lower stresses and then allowed to evolve under the higher stress along with critical damping For example,runs SFL-10 and SFL-11 were scaled from runs SFL-7 and SFL-8 respectively. Tables 5.3.2 through 5.3.4 summarize the details of the simulations under fixed external load. The quantities of interest for the quantitative evaluation of crack statics as calculated from the simulations, are the following.

$N_R$ , $NTM_{odd}$, $NTM_{even}$, l, $\sigma_{ext}$ , $\sigma_{true}$ , A, e, $E_{el}$, $E_S$, M, $d_c$ , $d_{c-1}$ and $d_{c+1}$ . (see the meaning of the notations in pp. x - xii).

bond is considered to be broken if the bond is longer than the range of the potential, R = 1.6d. It is clear from table 5.3.4 that all the samples are below critical stress level. The detailed evaluation of the results will be made in the following sections.

Fixed External Displacement

Fixed external displacement simulations to study crack statics (equilibrium) are designated by SFD. To cut down the cost of bringing the perfect samples (SFD 1, 3, 8, 12, 14, 17 and 19) to equilibrium the samples were scaled to appropriate external displacement and were allowed to relax with damping until they came to equilibrium as described under fixed external load condition.

All of the simulations with cracks were performed with a crack of half length $l_o$= 9.75d i.e., the number of broken bonds (NBB) in the half sample is 19. Because of the appearance of the crack geometry in the full sample it is found that the relation between l and NBB

$$l = \frac{2NBB+1}{4}$$

is the appropriate average.

Except for the simulations designated (SFD4 through SFD7 and, SFD16) the samples with cracks were brought to equilibrium by simply putting the crack in the perfect samples in equilibrium at the desired strains and letting the samples relax under critical damping until they come to equilibrium with the "knife" present. equilibrium with the "knife" in it.

Runs SFD4 and SFD16 were performed by scaling the samples appropriate to the external displacement, putting the knife and critical damping all together at the same time from the very beginning, and then allow the samples to relax until the attainment of equilibrium.

To obtain the equilibrium for samples with a crack under higher external displacements (e.g. SFD 2, 5, 6, 7, 9, 10, 11, 13, 15, 18, 20 and 23) the samples were scaled from samples with a crack under the lower external displacements as follows.

| RUN | SCALED FROM |
|---|---|
| SFD 2 | SFD 1 |
| 5 | 4 |
| 6 | 5 |
| 7 | 6 |
| 9 | 8 |
| 10 | 9 |
| 11 | 10 |
| 13 | 12 |
| 15 | 14 |
| 18 | 17 |
| 20 | 18 |
| 23 | 20 |

Runs SFD21 and SFD22 were obtained from runs SFD20 and SFD21, respectively, by scaling down from the slightly higher external displacements. Except for run SFD23 all the samples came to equilibrium. Table 5.3.8 shows that the sample in SFD23 started to propagate because the first unbroken bond at the crack tip ($d_{}$) went beyond 1.6d.

Three more simulations were carried out with the samples of runs SFD20, SFD21 and SFD22 by pulling out the knives, i.e., by restoring the bonds across the crack surfaces, to allow relaxation. The crack in run SFD22 heals (closes) by restoring the bonds across the crack surfaces below 1.6d, but the cracks in runs SFD20 and SFD21 are stable.

Tables 5.3.5 through 5.3.7 summarize the detailed results of the simulations under fixed external displacement. The quantities of interest for a quantitative enaluation of crack statics, as calculated from the simulations, are the following.

$N_R$, $NTM_{odd}$, $NTM_{even}$, A, $e_{ext}$, l, $E_{el}$, $E_S$, H, $\sigma_{ave}$, $d_{c-1}$, $d_c$, $d_{c+1}$, $\sigma^L_{c\pm i}$ and $\sigma^U_{c\pm i}$. (see the meaning of the notations used in this thesis in pp. x - xii ).

## 5.4 Detailed Properties Of The 2-D Triangular Lattice Interacting Via The L-J Potential

(a) The Perfect Solid

The elastic constants of a 2-D triangular L-J solid are well known (section 5.2), i.e., the response to an infinitesimal stress ( $\sigma$) or strain ( $e$ ). As the strain is increased the system shows a highly nonlinear behavior, i.e., M is a function of e , arising from the highly nonlinear force of the L-J interaction (Paskin, Som and Dienes 1981). From a uniform tensile strain the modulus (M) can be calculated directly from a balance of forces on one deformed triangular cell as shown in the figure 5.4.1, where the solid triangle is the deformed configuration. If the vertical elongation is $\Delta$ (under an applied load F) then the vertical strain is

$$e = \frac{\Delta}{\sqrt{3}/2} \qquad 5.4.1$$

The undeformed triangle is an equilaterial triangle with each side (d) equal to 1. The deformed sides $r_1$ and $r_2$ can be

$$r_1^2 = \frac{3}{4}(1+e)^2 + \frac{1}{4}(1-\nu e)^2 \qquad 5.4.2$$

$$r_2 = (1-\nu e) \qquad 5.4.3$$

where $\nu$ = Poisson's ratio. The tensile force, F, is given by

$$F = \sqrt{3}\,\frac{1+e}{r_1}\left[\frac{d\phi}{dr}\right]_{r=r_1} \qquad 5.4.4$$

where $\phi(r)$ is the interatomic potential. Since the energy of the triangle is a minimum at equilibrium, $\nu$ can determined by minimizing the energy with respect to $\nu$ , namely

$$2\frac{d\phi}{dr_1}\cdot\frac{dr_1}{d\nu} + \frac{d\phi}{dr_2}\cdot\frac{dr_2}{d\nu} = 0 \qquad 5.4.5$$

with $\frac{dr_2}{d\nu} = -e$ & $\frac{dr_1}{d\nu} = -\frac{1}{4}(1-\nu e)\frac{e}{r_1}$ 5.4.6

Young's modulus M can be written as

$$M = \frac{F}{e(1-\nu e)} \qquad 5.4.7$$

Using the L-J potential equation 5.4.5 can be reduced to

$$e(1-\nu e)\left(\frac{1}{r_1^{14}} - \frac{1}{r_1^{8}}\right) + 2\left(\frac{1}{r_2^{13}} - \frac{1}{r_2^{7}}\right) = 0 \qquad 5.4.8$$

For a particular value of the strain (e) this equation was solved for by an iterative process with an error in the sixth figure. Values of Poisson's ratio ( $\nu$ ) corresponding to different values of the strain (e) and also the corresponding values of Young's modulus (M) and of the stress ( $\sigma$ ) is listed in table 5.4.1. Three graphs showing the variations of $\nu$ , M and $\sigma$ against a wide range of e are shown in figure 5.4.2 through 5.4.4.

A series of computer calculations was performed over a range of applied strains and sample sizes (section 5.3; runs SFD1, 12, 14, 17 and 19). The data for M are shown in figure 5.4.5 together with the theoretical modulus (solid line) calculated by the above equations. The excellent agreement of the theory and the computer calculations, and the observation of no size dependence in the modulus over a factor of four in the sample area, show that the strain dependence of the modulus is understood in a fundamental way for this nonlinear solid. Results from fixed load static simulations are also in good agreement with figure 5.4.5.

In the region of interest in subsequent calculations the modulus-strain dependence is accurately given by the linear relation of figure 5.4.5, namely

$$M = M_0 - \eta e \qquad 5.4.9$$

where $M_0$ = 83.14 and $\eta$ = 414

(b) The 2-D Solid Containing a Crack

When a crack is introduced into the sample, with a fixed external displacement, Young's modulus is reduced. The reduction in modulus occurs because the introduction of a crack, at fixed displacement, reduces the strain energy of the system. As the

effective modulus is related to the stored elastic energy, a reduction in modulus results. Data obtained from static simulations SFD2, SFD9 and SFD20 (under the same strain = 0.029) are used to obtain a plot of the variation of the modulus with the area of the different samples as shown in figure 5.4.7. The linearity in the variation of (1/modulus) vs. (1/area) and the small percentage difference of (1/M') for the large sample and that for infinite sample (extrapolated) confirms that the large sample used in the simulation ( $N_R$ = 79, $NTI_{odd}$ = 135) would give results very close to the results given by the infinite sample. The size dependence of M for a sample with a crack may be analyzed by a procedure analogous to that given by Berry (1960) (see section 3.1) for a linear elastic continuum.

The system under consideration is nonlinear in the region of interest and, therefore, Berry's procedure nees to be modified. The following scheme was desired for describing and understanding the basic mechanical properties of the sytem. From figure 5.4.5 one can write, for a sample with a crack

$$M' = M_0' - \eta' e \qquad 5.4.10$$

Let a perfect sample of area A be strained under a fixed external displacement e and let $\sigma$ and M be the average external stress and effective modulus at equilibrium under the above strain. If the sample with a crack in the center is under the same external displacement the average external stress and the effective modulus would be somewhat lower at equilibrium. Let us assume that they are $\sigma'$ and M' respectively, and the plot of stress vs. strain would look like figure 5.4.6.

The elastic stored energy ($E_{el}$) of the perfect sample can be written as

$$E_{el} = A\int \sigma \cdot de = A\int (M_0 e - \eta e^2)de$$

$$= \frac{Ae^2}{2}\left(M_0 - \frac{2}{3}\eta e\right) \qquad 5.4.11$$

Similarly for a sample with a crack of length $2\ell$

$$E_{e\ell} = A\int \sigma' de = A\int (M_o' e - \eta' e^2) de$$

$$= \frac{Ae^2}{2}\left(M_o' - \frac{2}{3}\eta' e\right) \qquad 5.4.12$$

Making a simplifying assumption that the nonlinearity of the modulus is the same with and without a crack, $\eta = \eta'$, one can write the difference in the stored energy with and without a crack as

$$\Delta E_{e\ell} = \frac{Ae^2}{2}\left[(M_o' - M_o) - \frac{2}{3}(\eta - \eta')e^2\right]$$

$$= \frac{Ae^2}{2}(M_o' - M_o) \qquad 5.4\ 13$$

To evaluate M', however, a theoretical estimate of $\Delta E_{e\ell}$ is needed. As the exact form of the strain energy of a crack in a nonlinear elastic solid is not known, it was assumed that it is of the usual form with the linear modulus M replaced by the effective nonlinear modulus M', namely

$$\Delta E_{e\ell} = -\pi \ell^2 \sigma^2 / M'$$

$$= \pi \ell^2 e^2 M' \qquad 5.4.14$$

combining equns. 5.4.13 and 5.4.14 and since $(M'_o - M_o) = (M' - M)$ one can write

$$-\pi \ell^2 e^2 M' = \frac{Ae^2}{2}(M' - M) \qquad 5.4.15$$

which gives

$$M' = \frac{M}{1 + \frac{2\pi\ell^2}{A}} \qquad 5.4.16$$

This is similar to the form obtained by Berry (1960) with the linear modulus $M_o$ replaced by M. According to these results (1/M') should be a linear function of (1/A), which is indeed the behavior of the computer calculation as shown in figure 5.4.7. The behavior of the modulus as a function of sample area is in excellent agreement with equation 5.4.16.

The size dependence of the strain energy difference is, within the same approximation, given by

$$\Delta E_{el} = -\pi \ell^2 e^2 M' \qquad 5.4.17$$

and substitution of M' from equation 5.4.16 gives

$$\frac{1}{\Delta E_{el}} = \frac{1 + 2\pi \ell^2/A}{\pi \ell^2 e^2 M} \qquad 5.4\ 18$$

Thus $(1/\Delta E_{el})$ is also expected to be linear in (1/A). As indicated in figure 5.4.7 the strain energy response also shows the correct functional dependence, but the slope is larger than calculated from equn. 5.4.18. On the basis of this functional dependence the extrapolation to infinite size $(1/A \rightarrow 0)$ can be carried out. Using this procedure, an infinite sample strain energy $(\Delta E_{el}^{\infty})$ of $21.3\epsilon$ is obtained, which is about 12% larger than that for the largest sample $(19\epsilon)$ in the computer simulations.

Thus, the mechanical properties of the triangular 2-D L-J solid are well understood, both in the presence and absence of a crack. It is to be noted for the subsequent discussion in the following sections and chapters that sample size effects are small for the largest sample used in our simulations.

## 5.5 Discussion Of The Griffith Theory

The Griffith theory was tested for the case of fixed external displacement. The basic idea behind the Griffith approach is based on thermodynamic principle whose validity is unquestionable. But the assumptions made to arrive at the quantitative criterion for the equilibrium condition for fracture are not quite correct. Griffith used the expression of the change in strain energy ($\Delta E_{el}$) and surface energy ( E ) due to the introduction of crack of length 2l from linear elasticity theory.

$$\delta \Delta E_{el} = \frac{-2\pi\sigma^2 l \delta l}{M_o} \qquad 1.2.4$$

$$\delta E_s = 4\gamma l \delta l \qquad 1.2.5$$

If there is no plasticity at the crack tip, then the second equation is correct. But the expression for $\Delta E_{el}$ deserves checking. In Chapter 5.4 it was notedd that (for a finite sample)

$$\Delta E_{el} = \frac{-\pi\sigma^2 l^2}{M'} = -\pi e^2 l^2 M' \qquad 5.4.14$$

is in better agreement with our simulation than the linear elastic expression used by Griffith.

Using equation 5.4.14 in the Griffith condition of equilibrium (cf. equation 1.2.2) under fixed external displacement the following can be written

$$\frac{\delta}{\delta l}\left(-\pi l^2 e^2 M' + 4 l \gamma\right) = 0 \qquad 5.5.1$$

where, $$M' = \frac{M}{1 + \frac{2\pi l^2}{A}} \qquad 5.4.16$$

or, $$2\pi l M' e^2 \left(1 - \frac{2\pi l^2/A}{1 + 2\pi l^2/A}\right) = 4\gamma$$

$$\text{or,} \quad e = \left(\frac{2\gamma}{\pi M' \ell}\right)^{1/2} \left(1 + \frac{2\pi \ell^2}{A}\right)^{1/2} \qquad 5.5.2$$

For an infinite sample equation 5.5.2 reduces to

$$e = \left(\frac{2\gamma}{\pi M \ell}\right)^{1/2} \qquad 5.5.3$$

whereas the Griffith condition under constant strain (cf. equation 1.2.7) is

$$e = \left(\frac{2\gamma}{\pi M_0 \ell}\right)^{1/2} \qquad 5.5.4$$

Runs SFD7, SFD11 and SFD20 (cf. section 5.3, tables 5.3.5 and 5.3.6) and DFD1 and DFD3 (cf. section 6.2., table 6.2.1) are found suitable to compare the Griffith condition with our present calculations. In all these runs, samples of different sizes with a crack of the same length were brought to equilibrium at strains a few percent below the actual critical strain.

The Griffith condition (equation 5.5.4) gives a critical value of e = .028 using $\gamma = 1$, $l = 9.75$ and $M_0 = 83.14$. This value of the critical strain is true for an infinite sample. Our simulation result for the largest sample is .029. It is seen that the smaller the sample (cf. Table 5.5.1 - Column 2) the higher the critical strain. This is exactly what is expected. The smaller the sample the narrower is the crack under fixed displacement. According to our simulation, unless the bond near the crack tip extends beyond 1.6d, the bond cannot break. Thus, for smaller samples higher strains are needed to allow the crack to grow wide enough so that the crack tip bonds can break. Using the value of M' for different runs the critical strains were calculated from equation 5.5.2 and are shown in table 5.5.1 (Column 4).

Comparing these values with the values used in the simulation, it is found that equation 5.5.2 gives better results for smaller samples. At this point, it is necessary to recollect that the change in the strain energy ( $\Delta E_{el}$ ) due to the crack for the largest sample is 12% off from the value for an infinite sample. Thus, our expression for the critical strain is not totally correct, but it does describe quite well how the finite sample size modifies the critical strain.

## 5.6 Discussion Of The Eringen Theory

In section 1.4 it was shown how Eringen removed the stress singularity at the crack tip using non-local elasticity theory. Here a comparison between the Eringen stress profile and the stress profile obtained by molecular dynamic simulation will be made. Run SFD20 (cf. tables 5.3.5 through 5.3.8) is best suited for this comparison. Before making this comparison, it is necessary discuss the stress profile of a finite sample under constant strain.

Under fixed displacement the stresses on the upper and lower surfaces of a finite sample are not uniform. The stress near the center is somewhat lower than the stress elsewhere as shown in figure 5.6.1 Thus, there is an ambiguity in the definition of the stress to be used to calculate the stress concentration factor (F).

If the average stress over the whole sample (L) = $\sigma_L$
and if " " " " " crack length 2l = $\sigma_{2l}$
and if " " " for the uncracked sample = $\sigma_{avg}$

Then $\sigma_L(L) = \sigma_{2l}(2l) + \sigma_{avg}(L - 2l)$

or,
$$\sigma_{2l} = \frac{\sigma_L(L) - \sigma_{avg}(L - 2l)}{2l} \qquad 5.6.1$$

Assuming $\sigma_{2l}$ is the effective average stress acting on the surface just above the crack to produce the maximum local stress at the crack tip, the stress concentration factor (F) can be calculated as

$$F = \frac{\sigma_{max}}{\sigma_{2l}} \qquad 5.6.2$$

Effectively this stress concentration is for an infinite sample, since for an infinite sample $\sigma_L = \sigma_{2l} = \sigma_{avg}$. In run SFD20 a sample of length, L= 135 and a crack of length, 2l = 19.5 was used and $\sigma_{avg}$ and $\sigma_L$ were found to be 2.003 and 1.894 respectively, and from

equation 5.6.1 $\sigma_{2\ell} = 1.248$. The maximum local stress ($\sigma_{max}$) was found to occur on atom ( $r_{c-2}^{U}$ ) (at a distance 2d in front of the original crack tip): $\sigma_{max} = 4.557$. Thus, the stress concentration factor F is given by

$$F = \frac{4.557}{1.248} = 3.65$$

Another important point to consider, before comparing the stress profiles is the proper definition of the crack length. To define a crack length equivalent to the Eringen continuum we need to consider the displacements of the atoms on the central two rows (figure 5.6.2). It is seen that, although not a single crack tip bond broke under the applied strain, the crack tip moved by 2d. Originally, the crack length (2l) was 19.5d. Now under the applied strain the crack length is seen to be somewhere between 19.5d to 23.5d. The stress concentration factor calculated from the Eringen theory depends on the length of the crack

$$F_{Eringen} = 0.73\sqrt{\frac{2\ell}{d}} \qquad 1.4.12$$

Thus, using a value of 2l/d = 21.5 $\pm$ 2

$$F_{Eringen} = 3.38 \pm 0.16$$

The stress profiles for run SFD20 and the Eringen stress profile for 2l/d = 21.5 are plotted in figure 5.6.6. The values of F are in good agreement though the width of the profile from the molecular dynamic calculation is somewhat larger than that of the Eringen profile. This difference may be accounted for by the use of the external stress as $\sigma_{2\ell} = 1.248$ instead of the actual stress acting on the external surface above the front region of the crack tip. Since the molecular dynamic simulation is limited to a finite sample, no further attempt was made to match the stress profile obtained from the simulation for a finite sample to that obtained by Eringen for an infinite sample. Nonetheless, the above discussion may be

summarized by saying that the Eringen non-local theory is a definite improvement over the usual continuum result which gives a stress singularity at the crack tip.

Some Stress Profiles

The Eringen stress profile shows the stress around the crack tip only when an infinite sample is under critical loading. It would be interesting to observe how the stress profiles around the crack tip region change at different external loadings below the critical value for a particular sample with a given crack length, and also for some external loadings on samples of different sizes (crack length remaining constant).

Figure 5.6.4 shows the stress profiles around the crack tip under fixed external displacement (strain = .029). Three different samples were used in the simulations (Runs SFD2, 9 and 20; tables 5.3.5 through 5.3.8).

Figure 5.6.2 shows the displacement of the atoms on the two central rows of the same three samples. It is clear that the smaller the sample the narrower is the crack and as the width (number of rows) of the sample increases not only the crack becomes wider but the crack also moves forward by stretching a few crack tip bonds, even though no bonds break and the crack is in equilibrium under the external displacement. Figure 5.6.4 also confirms this. The maximum in the stress profile of $row_c^U$ for the largest sample (run SFD 20) is seen to be moved by 2d from the orininal crack tip. The stress profile of $row_c^L$ is blunted which means that the crack tip bonds are stretched and the site of maximum force moved forward. Table 5.3.8 shows that the site of maximum force is shared by three atoms of $row_c^L$ in front of the crack tip.

For the smaller sample (run SFD 2), on the other hand, the site of maximum force is at the crack tip ($r_c^L$ ). As the bonds at the crack tip are not stretched as much as in the case of the large sample (run SFD 20), the site of maximum force is on the crack tip atom $r_c^L$ on the lower surface of the crack. The force on $row_c^U$ is 3.904, 1.5% below the maximum force on $row_c^L$ . This difference is due to the assymetry in the shape of the crack.

Comparing runs SFD 2 and SFD 9 it is clear that as one increases the number of rows in the sample, the crack becomes wider. In this case the displacement of the atoms at the crack tip on $row_c^L$ are larger (figure 5.6.2) and some stress is relieved. The site of maximum stress goes to the crack tip atom $r_{c-1}^U$ .

Figures 5.6.3 and 5.6.5 show the displacement and the stress field of the atoms of the central two rows of the same sample ($N_R$ = 79 and $NTM_{odd}$ = 135) under three external displacements. Figure 5.6.3 shows that, as the external strain is increased, the crack becomes wider and moves forward as the crack tip bonds are stretched. Because of the geometry of the crack tip, when the external strain is increased from .010 to .020 the displacements of the crack tip atoms on $row_c^U$ are comparetively larger than those of the crack tip atoms on $row_c^L$ . Thus the site of maximum force is located on atom $r_c^L$ on $row_c^L$ . Similarly, when the external displacement is increased from .020 to .029, the crack becomes wider again by stretched a few more bonds. This time the displacements of the crack tip atoms on $row_c^L$ are comparatively larger than those of the crack tip atoms on $row_c^U$ and the site of maximum force moves to atom $r_{c-2}^U$ on $row_c^U$ .

Thus, in summing up, as the number of rows is increased keeping the external displacement same, the crack becomes wider, the crack tip bonds start to stretch; the stretching of the bonds is achieved by a relatively larger displacements of the crack tip atoms

of one of the two rows, relieving the forces on those atoms and increasing the forces on crack tip atoms of the other row until the force on some atom is close to the theoretical $\sigma_{max}$( = 4.66$\epsilon$/d). If the sample is increased in size still further, the same process continues. But this time the site of the maximum force moves forward and to an atom of the other row and so on. Almost the same process is observed when the external displacement is increased keeping the size of the sample the same. But this time, as the external strain is increased above the critical strain, the stretched crack tip bonds start to break. This dynamic phenomenon will be described in detail in section 6.3.

Table 5.3.8 shows that the value of the maximum force never goes above 4.557 $\epsilon$/d compared to a value of 4.66 $\epsilon$/d as calculated in section 5.2 by disregarding the lateral contraction of the horizontal bonds. Thus, in our fixed external displacement runs, because of the horizontal deformation at the crack tip, the maximum force a crack tip can withstand is around 4.56 $\epsilon$/d.

## 5.7 Lattice Trapping

In section 2.2 the phenomenon of lattice trapping as first proposed by Thomson et al was discussed. The believed that lattice trapping is a consequence of the discrete nature of the lattice. To study lattice trapping, our largest sample (Runs SFD18 through SFD23 and Tables 5.3.5 through 5.3.7) was subjected to a series of external displacements until the system either came to equilibrium or the crack propagated by further bond breakage, or the crack healed upon restoration of the cut bonds. The results are shown in table 5.7.1.

As shown in the table, the crack was found to be stable at two strains 0.9% apart. At these equilibrium positions, the interatomic distances of the atoms across the crack surface exceeded 1.6d, the effective range of the potential, while the unbroken bond was stretched to less than 1.6d. Restoring the interaction, therefore, did not affect the equilibrium. Upon lowering the strain by 0.9%, $d_{c+1}$ became less than 1.6d and the system healed (with and without damping) upon restoration of the interactions across the crack. Conversely, upon increasing the strain by 1.7% the unbroken bond was stretched beyond 1.6d and the crack propagated by bond breakage (with and without damping). No attempt was made to obtain closer limits on the strain range of the stable region. It is concluded from these data that the range of lattice trapping is larger than 1% and less than 3%.

As already pointed out (cf. section 5.4), the strain energy difference in the largest sample differs from that in the infinite sample by only about 12% and, as the critical strain is approximately proportional to the square root of the energy, the estimate of any critical strain ratio is believed to be correct to better than 10%. Thus, the size effect would shift the critical

strains (an increase with decreasing sample size for a given critical energy) but leave the range in critical strains, and hence lattice trapping, essentially unchanged. A study of lattice trapping at half the size (runs SFD9 through SFD11) confirmed this analysis. Thus, size effects in this study are quite small and it is concluded that lattice trapping is less than 3% for potentials of the form used.

As discussed in section 2.2, Thomson et al obtained a value of the lattice trapping ratio $R_T = 2.14$ as compared to our ratio of 1.03 (at most). We checked into the calculation they did and found that the value of is correct but, from equn. 2.2.5 $R_T$ comes out to be 1.15 instead of 2.14 indicating small lattice trapping. Gohar (1979) did the same calculations using molecular dynamic simulation data and obtained a value of $R_T = 1.02$ in good agreement with our simulation results. In subsequent lattice statics calculations, incorporating bond snapping features, Thomson et al (1973) obtained larger lattice trapping ratios. For physical explanation of lattice trapping, they suggested an analogy to the Peierl's stress for dislocation.

This does not seem to be justified for continuous non-truncated interatomic potentials. If the stress that is applied is less than critical, indeed there will be a stress barrier against the crack propagation. However, there will be no stress opposing the crack healing. Any infinitesimal motion to close the crack will result in a lowering of the free energy; hence there will be no Peierl's stress to overcome healing. If the stress is slowly increased and the crack does not propagate it should heal. This should be the case until the maximum or critical stress is aplied; at this point a slight increase in stress should result in crack propagation. This is essentially the Griffith picture of fracture. Of course, if a material is not entirely brittle and some deformation can take place, then it is possible that the energy is approximately the same for a range of stresses at which a crack

neither propagates nor heals. This, however, does not seem to be the origin of the lattice trapping calculated by Thomson et al., particularly since even in their two-dimensional calculation, all motion is essentially transverse to the crack surface (i.e. Poisson's ratio is kept at zero). Hence, the Peierls-like barrier does not seem to be a simple consequence of the lattice periodicity independent of the potential and is not a universal phenomenon which yields lattice trapping as a fundamental property of a periodic array of atoms.

Credibility of The Present Result

There are major advangtages to the molecular dynamic simulation of the equilibrium properties of a crack. A realistic semi-empirical interatomic potential, in this case the Lennard-Jones, was used. The model system was completely unconstrained except for the correct boundary conditions. With appropriate attention to the required accuracy in the simulation, the results are exact within the framework of the model.

The major disadvantage of the molecular dynamic technique is the restriction of the system to a finite number of atoms. The basic question is, therefore, how large is large enough to simulate in a relevant way the properties of the corresponding infinite system. In the present case it was shown (section 5.4) that the properties of the finite system can be described and understood quantitatively on the basis of simple balance of forces and energies. Thus, extrapolation to infinite size became feasible and the error in using about 10,000 atoms could be estimated quantitatively. As already indicated, the error turned out to be small and did not affect in any significant way the negligible lattice trapping determined for this model. It should be noted that the finite search range of 1.6d used in practice renders the L-J potential a bond snapping potential but with a small snapping range.

The importance of the "cut off" may be illustrated in a simple way. In the sketch of Fig. 5.7.1 the extensions of the unbroken bond, $d_c$, and the first broken bond, $d_{c+1}$, are shown as a function of the applied strain, e. Let $r_{c1}$ and $r_{c2}$ be two cut-off bond distances, i.e., the force goes to zero at $r > r_c$. $e_p$ and $e_h$ are the applied strains for propagation and healing respectively. At $e > e_p$ the bond $d_c$ becomes "broken", while at $e < e_h$ the bond $d_{c+1}$ heals by coming within the range of the potential. In the simple linear sketch of figure 5.7.1 $e_{p1} - e_{h1} = e_{p2} - e_{h2}$. However, the ratio $e_p/e_h$ clearly increases as $r_c$ is decreased, and vice versa. Thus, a continuous potential, for which $r_c \to \infty$, would be expected to show no lattice trapping.

Finally it should be mentioned that all molecular dynamic simulations so far have been restricted to two dimensions as even modern computers cannot handle a three-dimensional atomic lattice of any sensible size.

## 5.8 Summary

In this chapter the mechanical properties of the 2-D system with and without a crack were studied extensively. Because this chapter is rather long it seems appropriate to summarize the results here.

Mechanical Properties Of The 2 Dimensional Triangular Lattice Interacting Via The L-J Potential

1) Young's modulus ($M_o$) of a perfect sample under infinitesimal stress or strain was found to be 83.14. This value agrees with linear elasticity theory.

2) Poisson's ratio ($\nu$) was found to be 1/3 which also agrees with linear elasticity theory.

3) The maximum local stress a triangular lattice can withstand (provided there is no lateral contraction) was calculated and found to be $4.66\,\epsilon/d$. Simulating cracks of vaous lengths under fixed external load and fixed external displacement it was always found that the crack tip stress above which the crack starts to propagte is a little less than $4.66\epsilon/d$. This slight deviation was attributed to the local deformation near crack tip.

4) By minimizing the energy of the perfect sample under fixed external displacement Young's Modulus, Poisson's ratio and the corresponding stress were calculated theoretically. Simulating perfect samples of different sizes under different external displacements the theoretical result was confirmed. It was found that in the non-linear region of interest, the modulus could be expressed in terms of strain as

$$M = M_o - \eta e \qquad 5.4.9$$

where, $M_o$ = 83.14 and $\eta$ = 414

The exact relationship among M, $\nu$, $\sigma$ and e are shown in figures 5.4.2 through 5.4.4.

5) When a crack is introduced a similar relation between Young's modulus (M') of the cracked sample and the corresponding strain (e) was observed

$$M' = M_o' - \eta' e \qquad 5.4.10$$

where $M'_o$ is Young's modulus of the cracked sample at infinitesimal strain and $\eta'$ is approximately equal to $\eta$.

6) The non-linear elastic strain energy was calculated from the above stress-strain relation for both the perfect and the cracked sample, and the change in elastic energy of the system due to the introduction of a crack was found to be

$$\Delta E_{el} = \frac{Ae^2}{2}(M' - M) \qquad 5.4.13$$

Replacing the linear modulus M by the non-linear modulus M' in the usual expression for $\Delta E_{el}$ for the linear regime and equating that expression with the above expression, a relation between M and M' was obtained as

$$M' = \frac{M}{1 + 2\pi l^2/A} \qquad 5.4.16$$

This theoretical expression is very similar to that given by Berry (1960) except that $M_o$ is replaced by M in our expression. The above behavior of the modulus (M') as a function of sample area is in excellent agreement (fig. 5.4.6) with our computer simulation result.

On the other hand, when the expression for

$$\Delta E_{el} = -\pi l^2 e^2 M' = \frac{-\pi l^2 e^2 M}{1 + 2\pi l^2/A} \qquad 5.4.14$$

was compared to the computer simulation results (fig. 5.4.8), the correct functional dependence was observed but the slope of the theoretical line ($1/\Delta E_{el}$) against ($1/A$) was found to be smaller than that obtained from the simulation.

7) On the basis of the above functional dependence of ($1/\Delta E_{el}$) with ($1/A$), an extrapolation to infinite sample size ($1/A \rightarrow 0$) was carried out. It was found that the infinite sample strain energy change ($\Delta E_{el}^{\infty}$) is only 12% larger than that for our largest sample.

The Griffith Theory

The Griffith Theory was tested for the case of fixed external displacement. For an infinite sample within the linear elasticity regime, the Griffith critical strain is given by

$$e_{Griffith} = \left(\frac{2\gamma}{\pi M_0 \ell}\right)^{1/2} \qquad 5.5.4$$

Samples of different sizes with a crack of the same size were simulated. It was found that the smaller the sample, the narrower is the crack under fixed displacement and the larger is the critical strain. The expression for critical strain based on the non-linear expression for the elastic energy change for finite size is given by

$$e_{critical} = \left(\frac{2\gamma}{\pi M \ell}\right)^{1/2} \left(1 + \frac{2\pi\ell^2}{A}\right)^{1/2} \qquad 5.5.2$$

This expression agrees better with the simulation results for smaller samples than that for larger samples. This must be because the expression of $\Delta E_{el}$ is not completely correct, nevertheless, the above expression for the critical strain gives a reasonable description of how the finite sample size modifies the critical strain.

Stress Profiles And The Eringen Theory

The Eringen stress profiles and the stress profiles obtained from the molecular dynamic simulation were compared. Making correction for the finite sample used in the simulation it was found that the stress concentration obtained from the simulation is in good agreement with the value given by Eringen. The stress profiles are also of same shape (figure 5.6.6) although the width of the profile obtained from the simulation is somewhat larger than that of the Eringen profile, a consequence of the finite sample used in the simulation. It was concluded that the Eringen non-local elasticity theory is a definite improvement over the usual continuum theory and is successful in removing the stress singularity at the crack tip in a natural way.

Stress profiles were also obtained at subcritical external strains for finite samples of different sizes. For a sample of particular size, if the external strain is increased from a low value towards the critical value it was observed that:

i) the crack grows wider.
ii) the crack tip bonds stretch.
iii) the site of maximum force moves from one crack tip atom on one of the two crack surfaces to another atom of the other surface in front of the crack tip. This is a repetitive process.
iv) the maximumforce never goes beyond $4.56\epsilon/d$ which is slightly below the theoratical value $4.66\epsilon/d$ calculated in section 5.2 where the lateral contraction of the horizontal bonds at the crack tip were neglected.

Similar phenomena were observed when the number of rows of a sample was increased keeping the external strain the same.

Lattice Trapping

Using a long range potential (L-J) it was shown that, for the largest sample in our simulation, lattice trapping is negligible ($1.01 < R_T < 1.03$). It was also shown that an infinite sample would be expected to show no lattice trapping. It was concluded that the large lattice trapping ratios obtained by several authors are due to the use of short range potentials and are not a consequence of the periodicity of the lattice.

# CHAPTER 6
# PRESENT CALCULATION: DYNAMICS

## 6.1 Molecular Dynamic Technique

The molecular dynamic technique has been described in connection with the static calculation in section 5.1. The same triangular array of atoms was used for dynamic calculations both under constant load and constant displacement. For constant load the samples were kept free to deform at the surfaces in order to allow dislocations to migrate and relieve strains by producing surface jogs (if the thermodynamics of the system required this configuration).

Dynamical calculations were made without any damping and, therefore, $\beta$ in equation 5.1.5 was taken as 1. The time step $\delta t$ was taken as $0.02d(m/\epsilon)^{1/2}$ for fixed displacement studies and $0.01d(m/\epsilon)^{1/2}$ for fixed load studies. These values were found to conserve energy to one part in $10^5$ and one part in $10^6$, respectively, in studies on a conservative system using the same lattice.

In order to allow for local structural changes or deformations the computer program was periodically updated to include the appropriate neighboring atoms in range R. A table of the atoms in this range was updated every 20 steps. The value of R was set to 1.6d for all simulations.

Crack propagation simulations were performed in the post loading mode. First, a sample was brought to equilibrium, with the knife inserted, by the application of critical damping as explained in the static simulation (section 5.1). The external load or displacement was then increased from the equilibrium value by a small increament and the system was allowed to relax without any damping, until the crack started to propagate by breaking the bonds in front of the crack, i. e., the crack tip bond stretched beyond 1.6d.

There is a procedural correction necessary on the work done in the simulations which arises from forces being effectively truncated beyond a range R. This is equivalent to a step function in the interaction energy (see figure 5.1.2a) which is equivalent to a $\delta$-function force (see figure 5.1.2b) which was neglected in our computations. This does not affect our equations of motion but does result in the necessity of making an energy correction of $|\phi(R)|$ whenever an interatomic distance is beyond the range R. Further, this range in practice was slightly larger than R because of our table update procedure. In our calculations a table of neighbors was formed initially and updated subsequently every 20 steps. The table includes all pairs of atoms whose interatomic distance is less than or equal to R at the time of update. If the crack is propagating or there is dislocation motion, an atom whose range is initially less than or equal to R in the table, may move beyond the range before the next table update. Forces are calculated for all atoms in the table. As the computer time necessary to find the atoms in a range R is long for a large sample, this procedure allowed us to perform the search once every 20 steps and hence minimize computational cost. Examining our simulations, it was found that the forces are calculated to an effective range $r_{max} = R + .04d$. The energy correction to the work done on the sample at $r_{max}$ is about $0.1\epsilon$ and this correction was included in all calculations, whenever necessary.

The separation of potential energy into elastic strain energy for crack formation plus a crack surface energy is somewhat arbitrary. While it is clear that the energy to break a bond for a perfect sample is $\epsilon$ and the surface energy per unit length (2-D) of a perfect sample is $2\epsilon/d$, appropriate for a cracked sample is less clear. Atoms near a crack tip may extend as much as about 10% of d. Should all the resulting changes in potential energy of a crack with this extension be included in the crack formation energy or should the crack be treated as having extended a fraction of an interatomic

distance and thus some fraction of $\epsilon$ be treated as crack surface energy. No attempt was made to rationalize this effect of crack extension into our analysis. Neither was any correction made for the crack surface energy because the surface energy might be calculated from the strained positions rather than from the perfect lattice configuration. The crack surface energy per unit length (2-D) was taken as $2\epsilon/d$ and the energy of $\epsilon$ was associated with each bond separation larger than R. For the initial crack formation it was taken as $\epsilon$ per bond broken by the "insertion of the knife."

In the dynamic calculations, obtaining the forces on each atom is a step in the numerical procedures. It is therefore convenient to give the forces on atoms rather than stresses which would involve some arbitrary element of area or length in these two-dimensional calculations. For the small changes in length perpendicular to the applied load, the forces and certain stresses are simply related by a dimensional constant (see Appendix) In order to analyse the present results in a conventional manner, the applied external atomic forces and the local forces on specified atoms were monitored. In the figures the forces above the reference row are described as sigma up and below as sigma down. These motions may be unequal when a dislocation or a crack is in motion.

## 6.2 Results

### External Fixed Displacement

Four samples of different sizes with cracks of the same length (l =. 9.75d) were used to study crack propagation under fixed displacement. The runs are designated by DFD. Details of these runs can be found in Tables 6.2.1 through 6.2.3. Samples of increasing size have both increasing number of rows and increasing number of atoms in each row. The samples were first brought to equilibrium under a fixed strain (e) just below the critical strain. The external strains were then increased to ( $e+\Delta e$ ) by approximately 1% by scaling the sample to that strain from the samples in equilibrium and were allowed to relax without damping the crack was found to propagate. In all situations cracks were found to propagate by breaking bonds at the crack tips. As these dynamic simultions are very slow (because no damping was used) compared to static simulations, it is very costly to allow the system to break a large number of bonds. Besides, as the crack tips approaches boundary surfaces the simulation results are not very reliable because of surface effects. For these reasons cracks were limited to expand by approximately 45 bonds ($NBB_{Tot}$) in the half sample.

For each sample, right after the external strain was increased to just above critical value, all the energies (surface, $E_s$ ; elastic, $E_{el}$ and kinetic, $E_k$) of the sample and Young's modulus, M', were recorded at different time steps.

The number of broken bonds is plotted against the time step for each sample in figure 6.1.2. Curves 1 through 5 correspond to runs DFD 1 through DFD 5. Crack velocities at different time steps were calculated from the slope of the curve at the corresponding time steps. Crack velocities in terms of numbers of bonds

broken/time step are plotted against the time step and are shown in figure 6.2.2. Breaking of one bond corresponds to a increase in crack length by d/2. As plotting of crack velocities ($v_c$) in units of the longitudinal sound velocity ($V_L$) of the material versus crack half length (l) is a usual practice, the crack velocities are plotted against l in figure 6.2.3.

The elastic response of the material during propagation is illustrated in figures 6.2.4 and 6.2.5. Figure 6.2.4 shows the variation of the effective non-linear elastic mudulus 1/M' with $l^2$. It is observed that their relationship is almost linear. Figure 6.2.5 shows the plot of the change in the elastic energy $\Delta E_{el}$ due to the crack versus $l^2M'$ as the crack propagates. This plot is also found to be linear within the simulation error.

To study the stress profiles around the crack tip of a moving crack the sample of run DFD 5 (the largest sample in equilibrium with fixed external strain $e_\infty$ = .029 ) was scaled to an external strain e = .0295 and allowed to propagate in a controlled fashion by applying critical damping from the very beginning.

The forces acting on atoms around the crack tip on two central rows (rows 39 and 40) were noted every 20 steps. The results can be found in table 6.2.3 and the stresses on the atoms of the two central rows are plotted against atom positions in figures 6.2.6 and 6.2.7

External Fixed Load

Fixed external load simulations designed to study the dynamics of crack propagation are designated by DFL. Dynamic simulations under fixed load were confined to only one sample containing 39 rows with 135 atoms in odd rows and 136 atoms in even rows. The sample was brought to equilibrium with a crack of length 39.5d (78 broken

bonds in full sample) under a fixed external load $0.6\epsilon/d$ . The sample came to equilibrium at step 15780. The length of the 1st unbroken bond ($d_c$) was found to be 1.208d. Deformations of the bonds near the crack tip were observed for different external loads by changing the applied load by small values from the equilibrium load of $0.6\ \epsilon/d$.

Several runs were made for the purpose of studying the difference in the nature of the propagation of a crack when the applied load was increased by slow increment and also by sudden change. The details of these simulations are tabulated in Table 6.2.4.

Run DFL 2 (continued from run DFL 1)

The external load was increased from .6 to .65 abruptly on the sample with a crack in equilibrium from run DFL 1 (obtained from Gohar, 1979) and the sample was allowed to relax without any damping upto time step 17920. The crack tip bonds were found to stretch but not beyond 1.6d. In other words the crack did not propagate.

Run DFL 3 (continued from run DFL 2)

The knife in the half sample of run DFL 2 was reduced to a smaller length (19.5d) allowing 20 bonds at each crack tip to interact. Then the sample was allowed to relax at step 17100 of run DFL 2. Within 200 steps, it was found that a few bonds at each crack tip shrank below 1.6d indicating that if enough time is given and if the knife is removed the crack would heal completely.

DFL4 (continued from DFL 2)

To confirm that run DFL 2 eventually comes to equilibrium the sample with the same external load was allowed to evolve in time with critical damping. The sample was found to come to equilibrium by time step 19200.

DFL 5 (continued from DFL 2)

The external load was increased from .65$\epsilon/d$ to .67$\epsilon/d$ on the sample from DFL 2 abruptly and allowed to relax with no damping from time step 17920 to 19200. The crack did not propagate.

Run DFL 6 (continued from DFL 1)

The external load was increased from .6$\epsilon/d$ to .67$\epsilon/d$ abruptly on the sample from DFL 1 and was seen to propagate when it was allowed to relax with no damping.

Run DFL 7 (continued from DFL 6)

The sample in run DFL 6 at step 16780 (before the critical bond broke) was allowed to relax with critical damping keeping the external stress same. It was found that the crack reached equilibrium.

Run DFL 8 (continued from DFL 6)

The sample in run DFL 6 at step 17330 (after the critical bond broke) was allowed to relax with critical damping keeping the external load the same. The crack was found to propagate.

## 6.3 Discussion Of The Mott Theory
(Crack propagation under fixed displacement)

As already pointed out, the boundary condition of fixed displacement is theoretically advantageous because no external work is done leading to a simpler energy analysis. Further, crack propagation can be initiated by a very small change in the applied strain, from essentially an equilibrium configuration.

In the dynamic simulations, detailed studies were made on four different samples of varying sizes containing same size crack (length 2l = 19.5d). To compare our results with Mott's theoretical prediction, the crack was allowed to propagate in a quasistatic manner by increasing the external strain from e (just below critical strain) to $e + \Delta e$ (just above the critical strain as described in section 6.2. The crack tip velocity, modulus of elasticity and all energies were monitored during propagation.

Figure 6.2.1 shows the plot of the number of bonds broken versus the time step. The origin of time is taken as the time when the external strain is increased beyond the critical strain. During the first 1000 steps or so, it is observed that the rate of bond breaking increases, and the rates are different for different samples, and then after step around 1000 the curves become straight lines indicating that the rates of bond breaking are constant. The rates of bond breaking are plotted against the time step and the crack half-length (l) in figures 6.2.2 and 6.2.3. In figure 6.2.3 the rate of bond breaking is expressed in terms of thelongitudinal sound velocity ($V_L$). The conversion can be obtained as follows:

1 broken bond $\equiv$ d/2

1 time step = $.02d\sqrt{m/\epsilon}$

1 broken bond/time step =

$d/2 \;/\; .02\, d\sqrt{m/\epsilon}$

$= 1/.04\sqrt{\epsilon/m}$ 6.3.1

Longitudinal sound velocity

$$V_L = \sqrt{M_o/\rho} \qquad 6.3.2$$

when $M_o$ = Young's modulus and

$\rho$ = density of the material

For our system (perfect - unstrained)

$M_o = 83.14\,\epsilon/d^2$

considering an unit triangular cell,

mass per triangle = $3(m/6)$

Area of triangle = $(\sqrt{3}/4)d^2$

So, $\rho = 2/\sqrt{3}(m/d^2)$ 6.3.3

$$V_L = 8.485(\epsilon/m)^{1/2} \qquad 6.3.4$$

Hence 1 broken bond/step = $2.946V_L$. 6.3.5

Figures 6.2.2 and 6.2.3 both show a rapid transition to the limiting terminal velocities. Not only are the terminal velocities different for samples of different sizes but the rate of attainment of the terminal velocity is also different for different samples. This fact indicates that our terminal velocity is dependent on the size of the sample, particularly on the number of rows of the sample.

As these experiments were performed under fixed displacement, i.e. the upper and lower boundaries were fixed, samples of larger number of rows will allow the crack to grow wider under comparatively smaller external strains compared to the situation where samples have smaller number of rows. This is clear from the data in table 6.2.2, wher the bonds near the crack tip are given for different samples under their corresponding approximate critical strain e. It is observed that the smaller is the sample higher the critical strain. How fast a crack would attain terminal velocity depends on several factors, namely

i) the width of the crack-tip at strain e
ii) closeness of e to the critical strain.
iii) % increase of e

As the terminal velocities are the points of most interest, and to bring all samples to the point of breaking (i.e. to find exact critical strain) is rather costly, no attempts were made to bring the samples to equilibrium exactly at critical strain.

As discussed in section 5.7, for an infinite sample the lattice trapping region is negligible but for small finite samples the lattice trapping region increases because of our fixed displacement boundary condition. Thus, cracks in each sample not only have different width, but the external strains (cf. table 6.2.2) are not equally close to the corresponding critical strains (higher values). Attempts were made to increase the strains to e + $\Delta$e (cf. table 6.2.1) by the same percentage (approx. $\sim$ 1%) for all of the samples. Comparing the two curves 4 and 5 of figure 6.2.2, it is seen that a wider crack favours earlier attainment of the terminal velocity (percentage increase of the strain is the same in both cases). Comparing curves 2 and 3 in the same figure it is clear that, if everything else remains same, the larger percentage increase in the strain favors early attainment of the terminal celocity.

As the process of the the attainment of terminal velocity is at least qualitatively understood, it is now necessary to understand why a terminal velocity is attained. According to Mott (section 3.1) the crack velocity attains a terminal velocity ($0.38V_L$) if the sample is infinite (cf. figure 3.2.1, $\delta$ = 0),but the terminal velocity is achieved when the crack length increases by at least a factor of 15 or 20 (for practical purpose). Actually

$$v_c = V_T \left(1 - \frac{l_0}{l}\right) \qquad 3.1.10$$

In all our simulations, the terminal velocities were attained much earlier ($1/l_o \sim 2$). Lawn and Wilshaw combined Mott's analysis with Berry's sample size criterion for a finite sample under a fixed strain and found that the increase in the compliances (i.e. decrease in the modulus $M' \rightarrow M/(1+2\pi l^2/A)$ (cf. equation 3.1.13) with crack extension leads to a diminishing applied force and the tendency toward terminal velocity is correspondingly lessened and the crack velocity decreases to zero after attaining a maximum as shown in figure 3.1.1.

Our simulation does not agree with the above prediction and the terminal velocity is maintained even upto $1/l_o \sim 3$ for all samples with no tendency toward a decrease in the velocity. To understand the attainment of terminal velocity quantitatively the following analysis is made following Mott.

As our simulations were done under quasistatic condition (small increment of strain) it is reasonable to apply our static results to study this type of crack propagation. But before applying those results, it is necessary to investigate well they fit these dynamic simulations. The elastic response of the material during propagation is illustrated in figures 6.2.4 and 6.2.5. According to equation 5.4.16 (obtained from the energy analysis of the static simulations),

$$\frac{1}{M'} = \frac{2\pi l^2}{AM} + \frac{1}{M} \qquad 5.4.16$$

$1/M'$ versus $l^2$ should be straight a line with a slope of $2\pi/AM$. Figure 6.2.4 shows that $1/M'$ versus $l^2$ is linear, with different slopes, for all the sample. The slopes ($S_1^{Dyn}$) of the lines are given in table 6.3.1. The value of the slopes ($S_1^{Sta}$) according to our static results are given in the previous column. The static and dynamic values are very close to each other (within 5 to 10%). The values of M and M' from static and dynamic calculations are also

compared in table 6.3.2. $M_{Sta}$ and $M'_{Sta}$ are obtained by using the theory developed from static simulations (cf. equs. 5.4.9 and 5.4.16), namely

$$M_{Sta} = M_o - 414.e \qquad 5.4.9$$

$$M'_{Sta} = \frac{M_{Sta}}{1 + \delta l^3/l_o^2} \qquad 5.4.16$$

$M_{Dyn}$ is obtained by extrapolating the straight lines to l = 0 in figure 6.2.4 and $M'_{Dyn}$ is the value of the effective modulus obtained from the simulation. Table 6.3.2 shows that the values of the modulus obtained from the theory developed for simulations are in close agreement with the values obtained from the dynamic simulations.

In figure 6.2.5 the change in the elastic strain energy ($-\Delta E_{el}$ /2) for the half sample, as the crack propagates, is plotted against l M' for all the samples.
According to equation 5.4.14 (static simulation)

$$-\Delta E_{el} = (l^2 M').\ \pi e^2 \qquad 5.4.14$$

giving the slope of the line: $-\Delta E_{el}/2$ (for the half sample) versus $l^2M'$ as $\pi e^2/2$. The plots in fig. 6.2.5 show the above functional form with different slopes for different runs. The slopes from the static simulations ($S_2^{Sta}$) and the slopes from the dynamic simulations ($S_2^{Dyn}$) are both given in table 6.3.1. Comparison of the two slopes for each run shows close agreement with a discrepancy of less than 10%. It should be noted that there was a similar discrepancy of about 12% in the static simulations. Overall the agreement with the approximate nonlinear elasticity treatment is satisfactory. The important observation to be made from the agreement of equilibrium static formulations with the dynamic results in the demonstraion that our dynamic configuration resembles the equilibrium static configuration.

Mott obtained the relationship for $E_k$, the kinetic energy, as (cf. equation 3.1.6)

$$E_k = \tfrac{1}{2} k \rho v_c^2 l^2 \sigma^2 / M_o^2 = \tfrac{1}{2} k \rho v_c^2 l^2 e^2 \qquad 6.3.7$$

where $\rho$ is the density, $v_c$ the crack tip velocity, $\sigma$ the external stress, $M_o$ the modulus and k a constant. For constant applied strain, $e = \sigma / M_o$ and the second form for the kinetic energy is applicable to the present simulations. This is the key Mott result, the rest of the details follow from conservation of energy and must be correct regardless of the form for the kinetic energy. In Fig. 6.3.1 the kinetic energies for all five runs are plotted against $l^2 v_c^2$ ; the agreement is striking. It should be noted that initially $v_c$ varies approximately linearly with l and, subsequently, becomes a constant as shown in Fig. 6.2.3, nevertheless $l^2 v_c^2$ describes the behavior of the kinetic energy, at least during the period during which the crack propagates to about 3 times its original length.

While the initial behavior of the kinetic energy is somewhat simple to explain, the $l^2$ dependence, when $v_c$ is a constant, is not so easy to understand nor is the fact that the asymptotic value of $v_c$ is much less than the Mott estimate of 0.38 times the longitudinal sound velocity $V_L (= 8.49\sqrt{\epsilon/m})$. For the smallest sample, the terminal velocity is $.053V_L$ and for the largest sample it is $.113V_L$ (Table 6.2.2). As the general nature of crack propagation is very much the same for all samples of different sizes, the results are first analyzed by focusing our attention on the largest sample (Run DFD5) which is closer to the infinite sample. Figure 6.2.3 shows that in the region where $v_c$ varies, $(l-l_o)/l_o < 1$ and a Taylor expansion can be made of the elastic energy for crack formation as a function of $(l-l_o)$. Inserting the conditions that the kinetic energy is zero at $l = l_o$ and

$$\left[\frac{\partial(\Delta E_{el} + E_s)}{\partial l}\right]_{l=l_o} = 0 \qquad 6.3.8$$

the following expression for the kinetic energy is obtained

$$\Delta E_k = -(\Delta E_{el} + \Delta E_S) = \frac{(l-l_o)^2}{2} \cdot \frac{\partial^2 \Delta E_{el}}{\partial l^2} \qquad 6.3.9$$

With $l_o$ =9.75d, from $l = l_o$ to 15.25d, $\Delta E_k/(l-l_o)$ only varies by about 15% from the average value, while $E_k$ changes by three orders of magnitude. Thus, the initial behavior of $v_c$ can be well described in terms of the initial constraints on the behavior of $(\Delta E_{el}+\Delta E_S)$. The behavior where $v_c$ = constant is not so easy to describe. Lawn and Wilshaw (1975) predicted that $v_c$ would vary rapidly and vanish much before the crack length is doubled. This does not happen in this simulation. The key difference between Lawn and Wilshaw's analysis and the present one is that they assume (in our notation)

$$\Delta E_{el} = -\pi l^2 e^2 (M')^2 / M_o \qquad 6.3.10$$

whereas it is found in the simulation that (cf. 5.4.14)

$$\Delta E_{el} = -\pi l^2 e^2 M' \qquad 6.3.11$$

As $M' \propto 1/(1 + \delta l^2/l_o^2)$, the Lawn and Wilshaw crack formation energy decreases with increasing $l$ much more rapidly and this makes the kinetic energy vanish at a small $l$. If the kinetic energy term is calculated using 6.3.11, it is found to vanish at 1~50d. While this is much larger than the Lawn and Wilshaw estimate, it is still not in accord with the present results. At first this is quite surprising in that the expression for $\Delta E_{el}$ is in accord with the dynamic results and thus the calculation for $E_k$ would also be expected to be valid. The reason for the discrepancy is that the agreement of $\Delta E_{el}$ with the dynamic results is to within several percent, but the $E_k$ is about as large in the region of interest as the error in $\Delta E_{el}$. Hence, the calculation of $E_k$ has an error of about 100% and thus, the expression for $E_k$ is just not described accurately enough to calculate $E_k$ directly from equation 6.3.7 with explicit forms for $\Delta E_{el}$ and $E_S$.

The constancy of $v_c$ may be approached somewhat differently in terms of the size effect. The main idea of how the size effect limits the velocity is that, because of sample size restraints, the crack height can only grow to some maximum value, $\delta y$, limited by the sample size in the y direction. The $v_c$ may be estimated by assuming an average acceleration near the crack tip of $\sigma_{max}/2m$, and thus

$$v_c = \sqrt{2\left(\frac{\sigma_{max}}{2m}\right)\cdot \delta y} \qquad 6.3.12$$

For the Lennard-Jones potential, $\sigma_{max} = 4.66\ \epsilon/d$, for the largest sample $\delta y \sim 0.5d$, and $V_T \sim 1.5\sqrt{\epsilon/m}$ compared to the observed value of $0.92\sqrt{\epsilon/m}$. This is in the right direction to explain both why $v_c$ becomes constant at a relatively small fraction of the sound velocity and also why it is a constant whereas quantitative examination of $(\Delta E_{el} + \Delta E_S)$ suggests a varying value for $v_c$[i.e., $(\Delta E_{el} + \Delta E_S)$ is not simply proportional to $l^2$ over any wide range of l]. However, if $v_c$ is limited by sample size constraints so that it cannot attain the limiting value of an infinite sample, simply because the available distance for the crack sufrface to expand is limited, the observed results seem reasonable. This analysis suggests a sample size effect: the smaller the sample, the smaller the limiting velocity, which is exactly what is observed. Going from the smallest sample with 27 rows to largest sample with 79 rows it is seen that the terminal velocity increase by a factor of 2.

The major argument favoring the credibility of the present molecular dynamic results is the close aggreement of the size dependence of the modulus (in the static calculations) with theory and the correct functional dependence of the modulus and crack energy of formation on the sample size and on the crack length during propagation. This suggests that the results for crack propagation are quantitatively quite good at the early stages of

propagation. Of course, as the crack grows, the size effect becomes more important. This may introduce some systematic size dependence in the crack velocity results but such systematics are outside the scope of the present analysis. The fact that the crack velocities rapidly attain a constant value less than the sound velocity, in accord with experiment, is another argument for the credibility of the dynamic results. As the fixed displacement results produced a number of results in agreement with our physical understanding of crack propagation and no surprising result inconsistent with this understanding, the fixed displacement results are regarded as highly credible.

Stress Profiles For Dynamic Runs

To study the time evolution of the stress profiles, as a crack starts to propagate, the largest sample was used (run DFD6, cf. section 6.2, table 6.2.3 and figures 6.2.6 and 6.2.7). At step 3600 under external strain .029 the crack was in equilibrium and the maximum force of 4.557 $\epsilon$/d was on atom 57 ($r_{c-2}^{U}$) of row 40. As the external strain was increased from .029 to .0295, two crack tip bonds were found to break at steps 3700 and 3790 respectively. Time evolutions of the stress profiles of row 39 and row 40 show that, as a crack tip bond breaks, the site of the maximum force is no longer on a single atom on a particular row but it is shared by few atoms. As for example, 20 steps after the first bond ($d_c$) broke, the force distribution on row 40 is 3.405, 4.139 and 3.980 on atoms 55, 56 and 57, respectively (curve 4 of figure 6.2.7). The same thing happened after the second bond broke, but because of the geometry of the lattice used, the site of the maximum force moved to row 39. At step 3800 the force distribution on row 39 is 3.362, 4.042 and 4.100 on atoms 54, 55 and 56 (curve 6 of figure 6.2.6). This curve shows that the sample is not in perfect equilibrium. The up and down forces acting on the new crack surfaces are still not equal because the profile was drawn only 10 steps after the second bond broke.

Curve 7 shows that if enough time is given the forces up and down at the crack surfaces become equal.

Thus, in brief, as the crack tip bonds break one after another the site of maximum force moves forward and hops from one row to the other. This is similar to the picture observed when the external strain was increased from a subcritical value to the critical value (section 5.6) where the maximum force was 4.557 $\epsilon$/d on row 40 of the largest sample. Close inspection of table 6.2.3 reveals a very interesting point. The force never went above .557 $\epsilon$/d during the propagation. Why did the crack propagate not at strain 0.029, even though the maximum force went upto 4.557 $\epsilon$/d? The question can be possibly answered by energy considerations. Although the maximum force is sufficient to break the crack tip bonds, the system may not have sufficient energy to provide the new crack surface. A slight increase in strain then provides energy for the crack to propagate.

## 6.4 Crack Propagation Under Fixed Load

The details of the results of the propagation of cracks under fixed displasement can be found in section 6.2. table 6.2.4 summarizes the essential points of crack propagation under a small increament of applied load from a load just below the critical. The stretching of the first ($d_c$) and second ($d_{c-1}$) unbroken bonds at the crack tip are plotted against the time step for different loads in figure 6.4.1. For a slow change of the external load, e.g., .60 → .65 → .67 (runs DFL2 and DFL5), the bonds $d_c$ and $d_{c-1}$ were seen to stretch and then to heal upon restoration of the interaction and finally came to equilibrium. In the static fixed load study, it was seen that a crack in equilibrium under a fixed load below critical is not stable in the sense that when the knife is taken out, or the knife is shrunk to a length smaller in size, the crack always heals. This was verified again in run DFL3 by reducing the size of the knife and relaxing the system under an external load without damping. The bonds $d_{c-1}$ and $d_c$ are seen to decrease in length confirming crack healing. On the other hand, with a more sudden change of $\sigma$: from .60 $\epsilon$/d to .67 $\epsilon$/d (Run DFL 6) with, no damping propagation occurred with d rapidly increasing past 1.6d. (the searching range)

From runs DFL 7 and DFL 8 it is seen that the crack does not propagate if the sample in run DFL 6 at step 16780 (before the breaking of the critical bond) is allowed to relax under critical damping, but the crack propagates if the critical damping is imposed on the sample at step 17320 (right after the critical bond broke).

Thus, at constant load, this system is very sensitive to the rate of change of the applied load. For sudden change of with no damping the crack propagates and for a slow change of $\sigma$ along with critical damping it required a higher value of the applied load to initiate propagation.

## 6.5 Summary

In this chapter the dynamical behavior of a crack under fixed external displacement and fixed external load was studied. Because this chapter is rather long it seems appropriate to summarize the important results here.

### Velocity Of Crack Propagation

Fixed external displacement boundary condition was used to study the velocity of crack propagation by increasing the external strain from a strain just below the critical (quasistatic condition). The present result was compared with the Mott prediction. Terminal crack velocity was obtained in simulations of samples of various sizes. The rate of attainment of terminal velocity was found to depend on several factors:

i) the width of the crack tip at a strain just below critical strain
ii) closeness of strain to the critical strain and
iii) percentage increase of strain.

The terminal velocity was dependent on the sample size (mainly on the number of rows). Going from the smallest sample of 27 rows to the largest sample of 79 rows, it was observed that the terminal velocity increased from $0.053V_L$ to $0.113V_L$ (factor of 2) compared to the Mott prediction of $0.38V_L$ for an infinite sample. Lawn and Wilshaw, following Mott and using Berry's sample size criterion for finite sample, predicted a phenomenon of crack arrest for finite samples. This was never observed in any of our simulations.

The elastic response of the system during crack propagation was found to be in close agreement with the results obtained from static simulations demonstrating that the dynamic configuration (under

quasistatic condition) resemble the equilibrium static configurations. The kinetic energy expression suggested by Mott was found to be in good agreement with the simulation results during the period the crack moved to about 3 times its original length. Although a reasonably good expression was obtained for the change in elastic energy due to the crack, it was not possible to obtain a good expression for the kinetic energy which can describe the change in kenetic energy during propagation. The reason for this is that the agreement of elastic energy with the dynamic results is to within several percent, but kinetic energy is about as large as the error in elastic energy in the region of interest.

The costancy of the crack velocity was explained in terms of the finite sample size effect. The finite size of the sample restricts the growth of the crack height to a maximum value. Taking into account the average acceleration at the crack tip for the largest sample used in the simulation, the terminal velocity was estimated to be $1.5\sqrt{\epsilon/m}$ compared to the simulation result $0.92\sqrt{\epsilon/m}$.

Stress Profiles For Dynamic Runs

The time evolution of the stress profiles as a crack starts to propagate under fixed external displacement showed that the crack tip bonds break one after another, the site of maximum force moves forward and hops from one of the two crack surfaces to the other. This is similar to the picture observed when the external strain was increased from a subcritical value to the critical value (section 5.6).

Critical study of the stresses around the crack tip as the crack propagates revealed that even if the maximum force on atoms near the crack tip reached its maximum value a bond can withstand, the crack might not propagate unless there is sufficient energy to provide new surfaces. It is necessary to increase the external strain to provide sufficient energy for the crack to propagate.

Crack Propagation Under Fixed Load

To study the crack propagation under a small increament of the external load from a load just below the critical was the point of interest of this study. At fixed load it was found that this system is very sensitive to the rate of change of the load. For a sudden change of load with no damping the crack propagtes and for a slow change of the load along with critical damping it required a higher value of applied load to initiate propagation.

# PART II

# INHOMOGENOUS MATERIAL

# CHAPTER 7
# PRESENT CALCULATION: DYNAMICS

## 7.1 Gaseous Embrittlement

Brittle fracture is known to occur in normally ductile metals under the influence of certain specific gaseous environments. Hydrogen is usually associated with such effects although there are many examples in the literature which show that other gaseous species often produce similar effects. For example, it has been shown [Purushothaman et al, 1978 and Frandsen et al, 1977] that oxygen increases fatigue crack growth rates in several iron and nickel base alloys when compared to growth rates in vacuum. Such phenomena must result from surface or very near surface effects whereas for the case of hydrogen no such conclusion can be made with certainty. The relatively small size of the hydrogen atom gives it a much higher degree of mobility than other species are likely to have in the metallic host at ambient temperatures.

If a universal mechanism of gaseous embrittlement exists it seems as though it must in principle involve what [Fuller et al, 1980] have termed chemically breaking or weakening of the crack tip bond by chemisorption of the gaseous environment and under suitable mechanical conditions fracture proceeds via a bond by bond rupture at the crack tip. Such a mechanism, however, does not seem to be entirely consistent with the experimental results in some well-studied systems. It is well known that in the case of high strength steels in $H_2$, $H_2S$, and $Cl_2$ environments [Sieradzki, 1981, 1982] a threshold pressure exists below which no environmental embrittlement effects are found to occur. This lower pressure threshold, which is typically on the order of $10^{1}$ to $10^{3}$ Pa, is at least four orders of magnitude larger than the pressures at which monolayer adsorption of these gases on the clean base metal surface is known to occur [Bozso et al, 1977 and Dowben et al, 1979]. If

the crack tip is extremely sharp, say of atomic dimensions, it may be argued that in some cases the environment cannot reach the critically stressed bond at the crack tip at low external gas pressures. In his discussion, Thomson [1980] refers to this effect as steric hindrance. However, for the specific cases discussed above, the bond lengths of the $H_2$ and $Cl_2$ molecules are $7.5 \times 10^{-2}$ and $1.99 \times 10^{-1}$ nm, respectively, so that even an atomically sharp crack is unlikely to present a geometric barrier to chemisorption. Furthermore, $H_2$, $H_2S$ and $Cl_2$ adsorption each occur via a mobile precursor [Bozso et al, 1977 and Dowen et al,1979] which increases the likelihood of adsorption occurring at the crack tip regardless of the geometric constraint which may be present.

Sieradzki [1982] has investigated the embrittlement of a high strength steel in gaseous chlorine and has shown that it results when the external chlorine gas pressure is large enough to produce a film at the crack tip of some 10 nm thickness. This critical film thickness was shown to be primarily a function of the elastic modulus of the film and metal substrate. The analysis was micromechanical in nature and was based on a model developed by Rice and Thomson [1974]. Sieradzki concluded that under a specialized set of circumstances the existence of an elastically hard film at a crack tip could inhibit dislocation generation at the tip and so result in brittle fracture.

## 7.2 Result

### Crack Coated With Hard Film

Our two dimensional system with the LJ potential under high applied load is inherently ductile (Paskin et al, 1980 and Gohar, 1979). The purpose of the present simulation is to investigate the fracture mode of an inherently ductile material when a pre-existing

crack is surrounded by a few layers of film of varied strength under fixed load condition. For these simulations a triangular array of 608 atoms arranged in 19 rows was used (only half of the sample is shown in the figures 7.2.1 through 7.2.3.)

The crack was coated with three layers of film surrounding all of the crack, i.e. the matrix atoms were replaced by "foreign" atoms as illustrated in Fig. 7.2.2. The strengths of the bonds joining the film and substrate atoms (FS) was made different from the strengths of the film-film (FF) bonds and substrate-substrate (SS) bonds. In these experiments the change in the strengths of the FF bonds was accomplished by changing only the depth of the potential for the appropriate bonds keeping the equilibrium bond length, d, unaltered.

The sample was scaled uniformly to a value of the strain corresponding to the applied external tensile load (below critical load) and the sample was allowed to evolve in time after the insertion of a crack of 7 broken bonds in the half sample and the application of an external load, $\sigma_1$ . The purpose of scaling is to reduce the computation time as otherwise the sample would take a much longer time to come to equilibrium. After equilibrium was reached the external load was increased to a value ( $\sigma_2$ ) a few percent higher (5 - 10% ) than the previous value at which the system came to equilibrium. The equilibrated sample was again scaled appropriate to the new external load and allowed to evolve in time along with damping. The purpose of the slow increment in the external load is to ensure that the atoms near the crack tip do not experience a large net force due to inaccurate scaling near the crack tip.

In order to analyze the present results in a conventional manner (see Appendix ), the applied external atomic forces and the local forces on specified atoms were monitored. In figures 7.2.4, 6,

7 and 9 the force above the reference row is described as $\sigma^{up}$ and below as $\sigma^{down}$. These may be unequal when a dislocation or a crack is in motion.

The results are presented in two series of computer generated pictures as the deformation and/or crack propagation proceeds: i) atomic positions; ii) local force profiles. The runs for these simulations are designated by DFLF. (Dynamic Fixed Load - Crack With Film) Details of the parameters used in the simulations are given in table 7.2.1.

(1) Atomic positions

The results for Run DFLF 1, representing the pure matrix material, are displayed in Figures 7.2.1a-1d. For these constant load data on small samples at high applied forces the behavior was ductile. Two dislocations were formed and propagated to the surface with concomitant widening of the crack. It is to be noted that in simiar loading conditions for a small sample, but under constant applied displacement rather than constant external force, brittle behvior was observed with no dislocation formation (Paskin et al, 1980 and Dienes et al 1981). Thus, if crack widening is prevented by preventing dislocation formation then brittle propagation results. Conversely, of course, dislocation formation and crack widening lead to a ductile type failure. At the higher loads used in subsequent fracture with films, the homogeneous sample failed in a ductile manner by shearing rather than by crack growth and fracture.

The results for Run DFLF 2, for the crack coated with a film (film atoms are indicated by large circles), are displayed in Figures 7.2.2a-2f, and show a mixed dislocation generation - crack nucleation behavior. A dislocation passed through at time step 1200, but instead of a second dislocation, a crack nucleus was

created at time step 1350 to 1400 in the weaker matrix ahead of the existing crack. The new crack is initially pinned and does not widen much as the crack begins to propagate.

The results for Run DFLF 3, for the crack coated with a very strongly bonded film, are displayed in Figures 7.2.3a-3d. Dislocation formation and crack widening is completely prevented by the strong films resulting in crack nucleation and brittle propagation in the matrix.

(2) Local stress profiles

The local force profiles for Run DFLF 1, the homogeneous sample, are shown in Figure 7.2.4. The theoretical critical, or maximum, force for a perfect triangular array with a LJ potential is 4.66 $\epsilon$/d. In Run DFLF 1 the maximum force observed at the crack tip in this simultion is 4.1 $\epsilon$/d. The local force sequences shown are to be compared to the corresponding atomic motions of Figure 7.2.1. The sequences show very clearly that the force at the crack tip is reduced when the dislocation is formed and the crack is blunted. It is of interest to display the force profile information in a somewhat different way, namely by the sequence of the local force at a given atom number on a given row. Such a graph for Run DFLF 1 is shown in Figure 7.2.5. The force relief as the first dislocation passes through is clearly seen at timestep 1150. The force then rises followed by a second, more gradual, relief as the second dislocation passes through at about time step 1600. This pattern is characteristic of dislocation generation near the crack tip and subsequent propagation to the surface.

For Run DFLF 2, a crack with a moderately strong film, the force profiles are first given in Figure 7.2.6 for a row that includes the film and the crack tip. The maximum near the crack tip is 7.4 $\epsilon$/d on row 9 at a position of about 11 (the theoretical

maximum is 4.66 X 2 = 9.32 $\epsilon$/d). As the dislocation is formed and slip occurs (see Figure 7.2.2) the maximum force is reduced to 5.2 $\epsilon$/d as shown in Figure 7.2.6 at time step 1150. As shown in Figure 7.2.2, crack nucleation occurs on row 6 and the force sequences on this row are shown in Figure 7.2.7 after the dislocation has passed through. Just prior to crack nucleation, at time step 1300, the maximum force is 4.85 $\epsilon$/d at atom position 10 (atom number 11). In 50 steps, at time step 1350, the maximum force is almost the same, 4.80 $\epsilon$/d, but has moved to atom position 9 (atom number 10) with a large reduction in the force where the previous maximum was located (to 1.80 $\epsilon$/d at atom position 10). In 50 more steps the maximum on this row moved two more atomic spacings to position 7. This corresponds to a moderately fast moving crack. At time step 1450, there is a clear double peak in the force profile on row 6 characteristic of the two crack tips of the newly formed crack.

The time sequence of the local forces for atom numbers 10 and 9 on row 6 is shown in Figure 7.2.8. This figure shows very clearly the rise in force prior to dislocation slip, relief as the dislocation passes through, the build up in the local force prior to crack nucleation and the drastic decrease upon crack nucleatin.

The data for Run DFLF 3, the very strong film, are presented in Figure 7.2.9. This stronger film shows no dislocation formation over a long time sequence. In Figure 7.2.9 the local forces on row 11 are shown as the new crack nucleates and grows. At time step 1550 the characteristic double hump of the developed crack is seen. In Figure 7.2.10 the time evolution of the forces is shown for atoms 8, 9 and 10 on row 11. Note that there is only a single maximum in these curves since the dislocation formation is absent (compare to Figure 7.2.8) and the system goes into crack nucleation directly. The maxima progress in time from atom 10 to 9 to 8. This progressive shifting of the maxima is characteristic of crack propagation. Thus, the new crack nucleates and begins to propagate at a moderately fast velocity almost simultaneously.

## 7.3 Propagation Of A Crack (Under Fixed Load) Coated With A Hard Film: Embrittlement

The semiquantitative nature of the analysis presented by Sieradzki (1982) (cf. section 7.1), in addition to the possible importance of such an effect in a number of systems, makes it desirable to analyze the film embrittlement mechanism from an entirely different approach. The size scale over which film effects are likely to dominate seems to preclude any continuum mechanics type of analysis. Additionally, such an analysis does not lend itself to kinetic factors which may dominate such situations. The purpose of this simulation is to study the propagation of a crack covered with an elastically hard thin film. To determine the manner in which such films could modify normal near tip deformation and subsequent fracture was the main object of this study.

### Model For Environmentally Triggered Embrittlement

On the basis of the simulation results and analysis (cf. section 7.2), the following sequence of steps has been deduced as a model for how the environment can trigger a brittle behavior in a material that is inherently ductile.

(1) An elastically hard (strongly bonded interatomic force) film is formed on the surface of the crack. This strongly bonded film allows the local forces near the crack tip of strongly bonded film-film atoms to exceed the critical local force for brittle fracture in the substrate.

(2) Little or no dislocations are formed in a strong film or the substrate as the load is increased. Hence the coated crack does not widen nor does the crack tip blunt much compared to the homogeneous substrate.

(3) The local force in front of the crack tip eventually exceeds the critical force for the substrate material and a crack is nucleated quite abruptly.

(4) The region of the newly created crack is initially "pinned" near the coated surface of the old crack. The newly created crack cannot widen appreciably and thus dislocation formation is inhibited.

(5) The newly created crack now propagates in a brittle manner because of the suppression of dislocation formation by the pinning of the crack by the hard film.

A consequence of the model, in its present simplest form, is that the hard film on the crack raises the critical force of the composite material. This is because, for a given applied force, the crack will not propagate until the local force on the film of the crack tip exceeds the "critical force of the film," not the substrate. (This of course is exclusive of the mode of crack nucleation in front of the film in the substrate.) Thus, fracture cannot occur even though the applied external force exceeds the critical force of the substrate material. It is the local forces in the material in the region of the crack tip that must exceed the local maximum force that is the determining factor.

There are a number of ways that a film on the crack surface can change the local forces near the crack tip. A lattice mismatch between film and substrate can create residual local forces which can promote fracture. A tough, strong film may also change the shape of the crack tip and thus increase the stress concentration at the crack tip. A lattice mismatch may produce the same effect and may also induce different rates of stress fall off in front of the crack tip and affect the overall critical stress for crack nucleation as well as crack propagation.

For the simple case considered here, a hard film with the same lattice paramter as the substrate, the critical load for the composite material with a hard film on the crack surfaces is greater than that of the substrate material itself. It is interesting to note that these inhomogeneous materials of atomic dimensions are particularly suitable for computer simulation studies and it is difficult to see how they could be studied by conventional continuum mechanics approaches.

Computer simulations of cracks coated with an elastic hard film thus show that brittle fracture can occur in substrates that are ductile. The brittle fracture occurs via cracks that are nucleated because of the presence of the hard films. This is an entirely new mechanism of environmentally induced fracture.

# CHAPTER 8
## SUMMARY AND CONCLUDING REMARKS

An atomistic study of brittle fracture was conducted. The study was performed, using molecular dynamic techniques, on a two dimensional triangular lattice whose atoms interact via a two body central (Lennard-Jones)) potential. A high speed CDC 7600 computer was used for the simulations. The purpose of this study was to try to obtain a clear understanding, and for confirmation, of some of the basic assumptions and models that have been proposed for the underlying mechanism of brittle fracture. While computer simulations are not the microscopically controlled experiments ultimately required for testing theory and experiment they can serve as interim steps in investigating the atomic interactions in fracture.

The basic procedure used in the molecular dynamic simulation consisted of solving Newton's equations of motions in a differece form for a finite number of atoms interacting via the L-J potential. Besides the atomic forces, if any atom (on the surface) experienced an external force that force was also taken into account in the equation of motion. The equation of motion for each atom is solved by Verlet's central difference method which is basically to find the position of each atom at an instant $t + \delta t$ from the position of the atom at time t and $t - \delta t$ and the net force acting on the atom at time t where $\delta t$ is a small interval of time of the order of the relaxation time of the material.

In all simulations only the first nearest neighbor interaction was taken into account and the interaction was cut off at a distance of 1.6 times the lattice constant (d), well beyond the distance (1.1d) where the atoms experience the maximum force. The crack was introduced into the perfect sample by removing the forces between the atoms forming the crack in the center of the sample.

For static study a crack under some external loading (stress or displacement) was allowed to come to equilibrium (i.e. the sample was allowed to evolve in time until the net force acting on every atom becomes zero). To enhance this process critical damping was used. At each step a fraction of kinetic energy was removed. Thus, when the sample reached its equilibrium state it was at absolute zero temperature.

About fifty percent saving in computer time was obtained by using the left-right symmetry of the sample. A number of mechanical and thermodynamic properties were monitored, such as: Young's modulus, average strain, average stress, Poisson's ratio, total kinetic energy, total potential energy of the system, local atomic positions, local interatomic forces, atomic velocities and the speed of crack propagation. The time step used in all simulations gave an accuracy of at least one part in $10^5$.

A brief summary of the work done in this thesis will be given here. The statics and dynamics of the homogenous system were studied. The details of the results can be found in chapters 5 and 6. The essential results are also summarized at the end of the two chapters (sections 5.8 and 6.5) and are not repeated here. The dynamic study of the inhomogenous material (chapter 7) is summarized here.

Brittle fracture is known to occur in ductile materials in special gaseous environments. To understand the effect of gaseous environments on crack propagation, cracks coated with a thin elastically hard film in our system (which is inherently ductile under high load) were simulated under fixed loading condition. It was found that under certain conditions secondary crack nucleation occurred in the simulations and brittle fracture was observed. The dynamics of the crack nucleation and the detailed spatial distribution of the local forces were examined. A model was

developed for this new mode of crack nucleation and brittle fracture. The role of the elastically hard film in suppressing dislocation generation and in initiating the secondary crack was discussed. This mode of initiating brittle fracture is entirely different from the usual models for gaseous embrittlement.

| Run | $\delta t$ $[ m/\epsilon ]^{1/2}$ | $\beta$ | No. of steps to equilibrate |
|---|---|---|---|
| TEST1 | .01 | .987 | 2580 |
| 2 | .02 | .974 | 1288 |
| 3 | .04 | .949 | 644 |
| 4 | .06 | .921 | 484 |
| 5 | .08 | .895 | 322 |

$$(\delta t)_1 / (\delta t)_2 = (1 - \beta)_1 / (1 - \beta)_2$$

$$= (\text{No. of steps})_2 / (\text{No. of steps})_1$$

Table 5.3.1 Search for damping parameter ($\beta$) by simulating a full sample of 20 rows with $NTM_{odd} = 13$ and a crack of length 5.5d. External load = $2.0\epsilon/d$. As the time step ($\delta t$) is increased, $\beta$ is less, i.e., it is necessary to take away more and more kinetic energy from the system as the time step is increased and it also takes less time to equilibrate. As the time step

| Run | $N_R$ | $NTM_{odd}$ | A $[d^2]$ | $\sigma_{ext}$ | e | l [d] |
|---|---|---|---|---|---|---|
| SFL1 | 39 | 135 | 4426.3 | 0.5 | .0062 | 0 |
| SFL2 | 39 | 135 | 4426.3 | 0.5 | .0064 | 4.75 |
| SFL3 | 39 | 135 | 4426.3 | 0.5 | .0158 | 19.75 |
| SFL4 | 39 | 135 | 4426.3 | 1.3 | .0172 | 0 |
| SFL5 | 39 | 135 | 4426.3 | 1.3 | .0211 | 9.75 |
| SFL6 | 79 | 135 | 9085.5 | 0.5 | .0062 | 0 |
| SFL7 | 79 | 135 | 9085.5 | 0.5 | .0063 | 4.75 |
| SFL8 | 79 | 135 | 9085.5 | 0.5 | .0067 | 9.75 |
| SFL9 | 79 | 135 | 9085.5 | 1.3 | .0172 | 0 |
| SFL10 | 79 | 135 | 9085.5 | 1.3 | .0175 | 4.75 |
| SFL11 | 79 | 135 | 9085.5 | 1.3 | .0187 | 9.75 |

$$NTM_{even} = NTM_{odd} + 1$$

Table 5.3.2 Summary of static fixed load results. Two samples of different sizes (perfect and with cracks of different lengths) under different external loads ( $\sigma_{ext}$). The average strains (e) were obtained at equilibrium.

| Run | $-E_{el}/2$ [$\epsilon$] | $E_s/2$ [$\epsilon$] | $\sigma_{true}$ [$\epsilon/d^2$] | Modulus [$\epsilon/d^2$] |
|---|---|---|---|---|
| SFL1 | 7749.014 | 0 | 0.5010 | 80.706 |
| SFL2 | 7739.884 | 18 | 0.5010 | 77.866 |
| SFL3 | 7704.455 | 78 | 0.5010 | 31.746 |
| SFL4 | 7726.910 | 0 | 1.3063 | 76.124 |
| SFL5 | 7700.310 | 38 | 1.3011 | 61.910 |
| SFL6 | 15835.34 | 0 | 0.5010 | 80.639 |
| SFL7 | 15826.21 | 18 | 0.5010 | 79.290 |
| SFL8 | 15815.78 | 38 | 0.5010 | 74.902 |
| SFL9 | 15789.95 | 0 | 1.3063 | 76.620 |
| SFL10 | 15779.84 | 18 | 1.3063 | 74.620 |
| SFL11 | 15765.77 | 38 | 1.3063 | 69.730 |

Table 5.3.3 Summary of static fixed load results. When the samples under fixed external load come to equilibrium the elastic strain energy ($E_{el}$), and the true stress acting on the boundary surfaces were monitored. Young's modulus (M) of the perfect samples and that (M') of the samples with crack were also monitored.

| Run | $d_{c-1}$ [d] | $d_c$ [d] | $d_{c+1}$ [d] |
|---|---|---|---|
| SFL2 | 1.011 | 1.017 | 1.054 |
| SFL3 | 1.054 | 1.099 | 1.267 |
| SFL4 | 1.012 | 1.012 | 1.012 |
| SFL7 | 1.011 | 1.016 | 1.051 |
| SFL8 | 1.017 | 1.025 | 1.082 |
| SFL9 | 1.012 | 1.012 | 1.012 |
| SFL10 | 1.033 | 1.054 | 1.157 |
| SFL11 | 1.056 | 1.114 | 1.283 |

Table 5.3.4 Summary of static fixed load results. Crack tip bond lengths. $d_c$ is the length of the crack tip bond, $d_{c-1}$ is that of the bond in front of the crack tip and $d_{c+1}$ is that of the first broken bond behind the crack tip.

| Run | $N_R$ | $NTM_{odd}$ | A $[d^2]$ | $e_{ext}$ | l [d] |
|---|---|---|---|---|---|
| SFD1 | 39 | 67 | 2188.4 | .029 | 0 |
| SFD2 | 39 | 67 | 2188.4 | .029 | 9.75 |
| SFD3 | 39 | 75 | 2451.7 | .0385 | 0 |
| SFD4 | 39 | 75 | 2451.7 | .038 | 9.75 |
| SFD5 | 39 | 75 | 2451.7 | .0383 | 9.75 |
| SFD6 | 39 | 75 | 2451.7 | .0384 | 9.75 |
| SFD7 | 39 | 75 | 2451.7 | .0385 | 9.75 |
| SFD8 | 59 | 95 | 4746.7 | .029 | 0 |
| SFD9 | 59 | 95 | 4746.7 | .029 | 9.75 |
| SFD10 | 59 | 95 | 4746.7 | .0312 | 9.75 |
| SFD11 | 59 | 95 | 4746.7 | .0315 | 9.75 |
| SFD12 | 79 | 135 | 9085.5 | .01 | 0 |
| SFD13 | 79 | 135 | 9085.5 | .01 | 9.75 |
| SFD14 | 79 | 135 | 9085.5 | .02 | 0 |
| SFD15 | 79 | 135 | 9085.5 | .02 | 9.75 |
| SFD16 | 79 | 135 | 9085.5 | .023 | 9.75 |
| SFD17 | 79 | 135 | 9085.5 | .028 | 0 |
| SFD18 | 79 | 135 | 9085.5 | .028 | 9.75 |
| SFD19 | 79 | 135 | 9085.5 | .029 | 0 |
| SFD20 | 79 | 135 | 9085.5 | .029 | 9.75 |
| SFD21 | 79 | 135 | 9085.5 | .02875 | 9.75 |
| SFD22 | 79 | 135 | 9085.5 | .0285 | 9.75 |
| SFD23 | 79 | 135 | 9085.5 | .0293 | 9.75 |

Table 5.3.5 Summary of static fixed displacement results. Samples of different sizes (perfect and with cracks of half length 9.75d) were simulated under fixed external displacement. Run SFD1 through SFD19 came to equilibrium with the knife separating the crack surfaces. Runs SFD20 through SFD23 were performed without any knife.

| Run | $-E_{el}/2$ [ $\epsilon$ ] | $E_s/2$ [ $\epsilon$ ] | Modulus [ $\epsilon/d^2$ ] | $\sigma_{ave}$ [ $\epsilon/d^2$ ] |
|---|---|---|---|---|
| SFD1 | 3807.849 | 0 | 71.109 | 2.0622 |
| SFD2 | 3795.875 | 38 | 56.117 | 1.6270 |
| SFD3 | 4236.594 | 0 | 67.233 | 2.5885 |
| SFD4 | 4231.190 | 38 | 52.749 | 2.0045 |
| SFD5 | 4230.452 | 38 | 52.435 | 2.0083 |
| SFD6 | 4230.206 | 38 | 52.260 | 2.0068 |
| SFD7 | 4229.964 | 38 | 52.083 | 2.0052 |
| SFD8 | 8222.506 | 0 | 71.120 | 2.0625 |
| SFD9 | 8212.077 | 38 | 62.238 | 1.805 |
| SFD10 | 8202.415 | 38 | 60.751 | 1.8954 |
| SFD11 | 8201.066 | 38 | 60.345 | 1.9009 |
| SFD13 | 15806.274 | 38 | 73.354 | .7336 |
| SFD14 | 15771.953 | 0 | 74.86 | 1.4972 |
| SFD15 | 15757.375 | 38 | 69.97 | 1.3994 |
| SFD16 | 15737.104 | 38 | 68.72 | 1.5806 |
| SFD17 | 15708.368 | 0 | 71.52 | 2.0024 |
| SFD18 | 15698.135 | 38 | 66.17 | 1.8528 |
| SFD19 | 15699.166 | 0 | 71.14 | 2.0630 |
| SFD20 | 15689.646 | 38 | 65.30 | 1.8938 |
| SFD21 | 15691.789 | 38 | 65.53 | 1.8713 |
| SFD22 | | Heals | | |
| SFD23 | | Propagates | | |

Table 5.3.6 Summary of static fixed displacement results. When the samples under fixed external displacement came to equilibrium the elastic strain energy ($E_{el}$), the crack surface energy ($E_s$), and the average stress on the boundary surfaces ( $\sigma_{ave}$) were monitored. Young's modulus (M) of the perfect samples and that (M') of samples with cracks were monitored.

| RUN | $d_{c-1}$ [d] | $d_c$ [d] | $d_{c+1}$ [d] |
|---|---|---|---|
| SFD2 | 1.063 | 1.137 | 1.313 |
| SFD4 | 1.429 | 1.532 | >1.6 |
| SFD5 | 1.460 | 1.561 | >1.6 |
| SFD6 | 1.476 | 1.575 | >1.6 |
| SFD7 | 1.491 | 1.594 | >1.6 |
| SFD9 | 1.125 | 1.284 | 1.446 |
| SFD10 | 1.328 | 1.446 | 1.579 |
| SFD11 | 1.403 | 1.521 | 1.621 |
| SFD13 | 1.022 | 1.034 | 1.108 |
| SFD14 | 1.014 | 1.014 | 1.014 |
| SFD15 | 1.051 | 1.100 | 1.258 |
| SFD16 | 1.064 | 1.141 | 1.323 |
| SFD17 | 1.019 | 1.019 | 1.019 |
| SFD18 | 1.215 | 1.379 | 1.517 |
| SFD19 | 1.020 | 1.020 | 1.020 |
| SFD20 | 1.438 | 1.549 | 1.640 |
| SFD21 | 1.387 | 1.510 | >1.6 |
| SFD22 | | Heals | |
| SFD23 | | >1.6 | >1.6 |

Table 5.3.7 Summary of static fixed displacement results. $d_c$ is the length of the crack tip bond, $d_{c-1}$ is that of the bond in front of the crack tip and $d_{c+1}$ is that of the first broken bond behind the crack tip.

| Run | $\sigma_c^L$ | $\sigma_{c-1}^L$ | $\sigma_{c-2}^L$ | $\sigma_{c-3}^L$ | $\sigma_c^U$ | $\sigma_{c-1}^U$ | $\sigma_{c-2}^U$ | $\sigma_{c-3}^U$ |
|---|---|---|---|---|---|---|---|---|
| SFD2 | 4.487 | 3.391 | 2.796 | 2.496 | 2.378 | 3.904 | 3.039 | 2.632 |
| SFD9 | 3.897 | 4.020 | 3.270 | 2.864 | 1.677 | 4.513 | 3.600 | 3.044 |
| SFD13 | 2.647 | 1.511 | 1.212 | 1.074 | 1.535 | 1.854 | 1.364 | 1.152 |
| SFD15 | 4.328 | 2.975 | 2.404 | 2.118 | 2.417 | 3.464 | 2.647 | 2.257 |
| SFD16 | 4.492 | 3.393 | 2.761 | 2.427 | 2.365 | 3.923 | 3.021 | 2.579 |
| SFD18 | 2.969 | 4.443 | 3.518 | 3.029 | 1.483 | 4.309 | 3.889 | 3.243 |
| SFD20 | 1.527 | 3.765 | 4.182 | 3.422 | 0.992 | 2.272 | 4.557 | 3.747 |

* in units of $\epsilon/d$.

Table 5.3.8 Summary of static fixed displacement results. Forces on atoms at the crack tip. $\sigma_c^L$ and $\sigma_c^U$ are the forces acting on the crack tip atoms on the lower and upper crack surfaces, respectively. (c-i) denotes the i-th atom in front of the crack tip.

| Strain | Poisson's ratio | Young's modulus $[\epsilon/d^2]$ | Stress $[\epsilon/d^2]$ |
|---|---|---|---|
| .000002 | .333334 | 83.1374 | .0002 |
| .0005 | .333334 | 82.8859 | .0414 |
| .001 | .330073 | 82.7339 | .0827 |
| .002 | .326824 | 82.3291 | .1647 |
| .003 | .323568 | 81.9240 | .2458 |
| .004 | .320395 | 81.5161 | .3261 |
| .005 | .317221 | 81.1082 | .4055 |
| .006 | .314128 | 80.6977 | .4842 |
| .007 | .311076 | 80.2862 | .5620 |
| .008 | .308055 | 79.8739 | .6390 |
| .009 | .305085 | 79.4603 | .7151 |
| .01 | .302145 | 79.0462 | .7905 |
| .10 | .139004 | 45.4419 | 4.5442 |
| .20 | .066233 | 23.4250 | 4.6850 |
| .25 | .046886 | 16.9424 | 4.2356 |
| .30 | .033585 | 12.3610 | 3.7083 |

(continued)

| Strain | Poisson's ratio | Young's modulus $[\epsilon/d^2]$ | Stress $[\epsilon/d^2]$ |
|---|---|---|---|
| .01 | .302145 | 79.0462 | .7905 |
| .02 | .274738 | 74.8810 | 1.4976 |
| .03 | .250525 | 70.7299 | 2.1219 |
| .04 | .229017 | 66.6556 | 2.6662 |
| .05 | .209819 | 62.7018 | 3.1351 |
| .06 | .192611 | 58.8975 | 3.5339 |
| .07 | .177128 | 55.2616 | 3.8683 |
| .08 | .163151 | 51.8046 | 4.1444 |
| .09 | .150495 | 48.5312 | 4.3678 |
| .10 | .139004 | 45.4419 | 4.5442 |
| .11 | .128544 | 42.5341 | 4.6788 |
| .12 | .119004 | 39.8030 | 4.7764 |
| .13 | .110283 | 37.2421 | 4.8415 |
| .14 | .1022967 | 34.8442 | 4.8782 |
| .15 | .094971 | 32.6013 | 4.8902 |
| .16 | .088242 | 30.5052 | 4.8808 |
| .17 | .082051 | 28.5477 | 4.8531 |
| .18 | .076348 | 26.7204 | 4.8097 |
| .19 | .071088 | 25.0155 | 4.7529 |
| .20 | .066233 | 23.4250 | 4.6850 |

Table 5.4.1 Material properties of the sample without crack at different strains.

| Run | $e^S_{Critical}$ | M' $[\epsilon/d^2]$ | $e_{Critical}$ | $(2\gamma/\pi M l)^{1/2}$ |
|---|---|---|---|---|
| DFD1 | .047 | 62.90 | .048 | .032 |
| SFD7 | .038 | 52.08 | .039 | .031 |
| DFD3 | .035 | 66.67 | .037 | .031 |
| SFD11 | .032 | 60.35 | .035 | .031 |
| SFD20 | .029 | 65.29 | .033 | .030 |

$e_{Griffith} = \sqrt{2\gamma/\pi M_0 l} = .028$ (for infinite sample)

$e_{Critical} = \sqrt{(2\gamma/\pi M' l)(1 + 2\pi l^2/A)}$ (for finite sample)

$e^S_{Critical}$ = Critical strain from simulations

Table 5.5.1 Comparis on of Griffith theory with the present result.

| Applied strain, e | $d_c$ [d] | $d_{c+1}$ [d] | Comments |
|---|---|---|---|
| 0.0285 | | <1.60 | crack heals |
| 0.02875 | 1.510 | 1.614 | crack stable |
| 0.0290 | 1.549 | 1.646 | crack stable |
| 0.0295 | >1.60 | >1.60 | crack propagates |

Table 5.7.1 Data of lattice trapping studies ( fixed displacement). The external strain of the large sample ($N_R$=79, NTM = 135) was lowered from .029 by a small percentage to find the external strain below which the crack (without knife) heals. The external strain was then increased from .029 by a small percentage to find the strain above which the crack propagates.

| Run | $N_R$ | $NTM_{odd}$ | e | e + Δe | Percent increase | $NBB_{Tot}$ | Curve |
|---|---|---|---|---|---|---|---|
| DFD1 | 27 | 55 | .047 | .0475 | 1.0 | 59 | 1 |
| DFD2 | 47 | 87 | .0349 | .0352 | 0.9 | 40 | 2 |
| DFD3 | 47 | 87 | .0349 | .0354 | 1.4 | 40 | 3 |
| DFD4 | 59 | 95 | .0315 | .0318 | 1.0 | 50 | 4 |
| DFD5 | 79 | 135 | .029 | .0293 | 1.0 | 45 | 5 |
| DFD6 | 79 | 135 | .029 | .0295 | 1.7 | 22 | |

$NBB_{Tot}$: Total number of broken bonds including 19 initial broken bonds.

DFD6 : This run was performed in a controlled fashion with the help of critical damping for the purpose of studying stress profiles.

Table 6.2.1 Summary of dynamic fixed displacement results. Four different samples with a crack of length 9.75d were first brought to equilibrium under an external strain (e) just below the critical strain. The external strain was then increased from e to e + Δ e by approximately one percent to study crack propagation.

| Run | Strain | $d_{c-1}$ [d] | $d_c$ [d] | $d_{c+1}$ [d] | $V_T/V_L$ | $l_T$ [d] |
|---|---|---|---|---|---|---|
| DFD1 | .0470 | 1.45 | 1.55 | 1.63 | .053 | 13.25 |
| DFD2 | .0349 | 1.44 | 1.55 | 1.63 | .093 | 14.75 |
| DFD3 | .0349 | 1.44 | 1.55 | 1.63 | .096 | 14.75 |
| DFD4 | .0315 | 1.40 | 1.52 | 1.62 | .108 | 15.75 |
| DFD5 | .0290 | 1.44 | 1.55 | 1.64 | .113 | 15.25 |

$l_T$ : Crack half-length at which terminal velocity is attained.

Table 6.2.2 Summary of dynamic fixed displacement results. Crack tip bond length ($d_c$, $d_{c-1}$ and $d_{c+1}$) at external strain e. $V_T$ is the terminal crack velocity. $V_L$ is the longitudinal velocity of sound.

Run DFD6

| Step | Strain | Force* on atom (row 39) | | | | | |
|---|---|---|---|---|---|---|---|
| | | 53 | 54 | 55 | 56 | 57 | 58 |
| 3600 | .0290 | 2.756 | 3.011 | 3.422 | 4.182 | 3.764 | 1.527 |
| 3640 | .0295 | 2.800 | 3.065 | 3.504 | 4.336 | 3.401 | 1.417 |
| 3680 | .0295 | 2.824 | 3.105 | 3.577 | 4.463 | 3.033 | 1.324 |
| 3720 | .0295 | 2.859 | 3.178 | 3.719 | 4.557 | 2.386 | 1.003 |
| 3760 | .0295 | 2.930 | 3.278 | 3.884 | 4.425 | 1.891 | 0.905 |
| 3800 | .0295 | 2.982 | 3.362 | 4.042 | 4.100 | 1.633 | 0.449 |
| 3840 | .0295 | 3.078 | 3.535 | 4.402 | 3.229 | 1.362 | 0.533 |

| Step | Strain | Force* on atom (row 40) | | | | | |
|---|---|---|---|---|---|---|---|
| | | 53 | 54 | 55 | 56 | 57 | 58 |
| 3600 | .0290 | 2.663 | 2.870 | 3.193 | 3.747 | 4.557 | 2.272 |
| 3640 | .0295 | 2.704 | 2.919 | 3.259 | 3.847 | 4.495 | 1.996 |
| 3680 | .0295 | 2.725 | 2.952 | 3.310 | 3.938 | 4.340 | 1.784 |
| 3720 | .0295 | 2.749 | 3.002 | 3.405 | 4.139 | 3.980 | 1.578 |
| 3760 | .0295 | 2.806 | 3.079 | 3.534 | 4.399 | 3.253 | 1.380 |
| 3800 | .0295 | 2.848 | 3.146 | 3.657 | 4.550 | 2.680 | 1.241 |
| 3840 | .0295 | 2.928 | 3.279 | 3.890 | 4.448 | 1.891 | 0.906 |

* in units of $[\epsilon/d]$

Table 6.2.3 Summary of dynamic fixed displacement results. Forces acting on atoms near the crack tip.

| Run | Steps from | to | Continued from run | $\sigma$ $[\epsilon/d^2]$ | Damp | NBB | Comments |
|---|---|---|---|---|---|---|---|
| DFL1 | | 15780 | | .60 | yes | 78 | Equilibrium |
| DFL2 | 15780 | 17920 | DFL1 | .65 | no | 78 | Bond stretching |
| DFL3 | 17100 | 17300 | DFL2 | .65 | no | 38 | Heals |
| DFL4 | 17920 | 19200 | DFL2 | .65 | yes | 78 | Equilibrium |
| DFL5 | 17920 | 19200 | DFL2 | .67 | no | 78 | Equilibrium |
| DFL6 | 15780 | 17420 | DFL1 | .67 | no | 78 | Propagates |
| DFL7 | 16780 | 17420 | DFL6 | .67 | yes | 78 | Equlibrium |
| DFL8 | 17330 | 17920 | DFL6 | .67 | yes | 78 | Propagates |

Table 6.2.4 Summary of dynamic fixed load results. Brittle to ductile transition. At fixed load the system is very sensitive to the rate of change of the applied load. For a slow load change local distortion at the crack tip is favored. For a sudden change, propagation occured.

| Run | $S_1^{Sta}$ [1/ ] | $S_1^{Dyn}$ [1/ ] | $S_2^{Sta}$ [1] | $S_2^{Dyn}$ [1] | $S_3^{Dyn}$ [m / $d^4$] |
|---|---|---|---|---|---|
| DFD1 | $8.04X10^{-5}$ | $7.77X10^{-5}$ | $3.55X10^{-3}$ | $3.55X10^{-3}$ | 1.05 |
| DFD2 | $2.66X10^{-5}$ | $2.36X10^{-5}$ | $1.95X10^{-3}$ | $2.11X10^{-3}$ | 1.37 |
| DFD4 | $1.89X10^{-5}$ | $1.94X10^{-5}$ | $1.59X10^{-3}$ | $1.79X10^{-3}$ | 1.34 |
| DFD5 | $.097X10^{-5}$ | $1.06X10^{-5}$ | $1.35X10^{-3}$ | $1.50X10^{-3}$ | 2.49 |

$S_1$ = Slope of the line: $(1/M')$ vs. $l^2$

$S_2$ = Slope of the line: $(-\Delta E_{el}/2)$ vs. $l^2M'$

$S_3$ = Slope of the line: $(E_k/2)$ vs. $l^2 v_c^2$

Sta : Static simulation

Dyn : Dynamic simulation

$S_1^{Theory} = 2\pi/MA$

$S_2^{Theory} = \pi e^2/2$

$S_3^{Mott} = k \rho e^2/2$

Table 6.3.1 Summary of static fixed displacement resutls. Comparis on with Mott theory.

| Run | A $[d^2]$ | $\delta$ | e | $M_{Sta}$ $[\epsilon/d^2]$ | $M_{Dyn}$ $[\epsilon/d^2]$ | $M'_{Sta}$ $[\epsilon/d^2]$ | $M'_{Dyn}$ $[\epsilon/d^2]$ |
|---|---|---|---|---|---|---|---|
| DFD1 | 1227.2 | .487 | .047 | 63.68 | 62.90 | 42.83 | 42.55 |
| DFD2 | 3445.9 | .173 | .0349 | 68.69 | 66.67 | 58.54 | 56.78 |
| DFD4 | 4746.7 | .126 | .0315 | 70.01 | 70.42 | 62.27 | 60.38 |
| DFD5 | 9085.5 | .066 | .029 | 71.13 | 71.43 | 66.75 | 65.29 |

$M_{Sta} = M_o - 414e$ $\qquad M_o = 83.14$

$M'_{Sta} = M_{Sta}/(1+\delta l^2/l_o^2)$ $\qquad \delta = 2\pi l_o^2/A$

$M_{Dyn}$ = Modulus obtained by extrapolating lines in figure 6.2.4

$M'_{Dyn}$ = Modulus obtained from simulation

Table 6.3.2 Summary of dynamic fixed displacement results. Comparis on of modulus obtained from static and dynamic simulations.

| Run | FF $[\epsilon/d^2]$ | FS $[\epsilon/d^2]$ | SS $[\epsilon/d^2]$ | $\sigma_1$ $[\epsilon/d^2]$ | $\sigma_2$ $[\epsilon/d^2]$ | $t_0$ |
|---|---|---|---|---|---|---|
| DFLF1 | 1.0 | 1.0 | 1.0 | 1.90 | 2.09 | 1000 |
| DFLF2 | 2.0 | 1.5 | 1.0 | 2.89 | 3.00 | 1000 |
| DFLF3 | 5.0 | 1.0 | 1.0 | 3.80 | 3.99 | 1300 |

$t_0$ = timestep at which $\sigma_2$ is applied

Table 7.2.1 Summary of dynamic fixed load studies of crack coated with 3 layers of film.

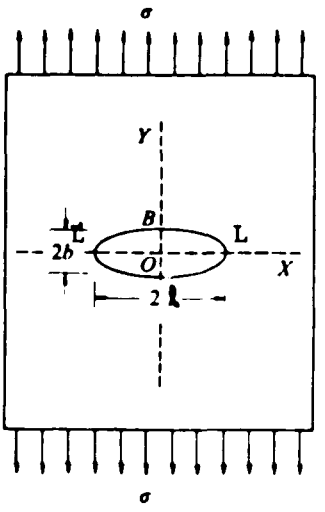


Figure 1.1.1 Plate containing elliptical hole, semi-axes b and l, subjected to uniform applied tension. (after Lawn and Wilshaw (1975))

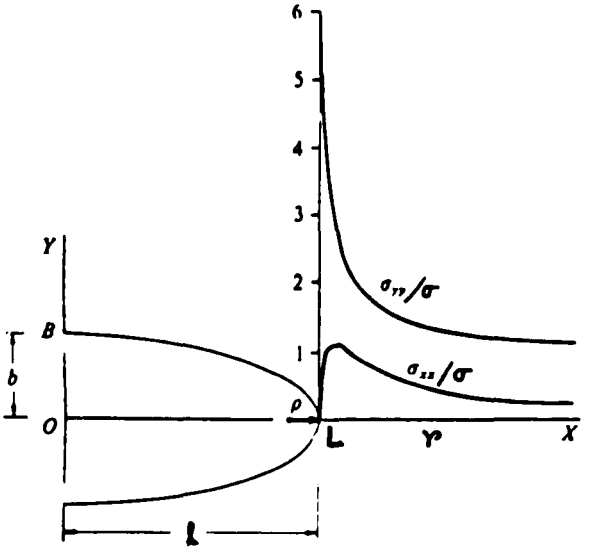


Figure 1.1.2 Stress concentration at elliptical hole, l=3b. Note that the stress cocentration is localised within ≈l from the tip, with stress gradient within≈ρ from the tip. (after Lawn and Wilshaw (1975))

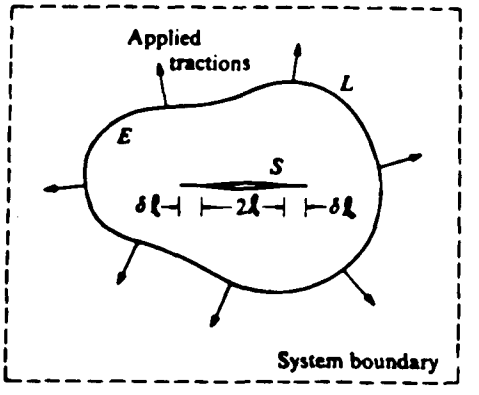


Figure 1.2.1 Static plane crack system. E, elastic medium; S, crack surface; L, applied loading. (after Lawn and Wilshaw (1975))

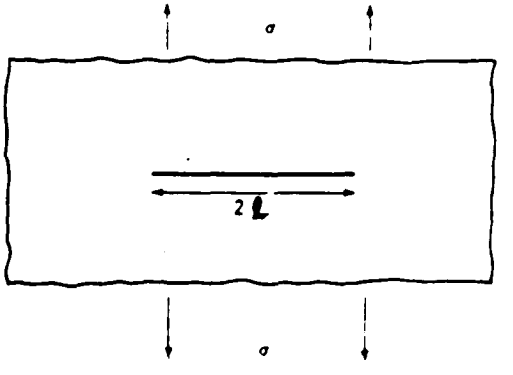


Figure 1.2.2 Griffith crack: gemetrical configuration. (after Lawn and Wilshaw (1975))

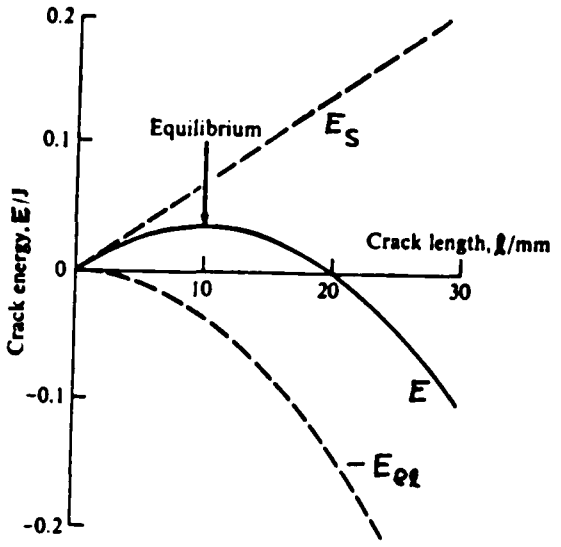


Figure 1.2.3 Energetics of Griffith crack in uniform tension. Data for glass from Griffith's paper: $\gamma$ =1.75J/m$^{-2}$, M=6.2X10$^{10}$ N/m$^{-2}$, =2.63X10$^{10}$ N/m$^{-2}$ (selected to give equilibrium at l=10mm. (after Lawn and Wilshaw (1975))

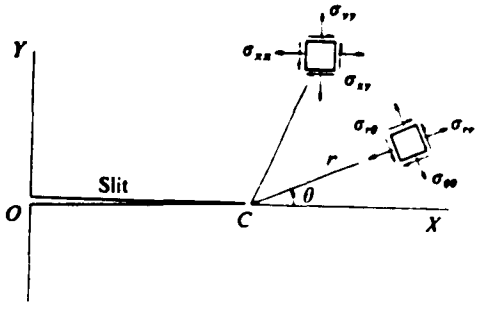


Figure 1.3.1 Crack tip stresses, showing triangular and polar components. (after Lawn and Wilshaw))

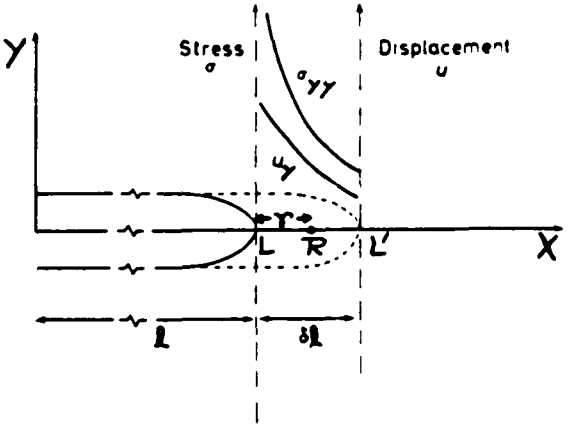


Figure 1.3.2 Calculation of G from work done by crack tip stress field. (after Knott (1973))

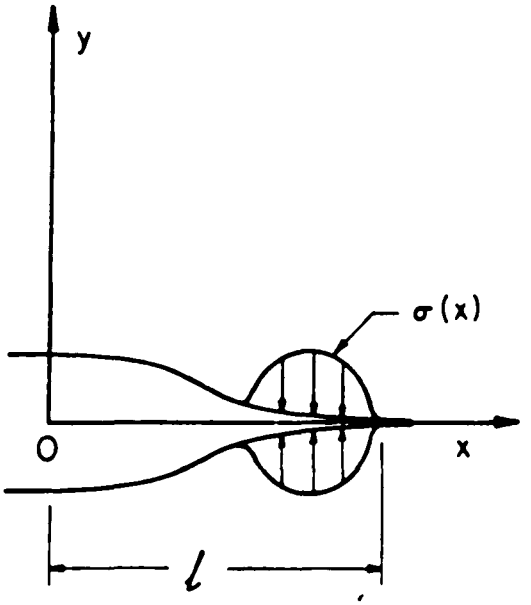


Figure 1.4.1 Barenblatt's hypothesis. (after Eringen (1977 ))

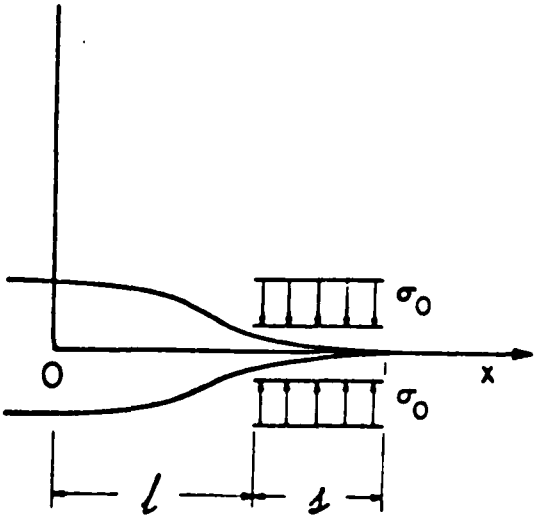


Figure 1.4.2 Khristianowich-Dugdale hypothesis. (after Eringen (1977))

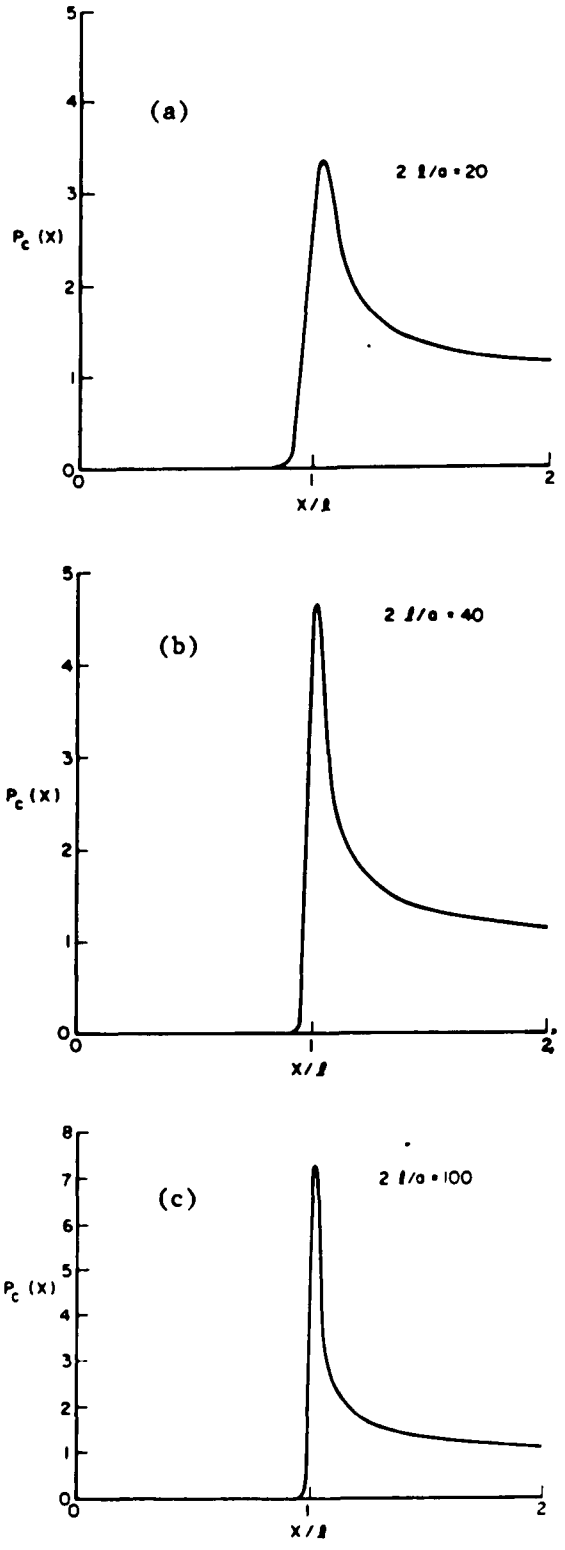


Figure 1.4.3 Stress concentration along crack direction. (after Eringen (1977))

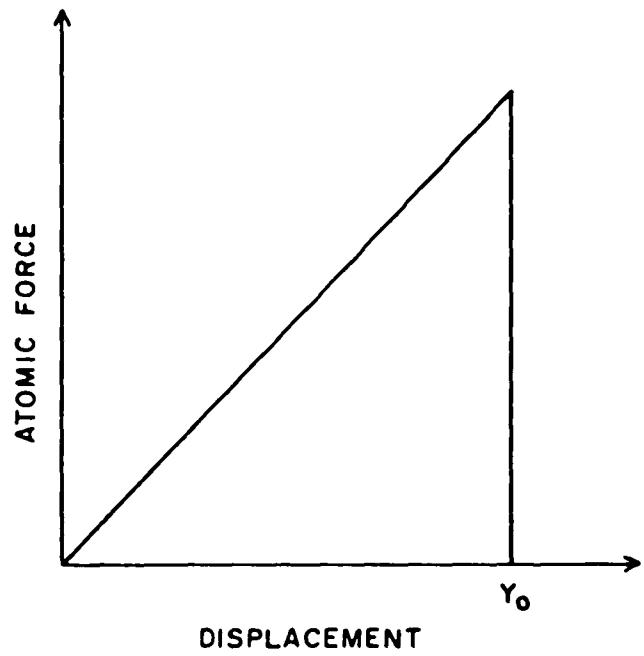


Figure 2.1.1 The assumed force law between the atoms is linear to a displacement $y_o$ at which point the bond snaps discontinuously and the force falls to zero. (after Thomson et al (1971))

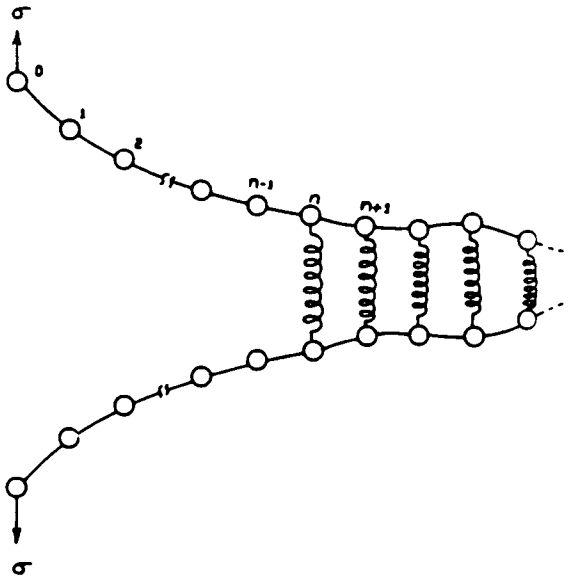

Figure 2.1.2 One dimensional model of a crack. Two semi-infinite chains of atoms are bonded together horizontally by bendable bonds and vertically by stretchable bonds. (after Thomson et al (1971))

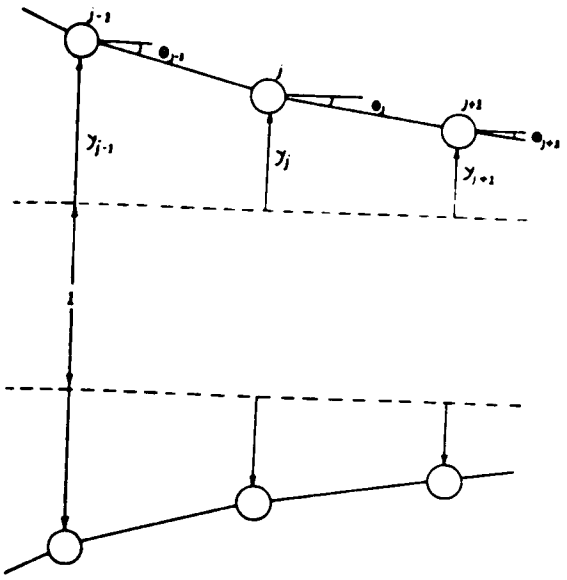

Figure 2.1.3 Schematic drawing depicting the calculation of the energy in the bendable bonds. (after Thomson et al (1971))

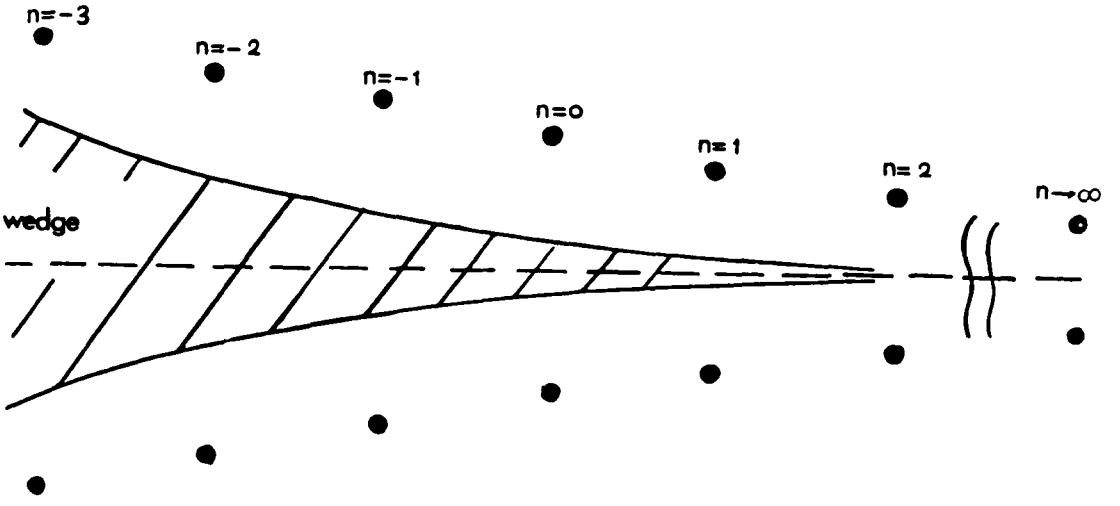


Figure 2.1.4 Atomic model of a crack. The atoms are considered to be forced apart by the wedge which is driven to the right under the force $\sigma$. (after Thomson et al (1971))

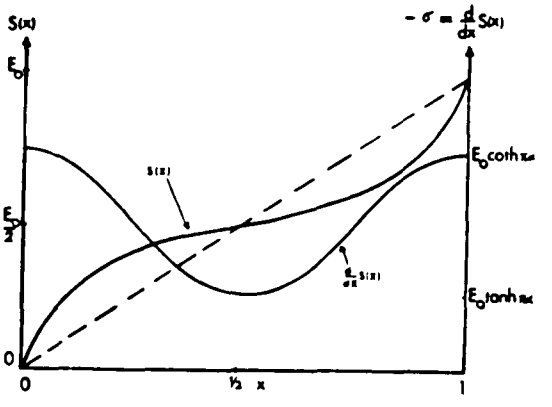


Figure 2.1.5 Functional form of the surface energy for moving a crack S(x) (plotted on the left axis), and the corresponding force $\sigma = -dS/dx$ (plotted on the right). The dashed line represents the average surface energy used in the continuum approximation. (after Thomson et al (1971))

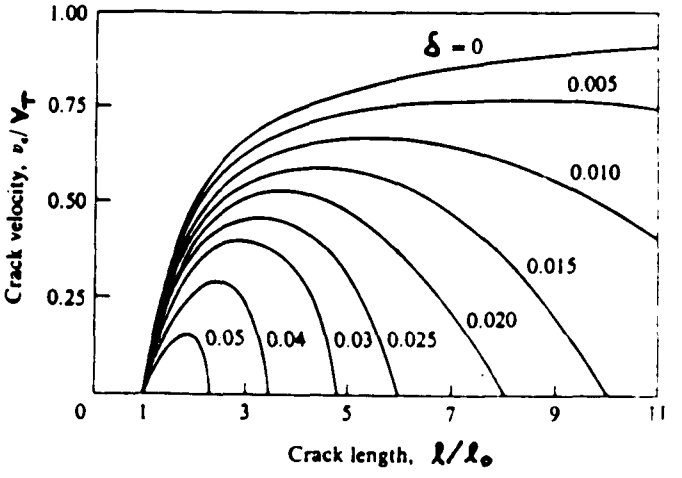


Figure 3.1.1 Crack velocity as function of crack length for a tensile system. In the small-crack limit, $\delta \rightarrow 0$, fixed load and fixed displacement loading give identical result. Curves $\delta > 0$ refer to fixed displacement loading only. (after Lawn and Wilshaw (1975))

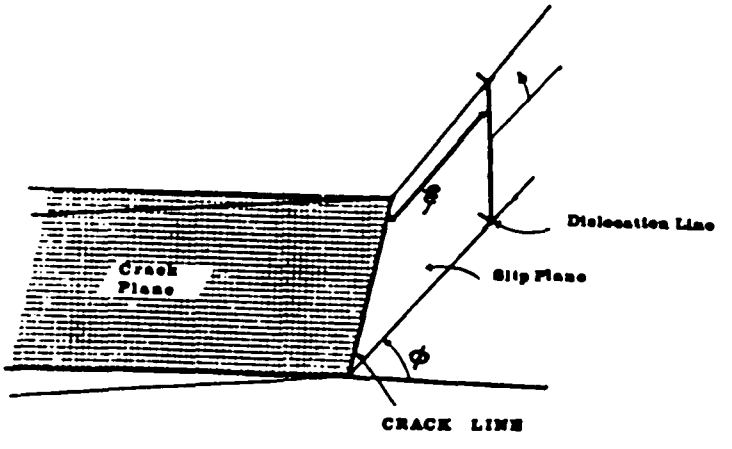


Figure 3.2.1 Geometry of the dislocation-crack configuration in two dimensions. b is the burger vector. (after Rice and Thomson (1974))

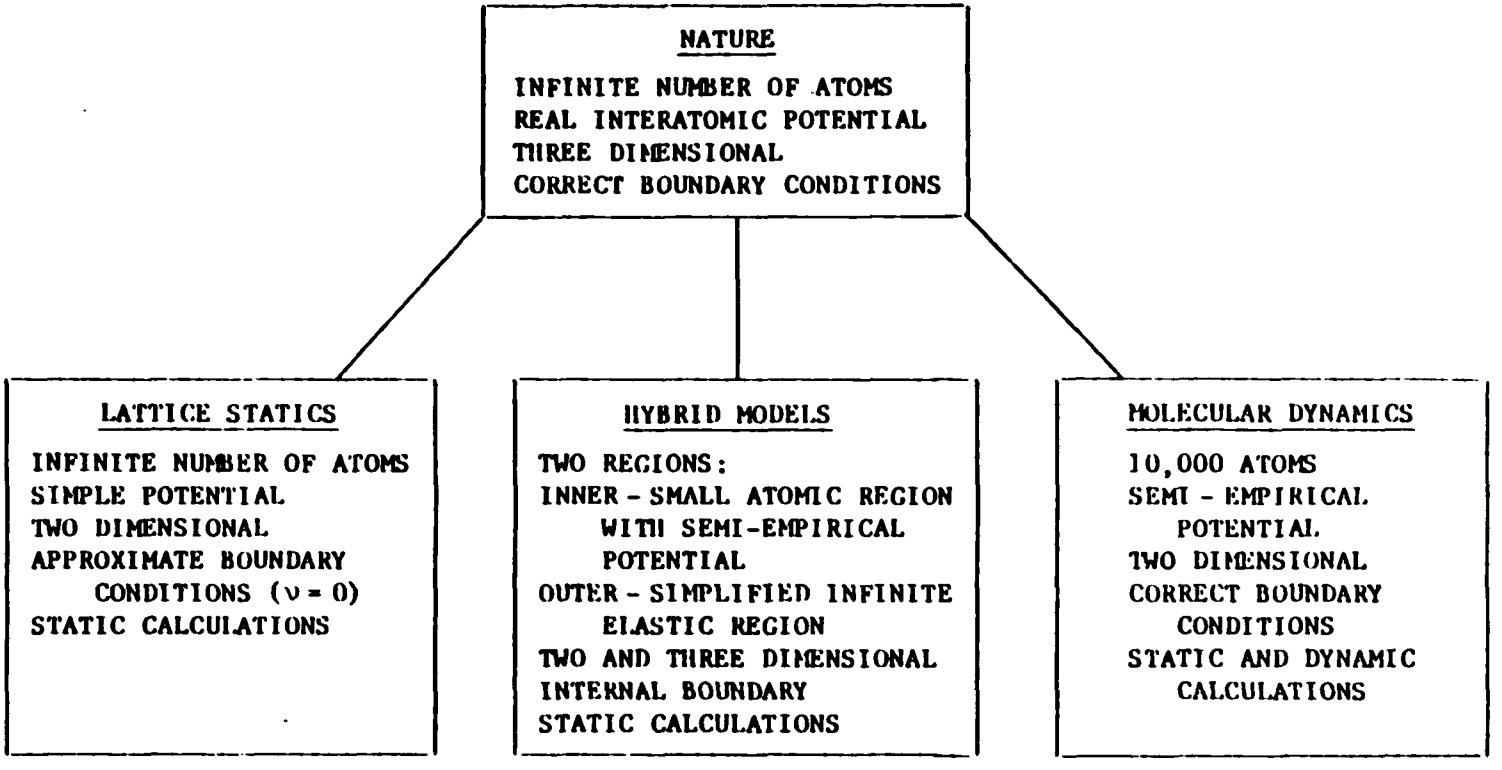


Figure 4.1.1 Illustration of the various approaches to the modeling of cracks in crystalline solids.

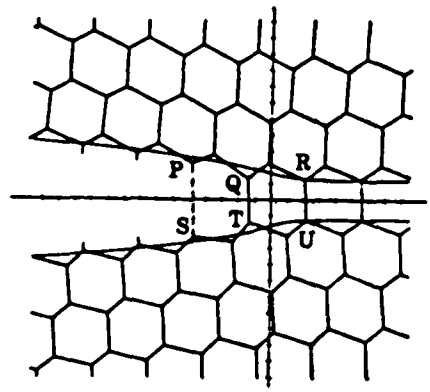


Figure 4.2.1 Computer-relaxed atomic configuration near an equilibrium (111) crack tip in silicon. (after Sinclair and Lawn (1972))

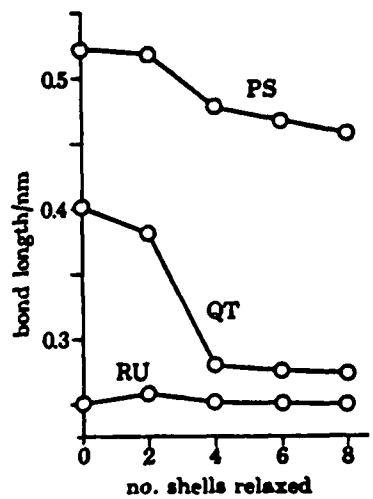


Figure 4.2.2 Dependence of Si-Si bond lengths PS, QT, RU on size of relaxed region. As region I is increased from 2 to 4 rectangular shells, the bond QT contracts from the 'ruptured' to the 'stretched' state, thus enclosing the crack by one atomic spacing.

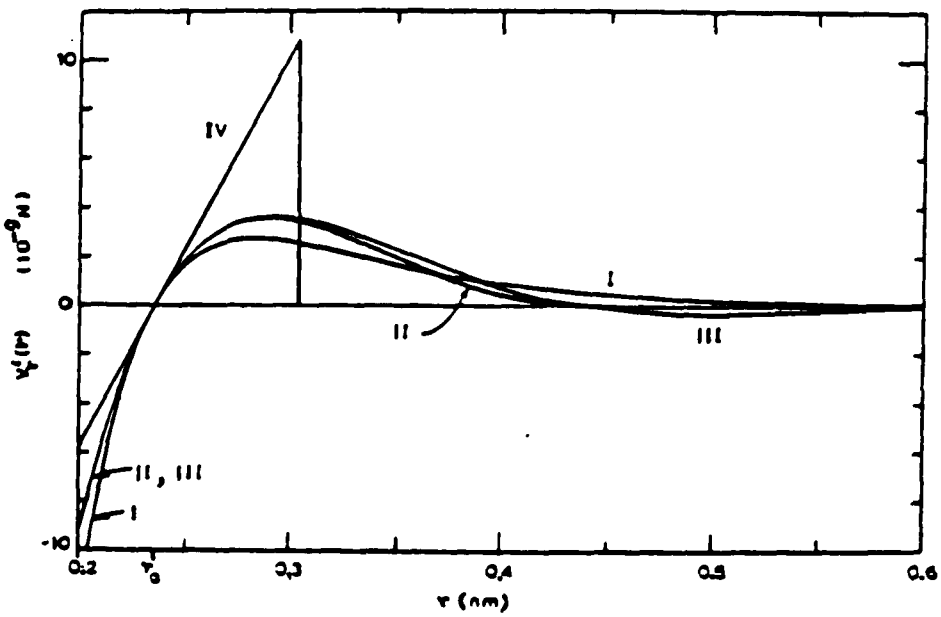


Figure 4.2.3 The radial component of the force laws derived from potentials I to IV.

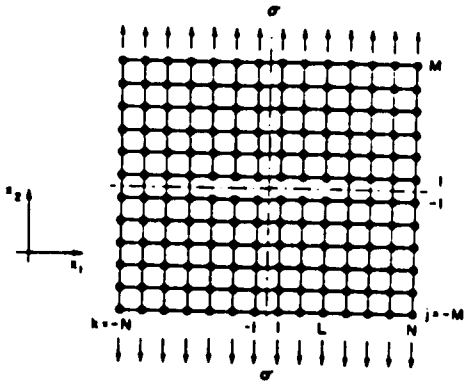

Figure 4.2.4 Idealised crystal model. Atomic motion in y direction alone is permitted. (after Weiner and Pear (1975))

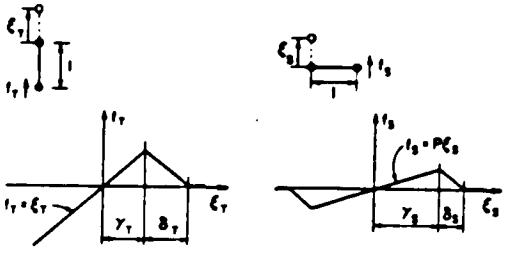

Figure 4.2.5 Plot of $f_T$ vs. $\xi_T$ shows piecewise linear tensile force law for neighboring atoms in the same column. Plot of $f_S$ vs. $\xi_S$ shows piecewise linear shear force law for atoms in neighboring columns. (after Weiner and Pear (1975))

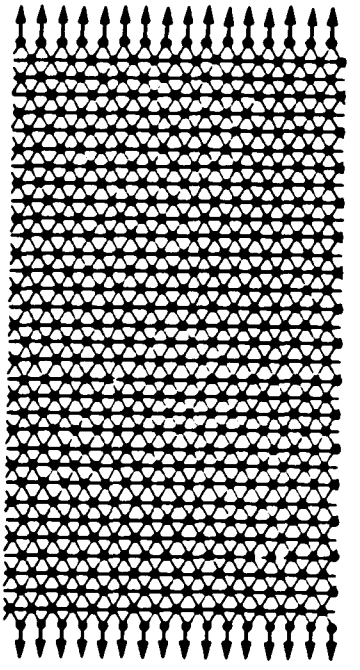

Figure 4.2.6 A triangular lattice of mass points joined by Hooke's law springs. The particles interact with 32 additional boundary particles which in turn interact with fixed external force on the upper and lower boundary particles (under fixed external load condition). (after Ashurst and Hoover (1976))

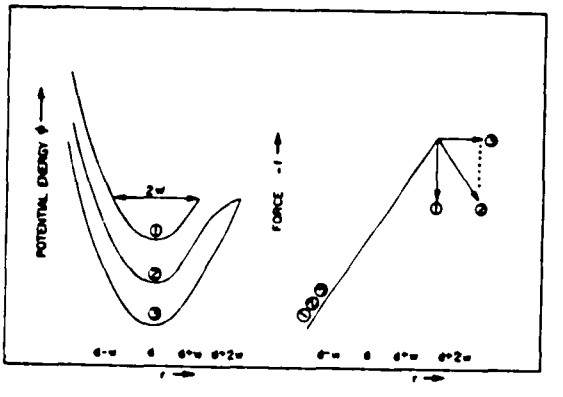


Figure 4.2.7 Interparticle potentials $\phi(r)$ and forces $f(r) = -\phi'(r)$. All these potentials have the same curvature at the minimum and hence the same linear elastic properties. The tensile strength of the crystal depends on the potential width $\omega$. (after Ashurst and Hoover (1976))

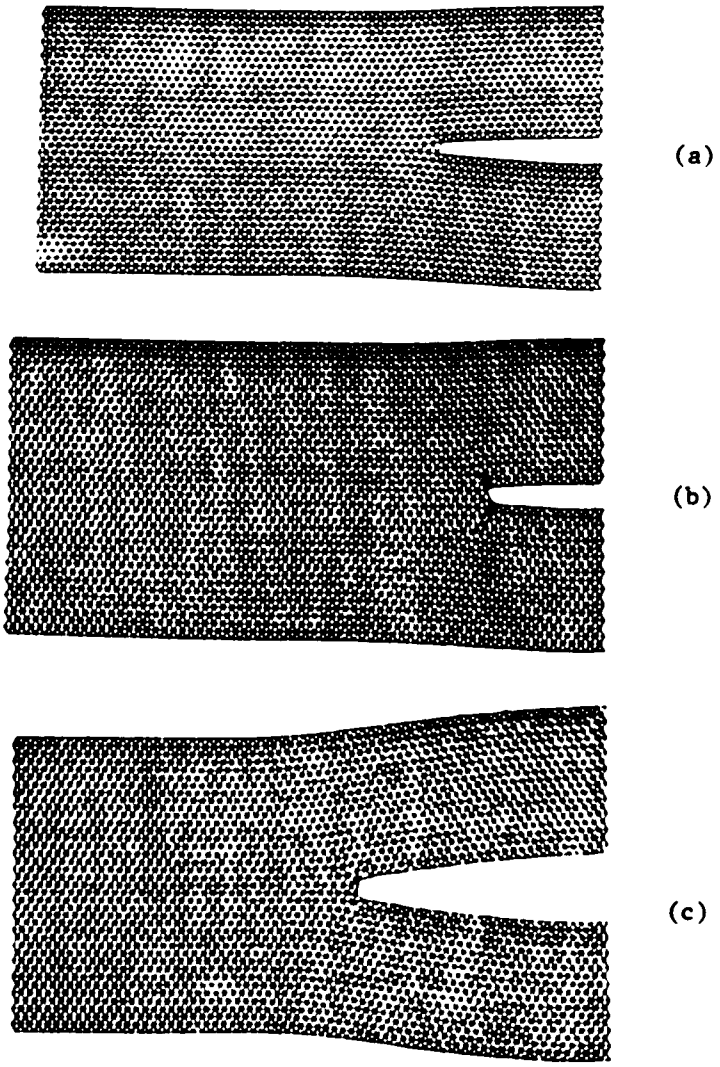


Figure 4.2.8 A two dimensional triangular lattice with a crack. Because of the mirror symmetry the entire sample can be obtained by refection about the right-handed side of the figure. Forces are applied to atoms in the 1st and 39th rows (applied $\sigma$). Lines are drawn between atoms that are less than 1.6d apart. (a) Clean brittle fracture at $\sigma$=0.5 and NBB = 39 ( NBB is the number of initially broken bonds for the half sample). (b) Incipient dislocation formation at $\sigma$ = 1.3 and NBB = 19. The extra lines designate the atoms that have moved into the range of interaction. (c) Dislocation formed at the lower end of the crack tip at $\sigma$ =1.3 and NBB = 39. This dislocation later on propagated to the surfaces. (after Paskin et al (1980))

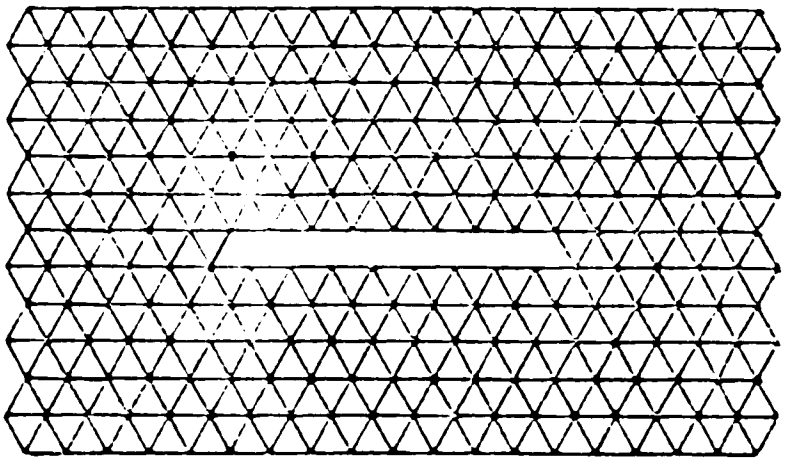

(a)

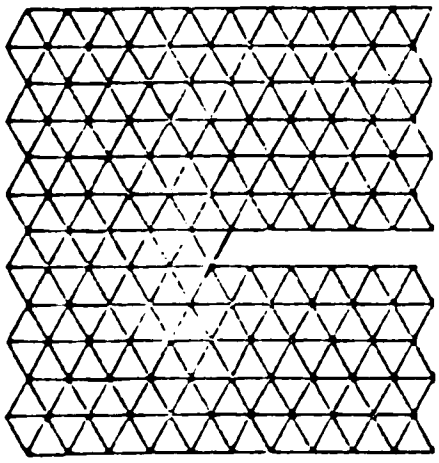

(b)

Figure 5.1.1 Arrangement of atoms in a triangular lattice.
(a) Full sample and (b) Half sample.

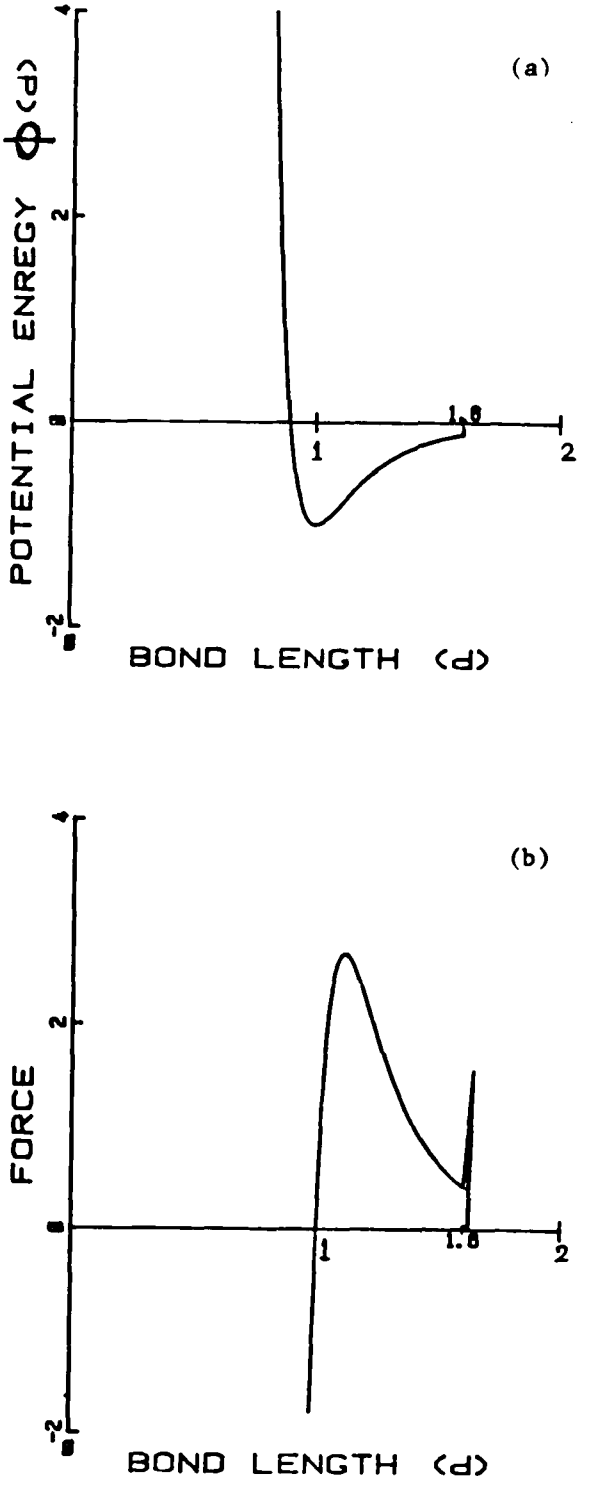


Figure 5.1.2 (a) Truncated Lennard Jones potential as used in all simulations. (b) Corresponding truncated force.

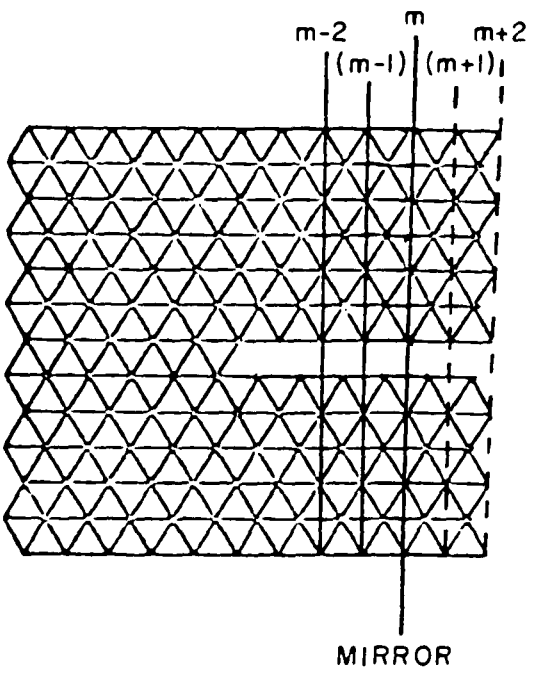


Figure 5.1.3 Half sample with two extra columns of atoms. The columns (m+1) and (m+2) are mirror images of columns (m-1) and (m-2) respectively.

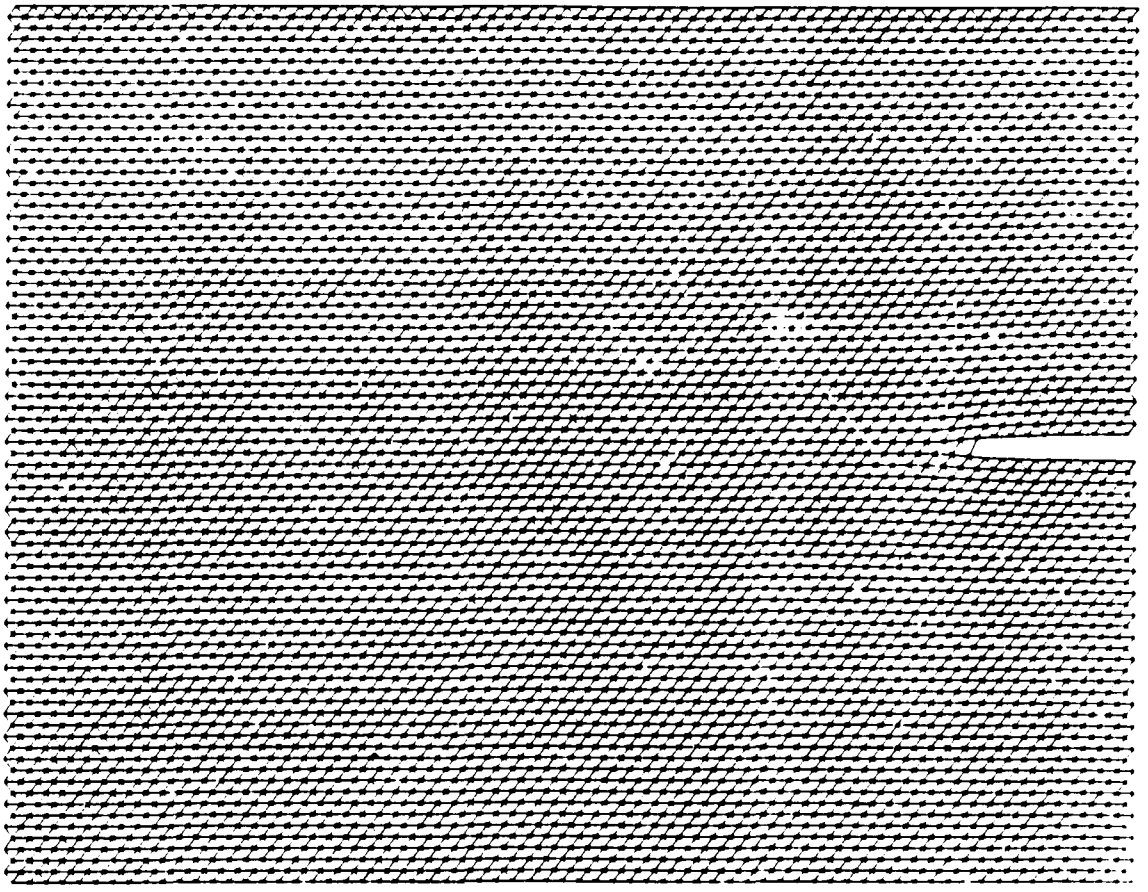

Figure 5.1.4 Half sample (~5,000 atoms) used in the static and dynamic studies of homogenous material.

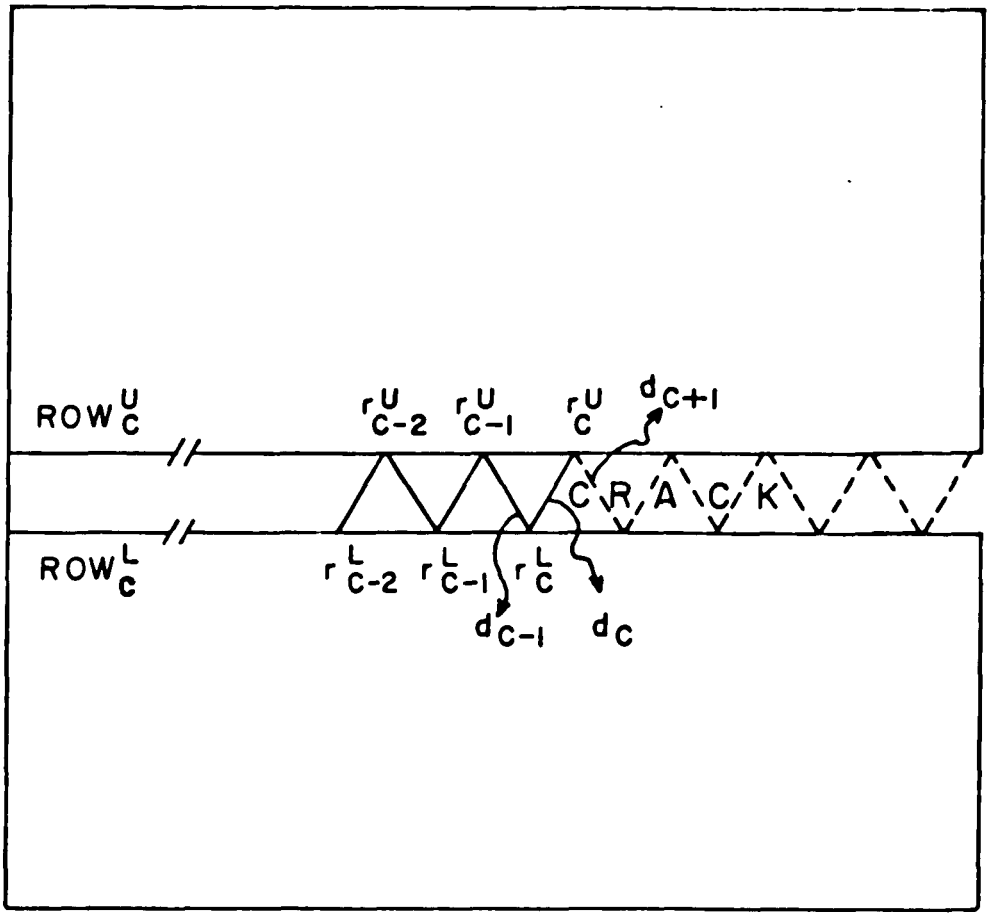


Figure 5.1.5 Labelling of bonds and atoms near the crack tip.

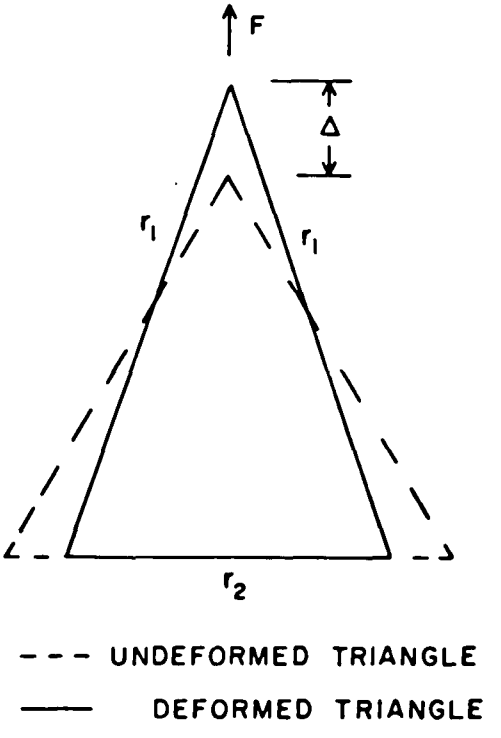


Figure 5.4.1 Tensile deformation of the elementary triangle.

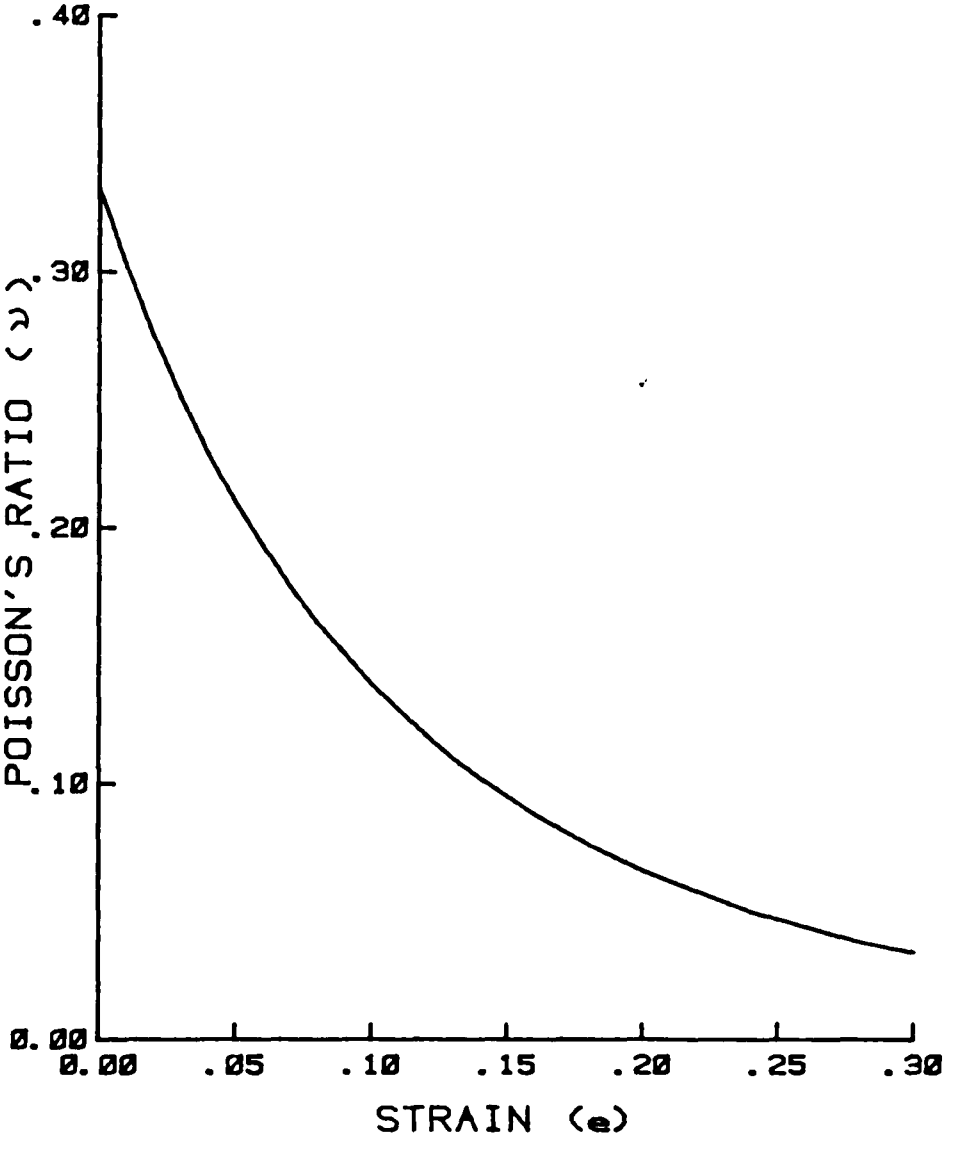


Figure 5.4.2 Variation of Poisson's ratio with strain for the perfect sample.

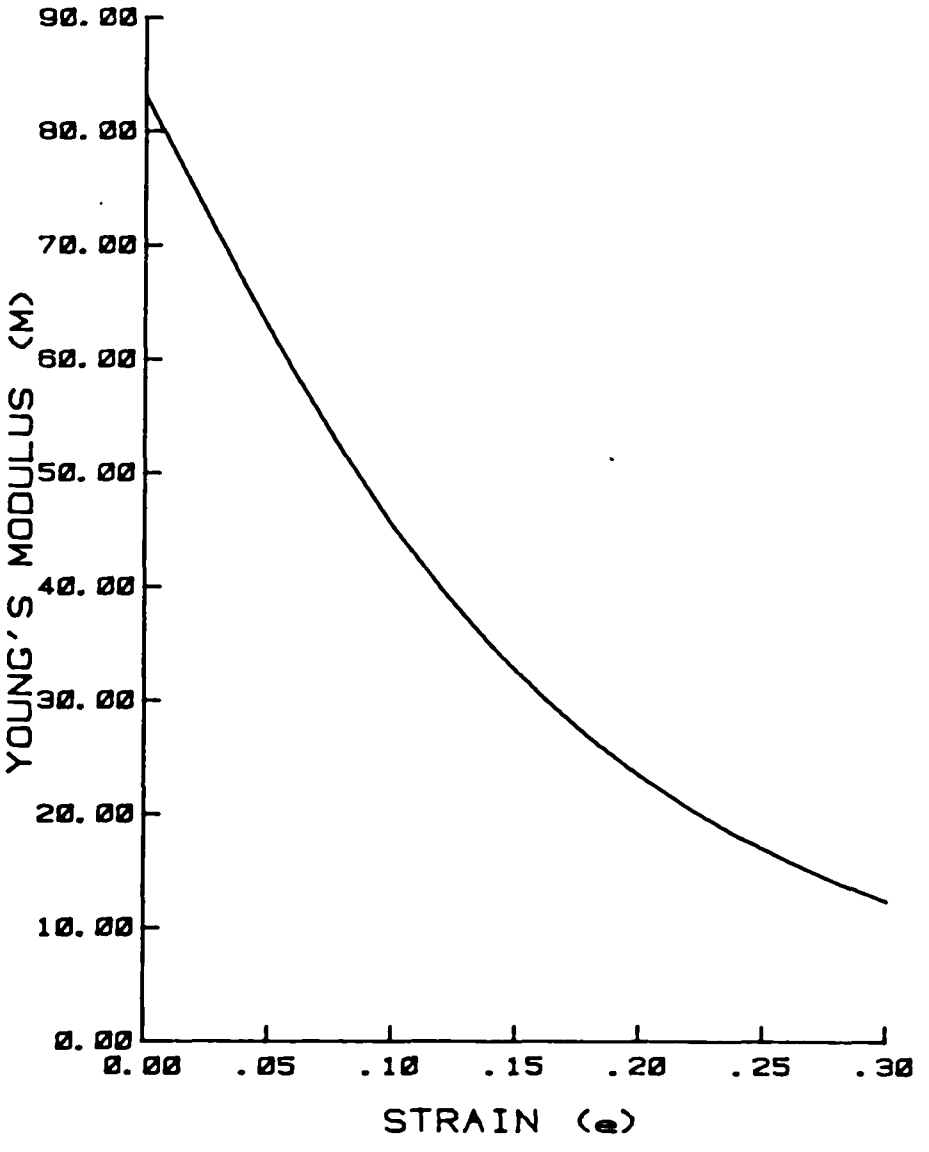


Figure 5.4.3 Plot of Young's modulus vs. strain for the perfect sample.

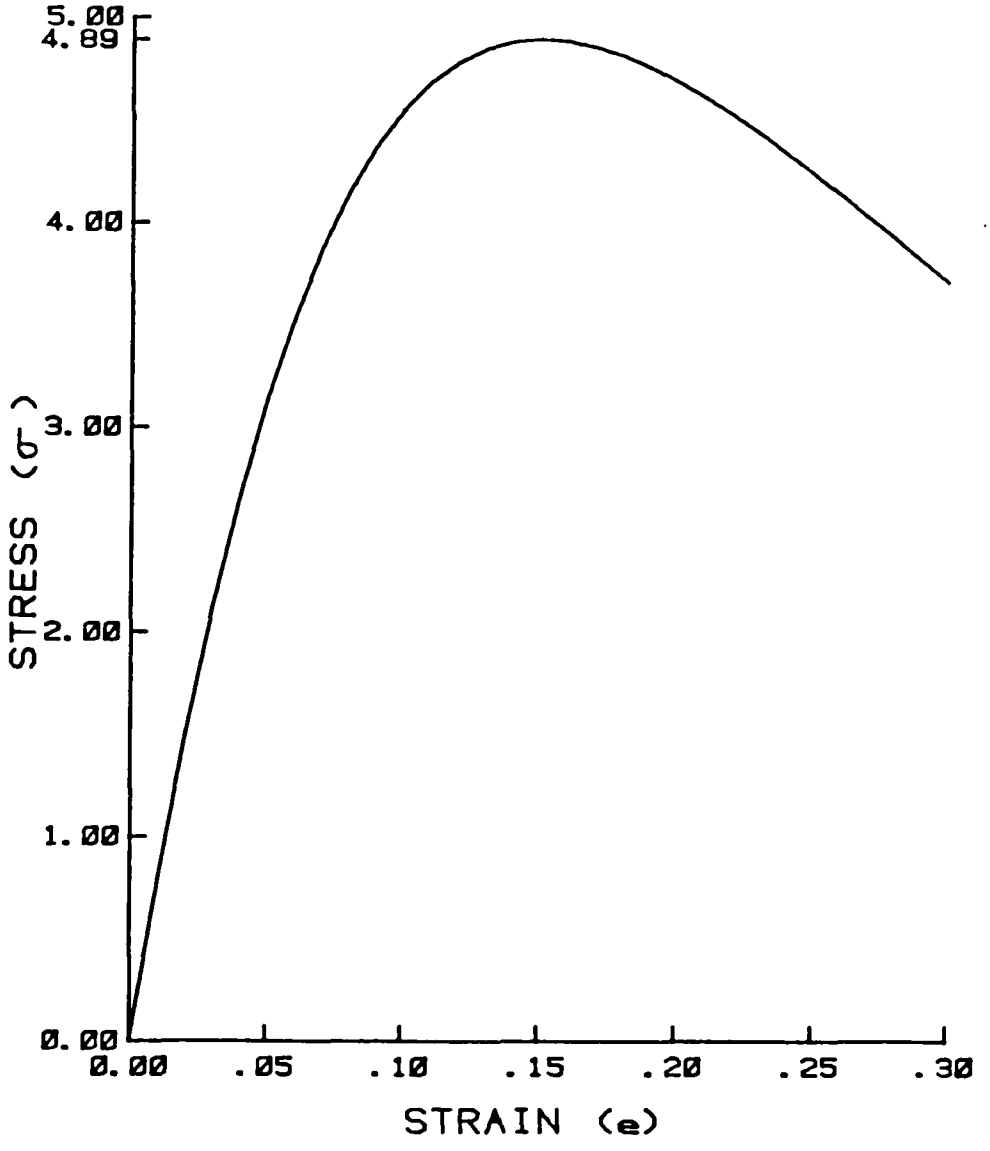


Figure 5.4.4 Plot of stress vs. strain for the perfect sample.

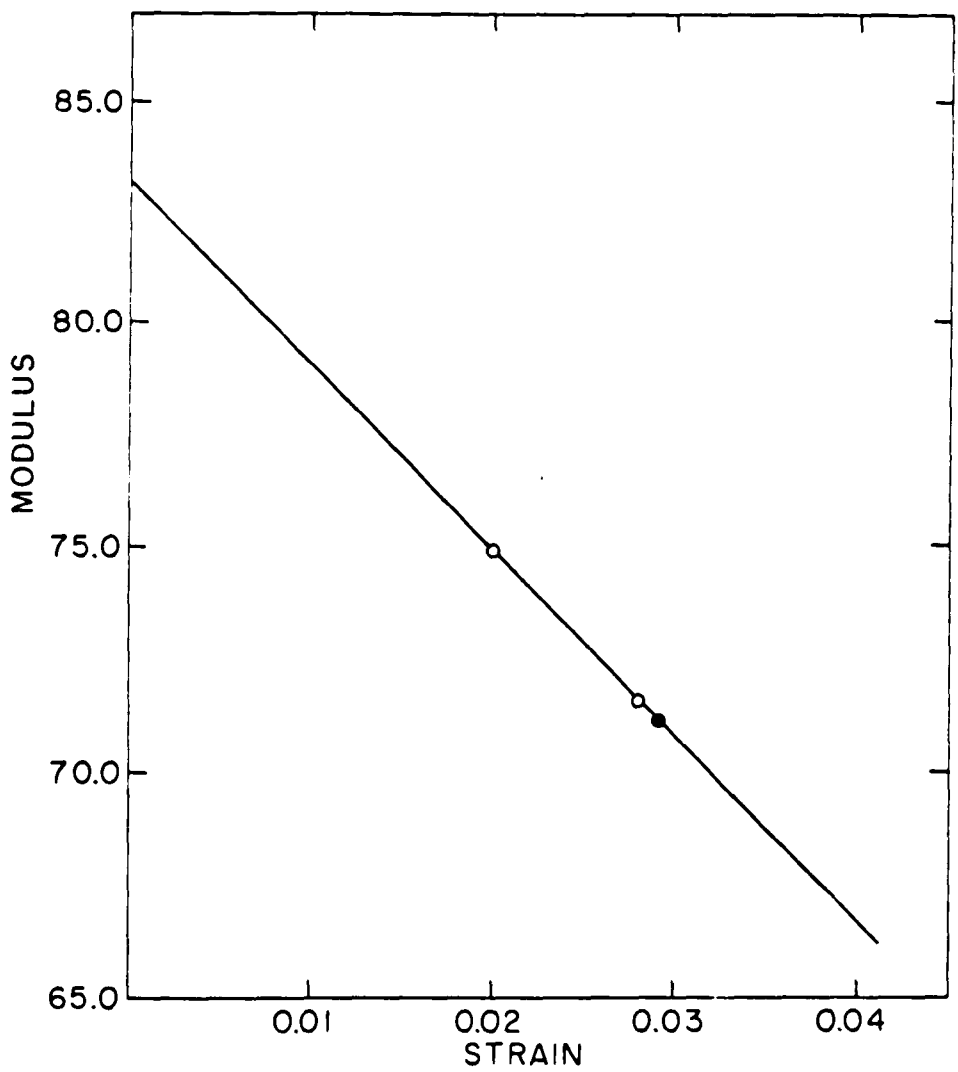


Figure 5.4.5 Young's modulus M vs. strain. The full circle represents three sample sizes spanning a factor of 4 in area; the moduli were identical within 0.1% independent of size. The straight line is the theoretical behavior of the modulus against strain for a perfect sample.

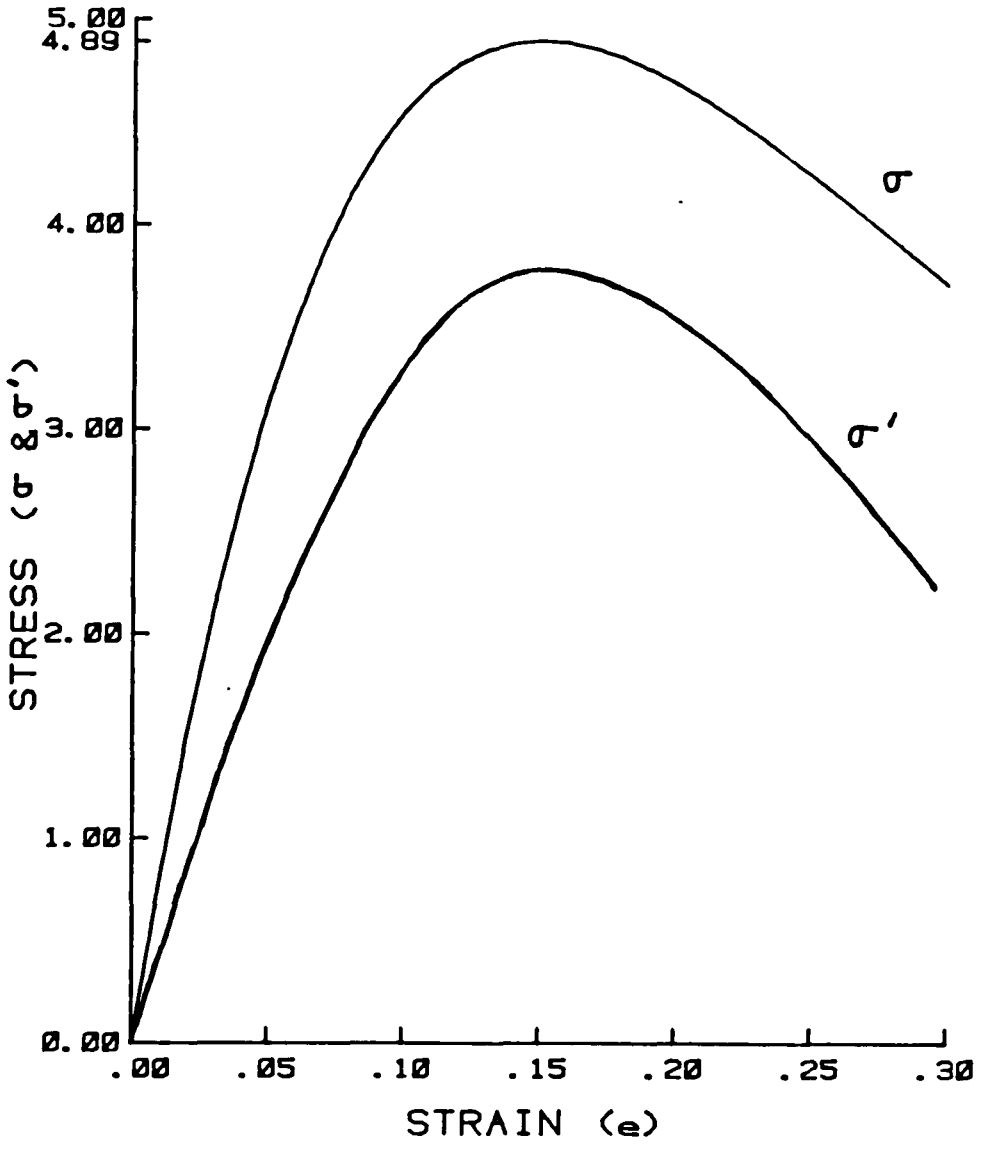


Figure 5.4.6 Stress-strain relation for the sample with and without crack (schematic)

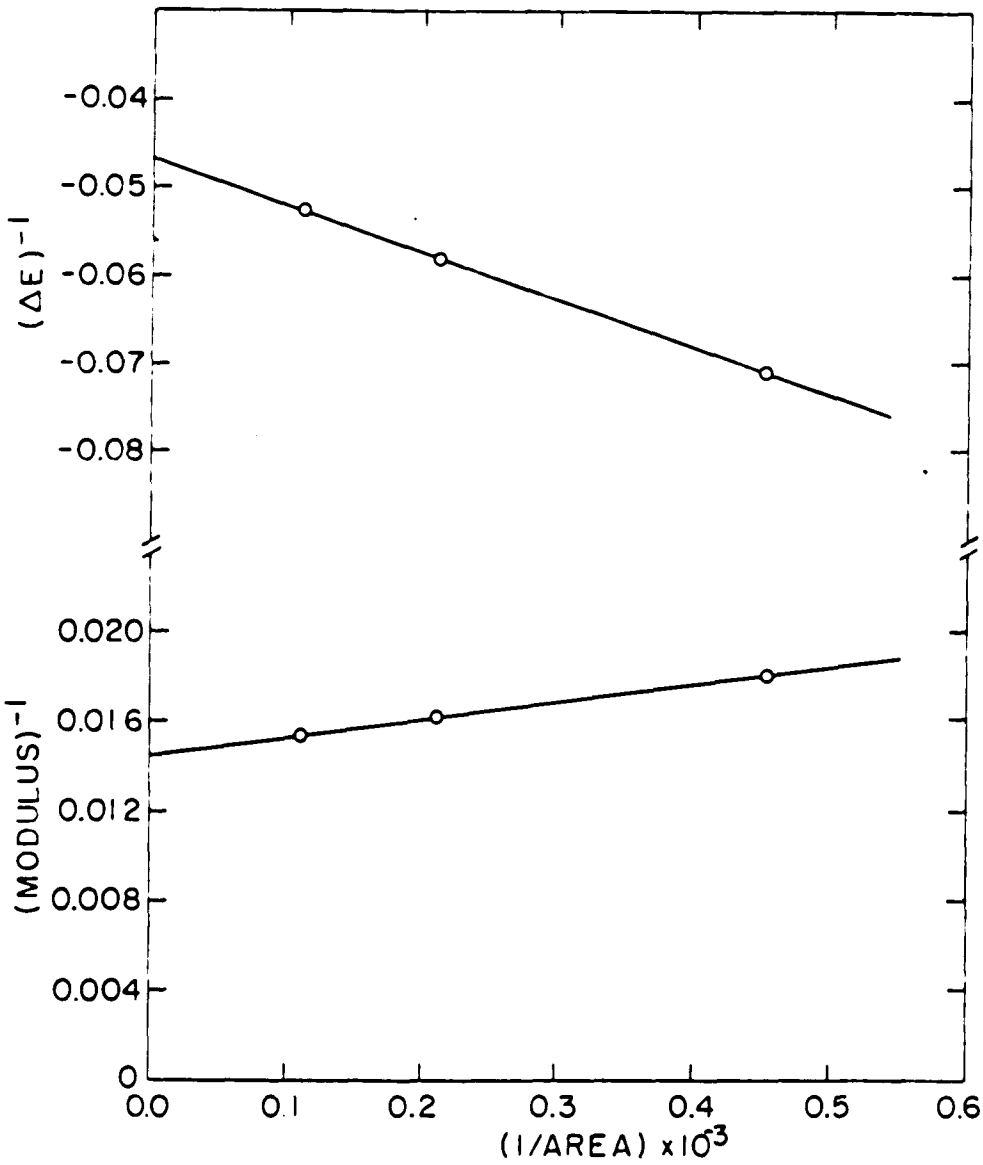


Figure 5.4.7 The functional dependence of the modulus and the strain energy difference $\Delta E_{el}$ on sample size Data plotted against 1/area as indicated by equations 5.4.16 and 5.4.18. (all values for full sample). The straight line is the empirical fit to the data . All samples have a crack of 38 broken bonds in the full sample.

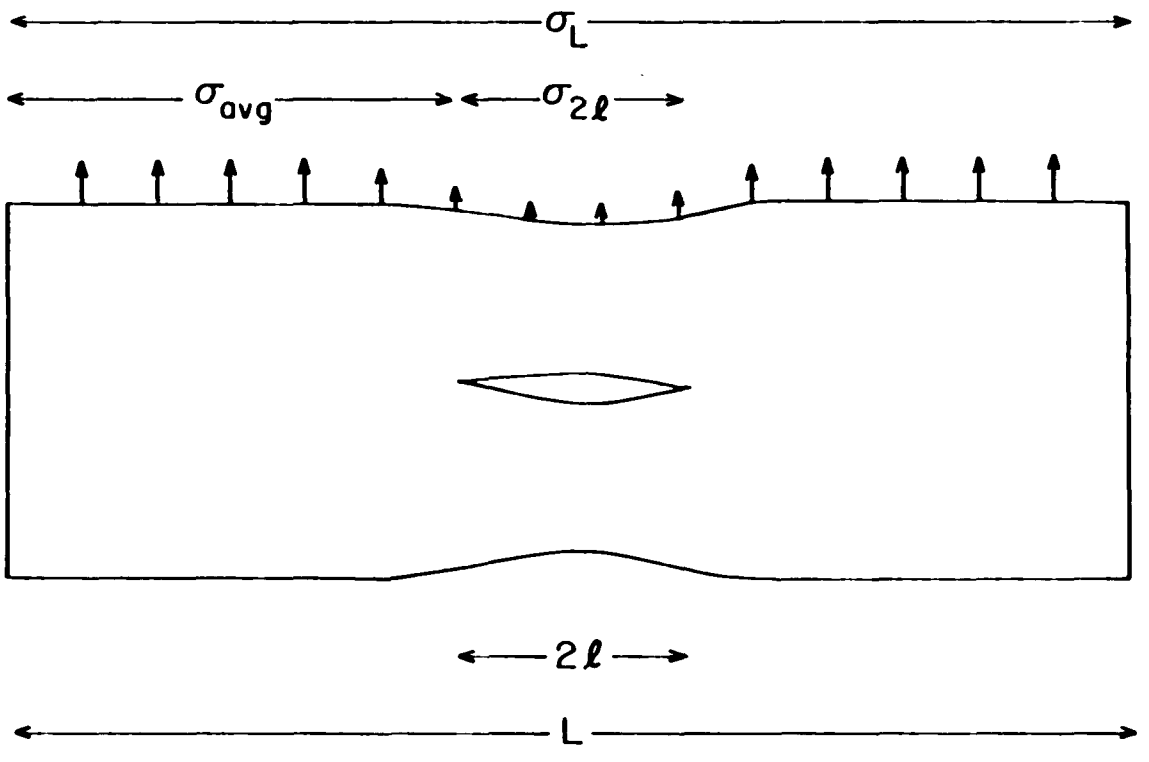


Figure 5.6.1 Stress distribution on the surface of the sample with a central crack under fixed displacement.

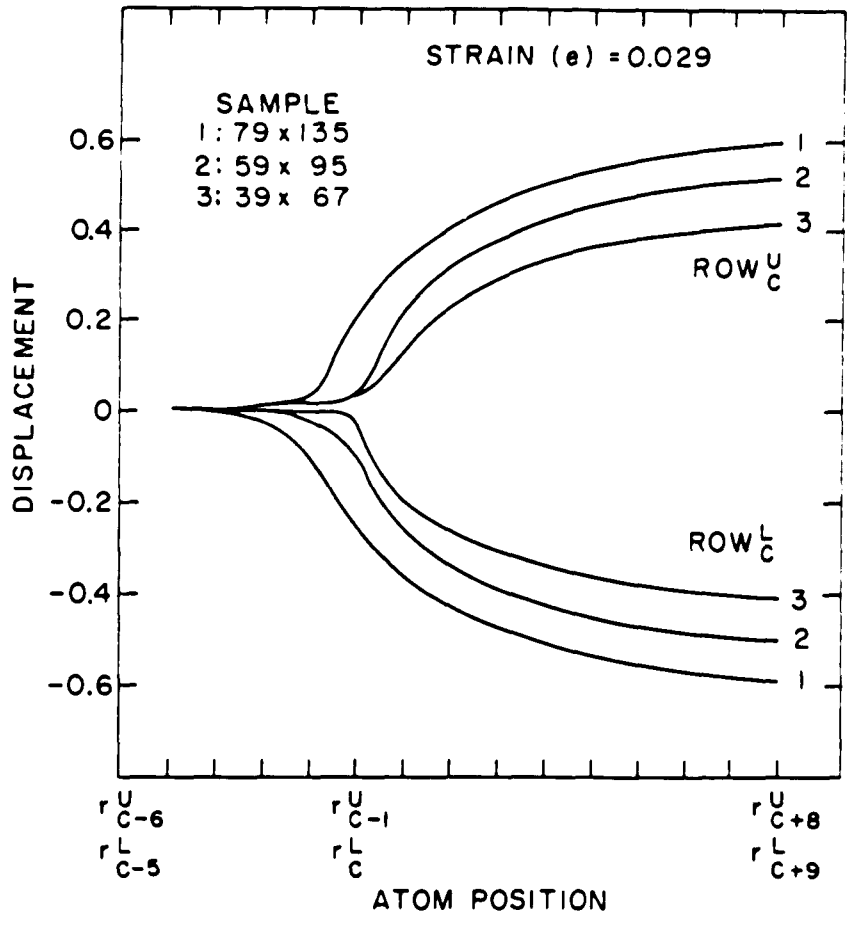


Figure 5.6.2 Plots of displacement of atoms on the central two rows against the atomic positions for three different samples under the same external displacement.

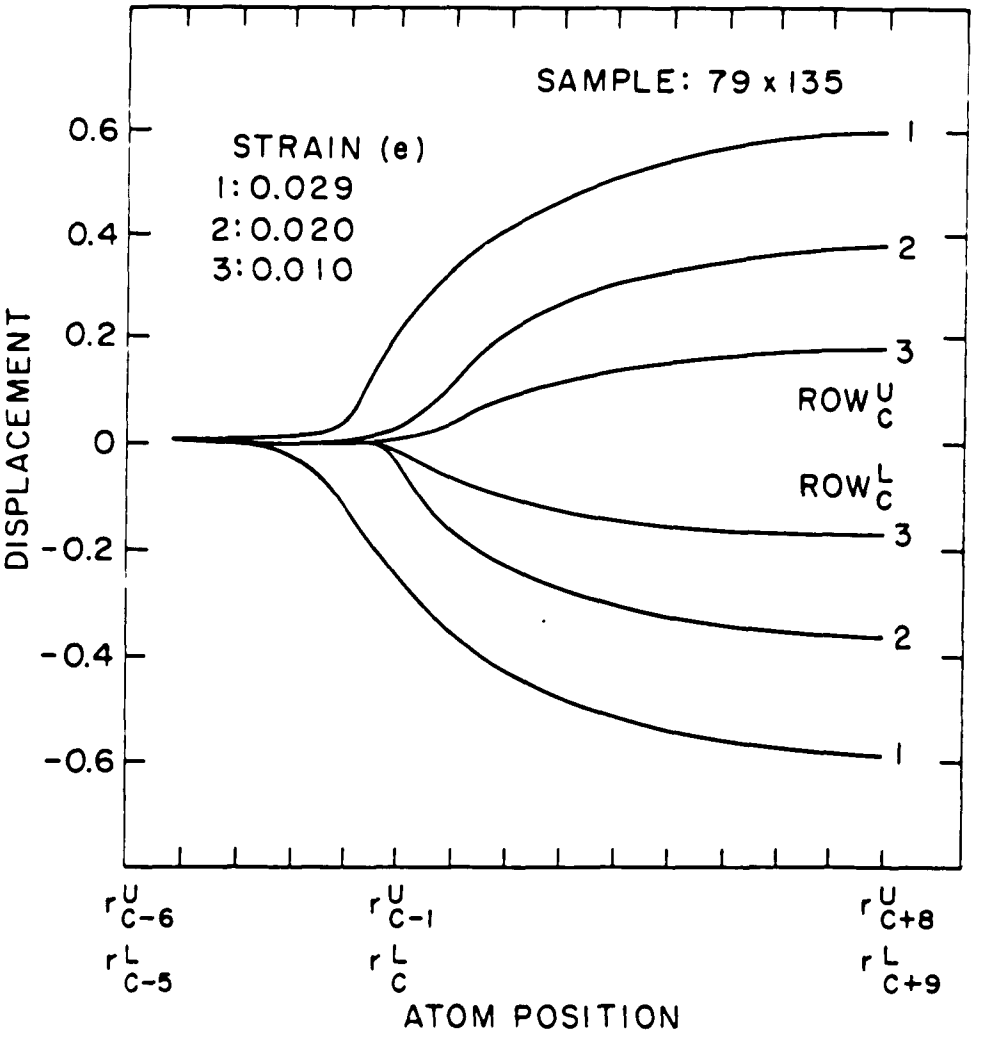


Figure 5.6.3 Plots of displacements of atoms on the central two rows against the atomic positions for the largest sample under different external displacements.

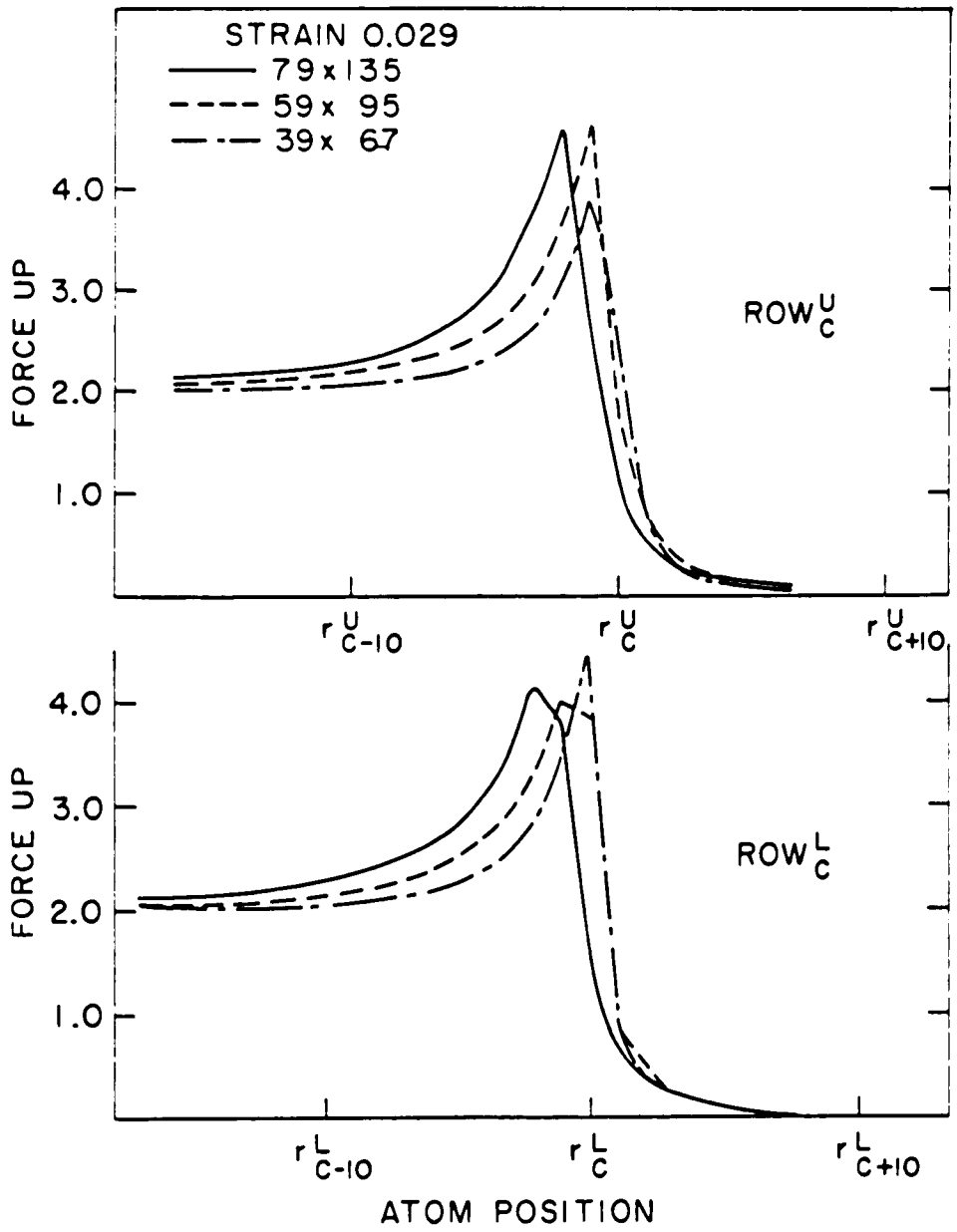


Figure 5.6.4 Plot of forces acting on atoms on the central two rows against the atomic positions for three different samples under the same external displacement.

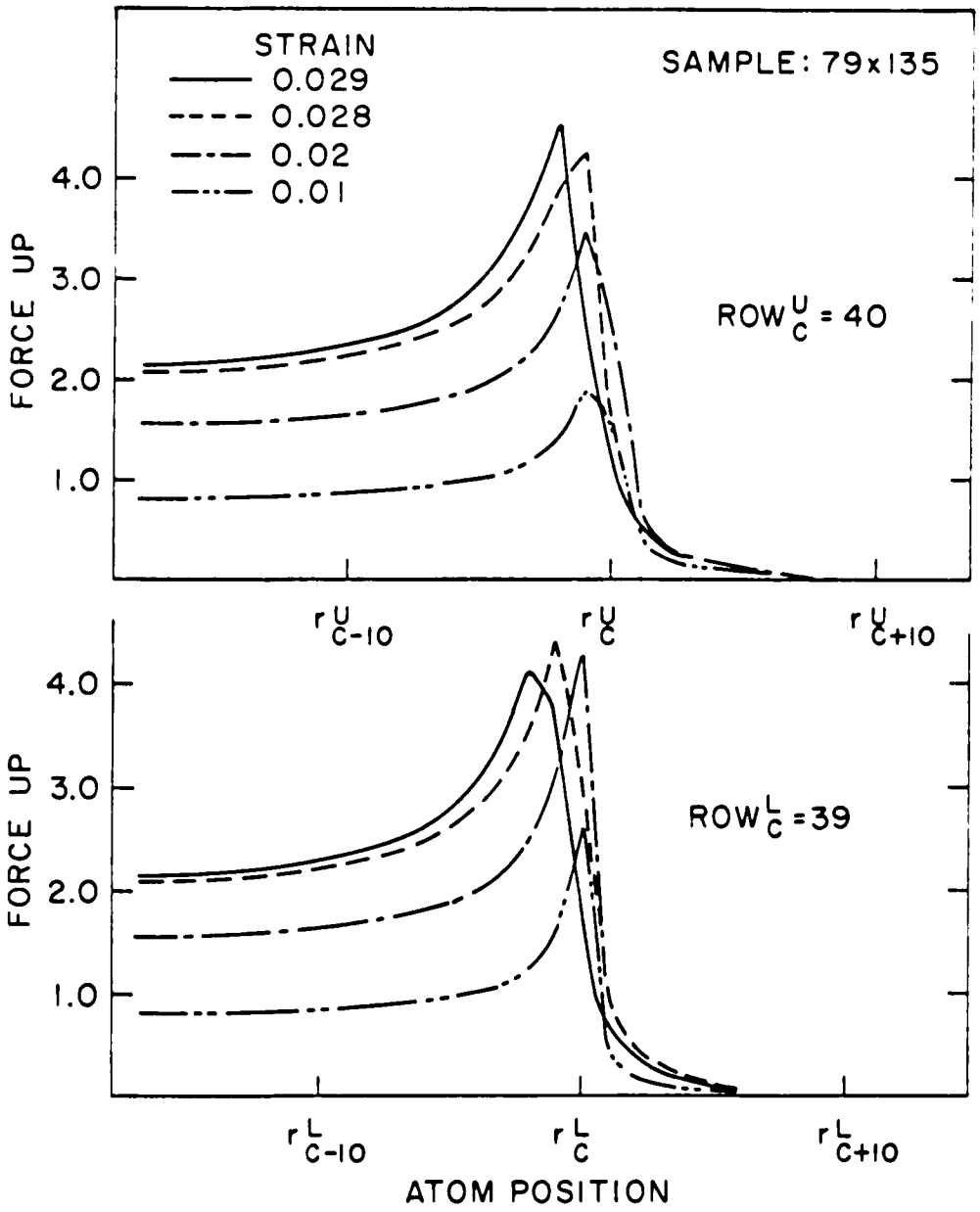


Figure 5.6.5 Plots of forces acting on atoms on the central two rows against the atomic positions for same sample under four different external displacement.

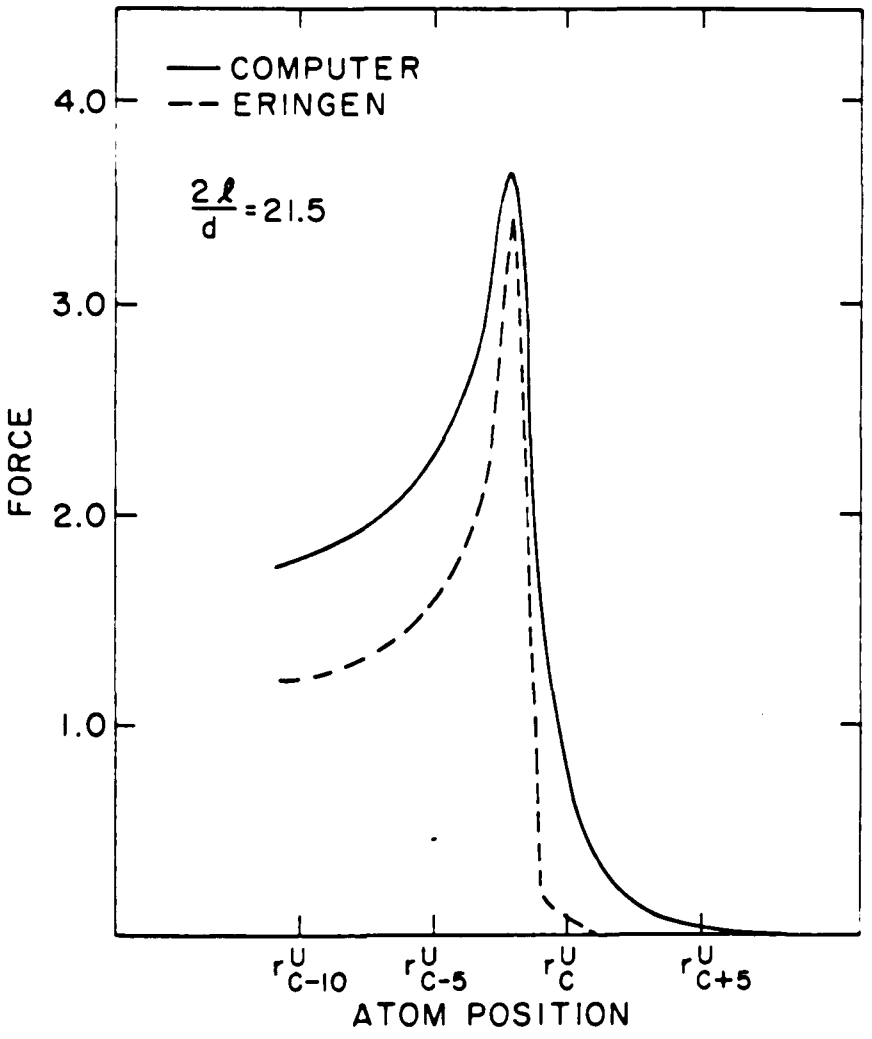


Figure 5.6.6 Comparison between Eringen and molecular dynamic stress profiles.

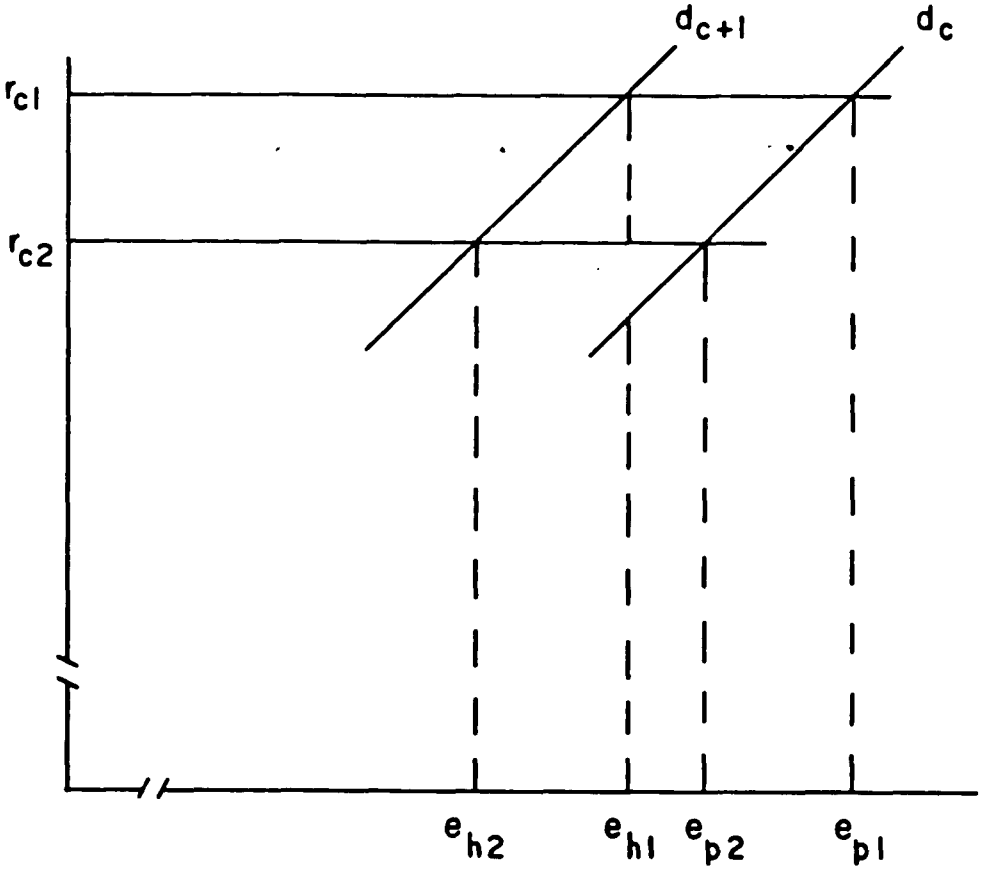


Figure 5.7.1 Sketch of the influence of the 'cut-off' in the potential on the lattice trapping ratio.

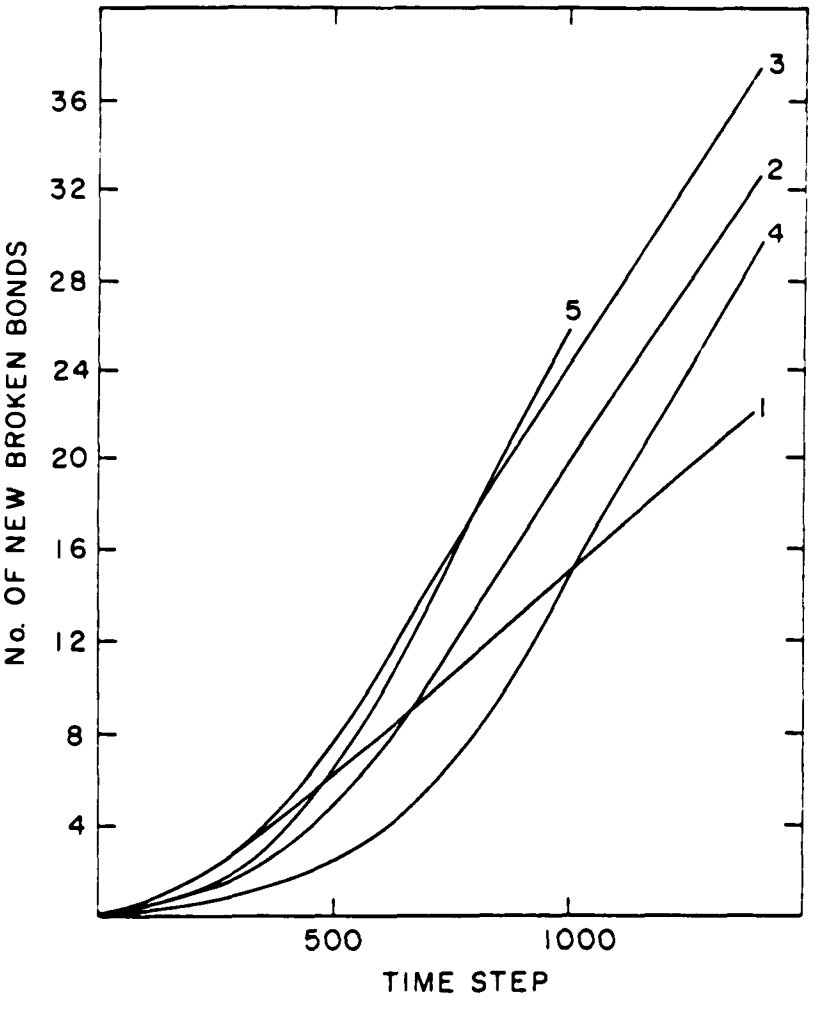


Figure 6.2.1 Plots of number of broken bonds against time step for different samples.

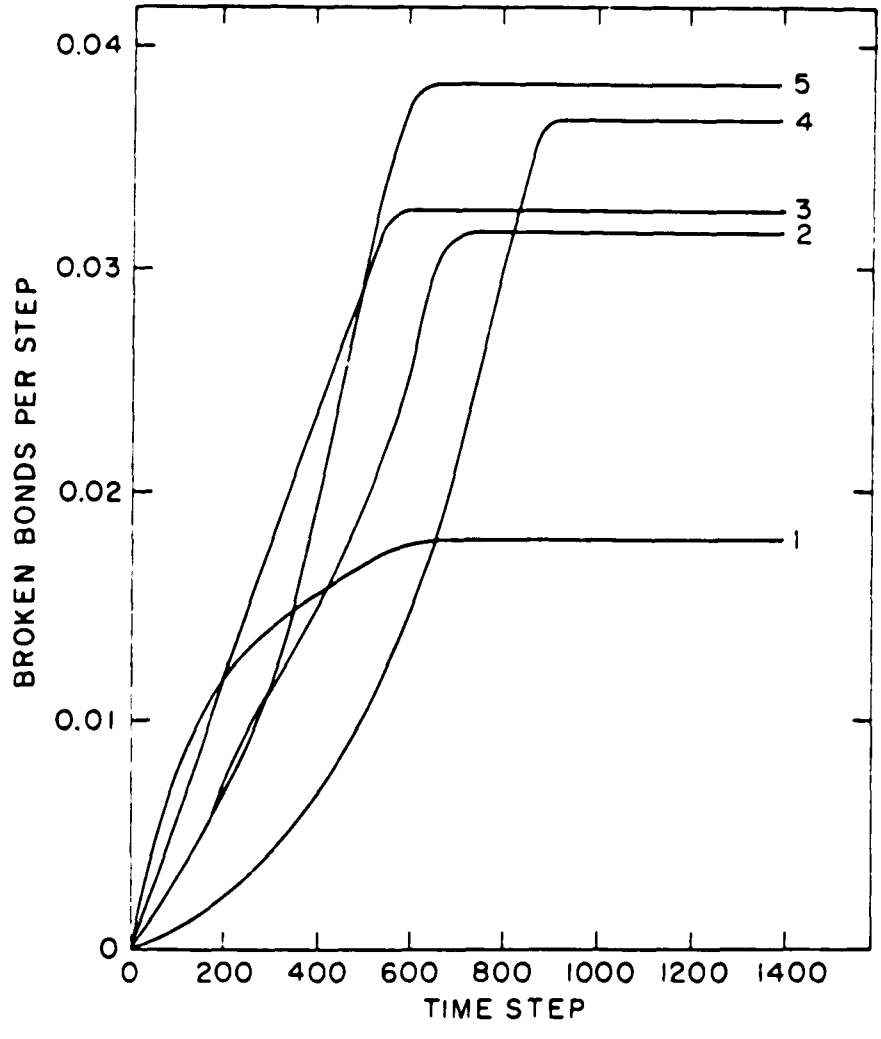


Figure 6.2.2 Plots of broken bonds per time step against time step.

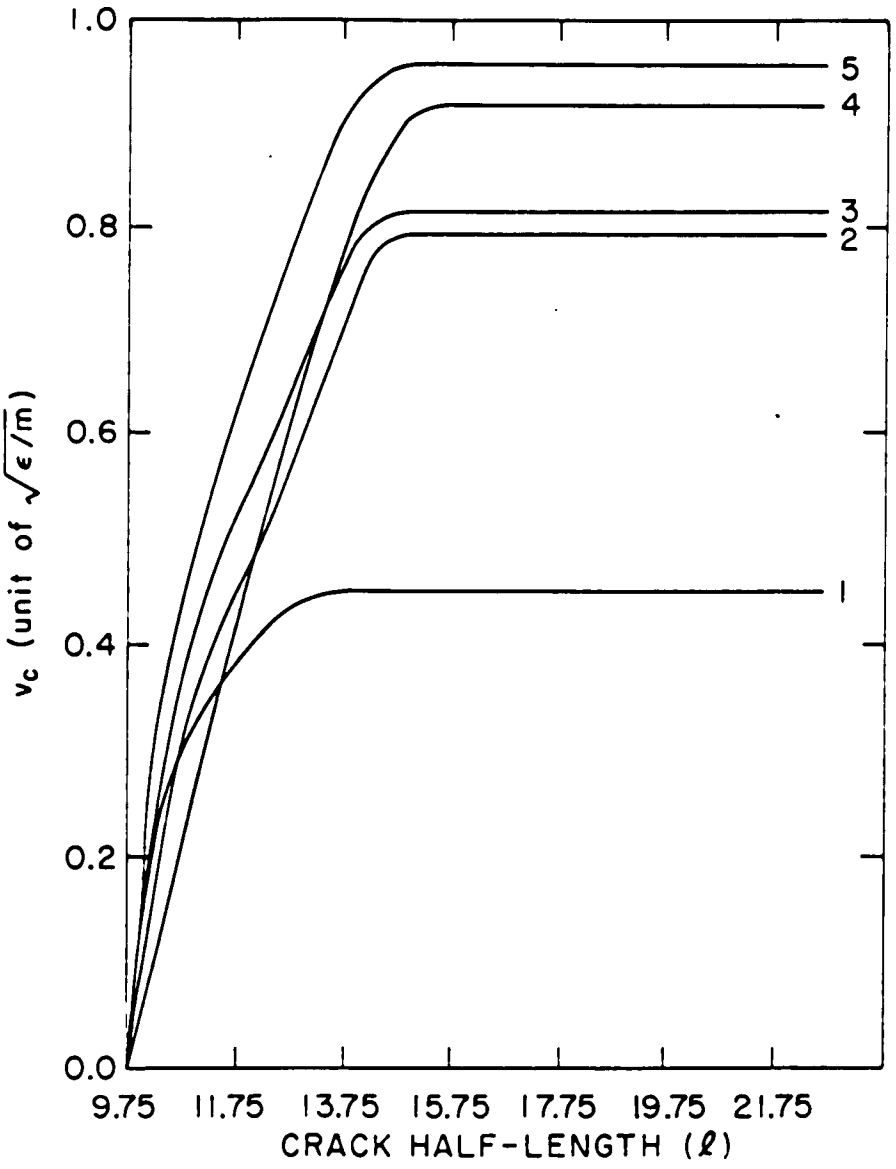


Figure 6.2.3 Plots of crack tip velocity against crack half-length.

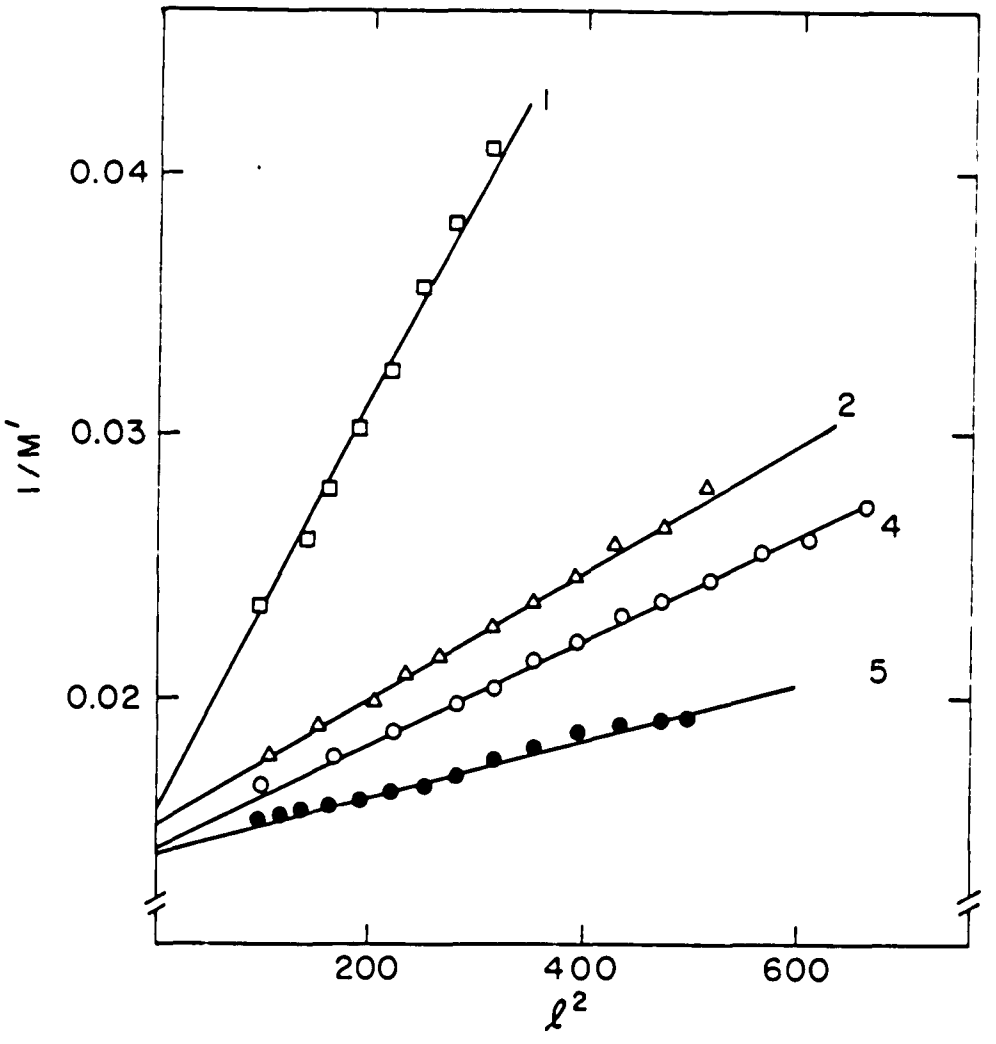


Figure 6.2.4 Plots of 1/Modulus against $l^2$ for four samples of differnet sizes.

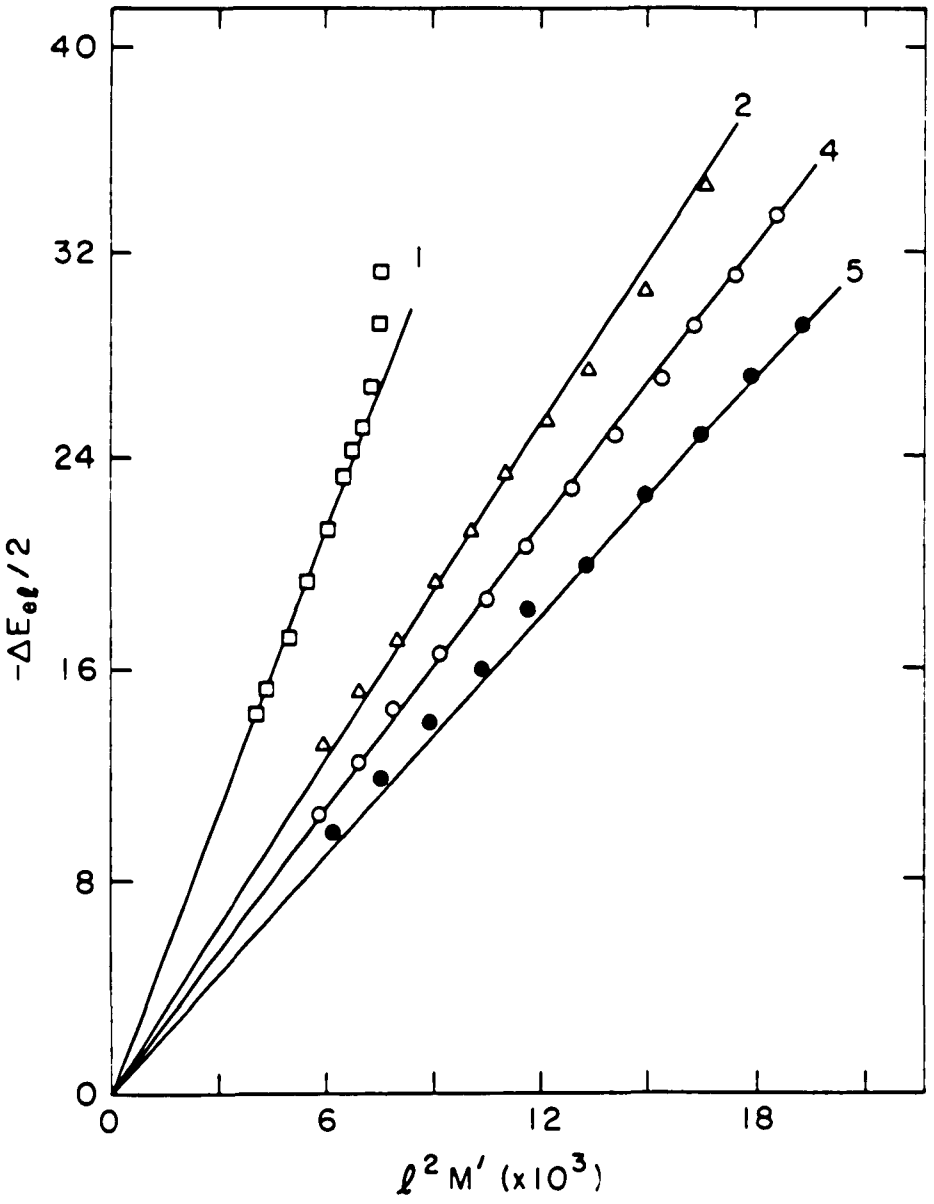


Figure 6.2.5 Plots of $-\Delta E_{el}/2$ against $l^2M'$ for four samples of different sizes.

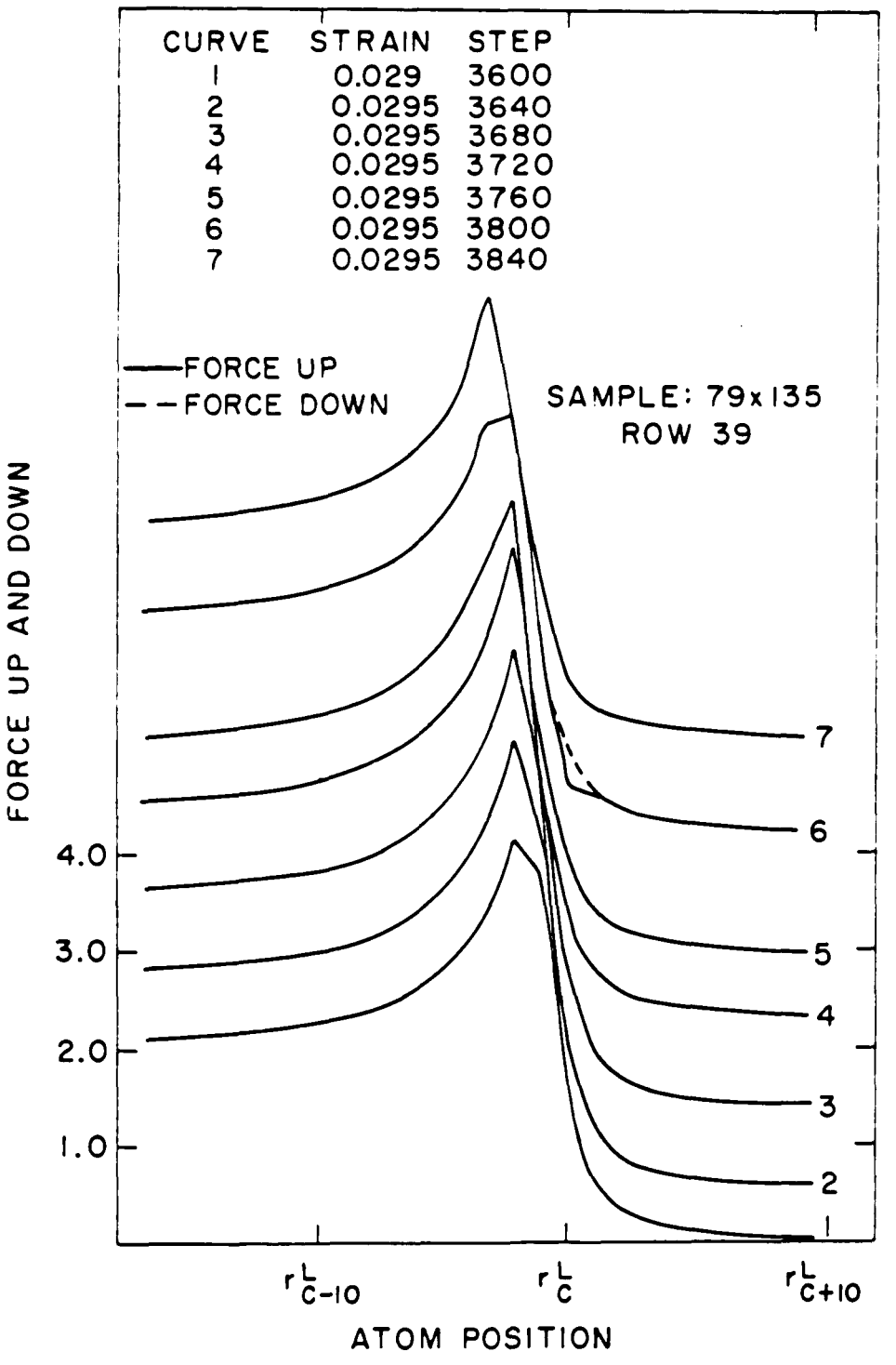


Figure 6.2.6 Plots of forces acting on atoms on row 39 of the largest sample against the atomic positions at different time steps as the crack propagates.

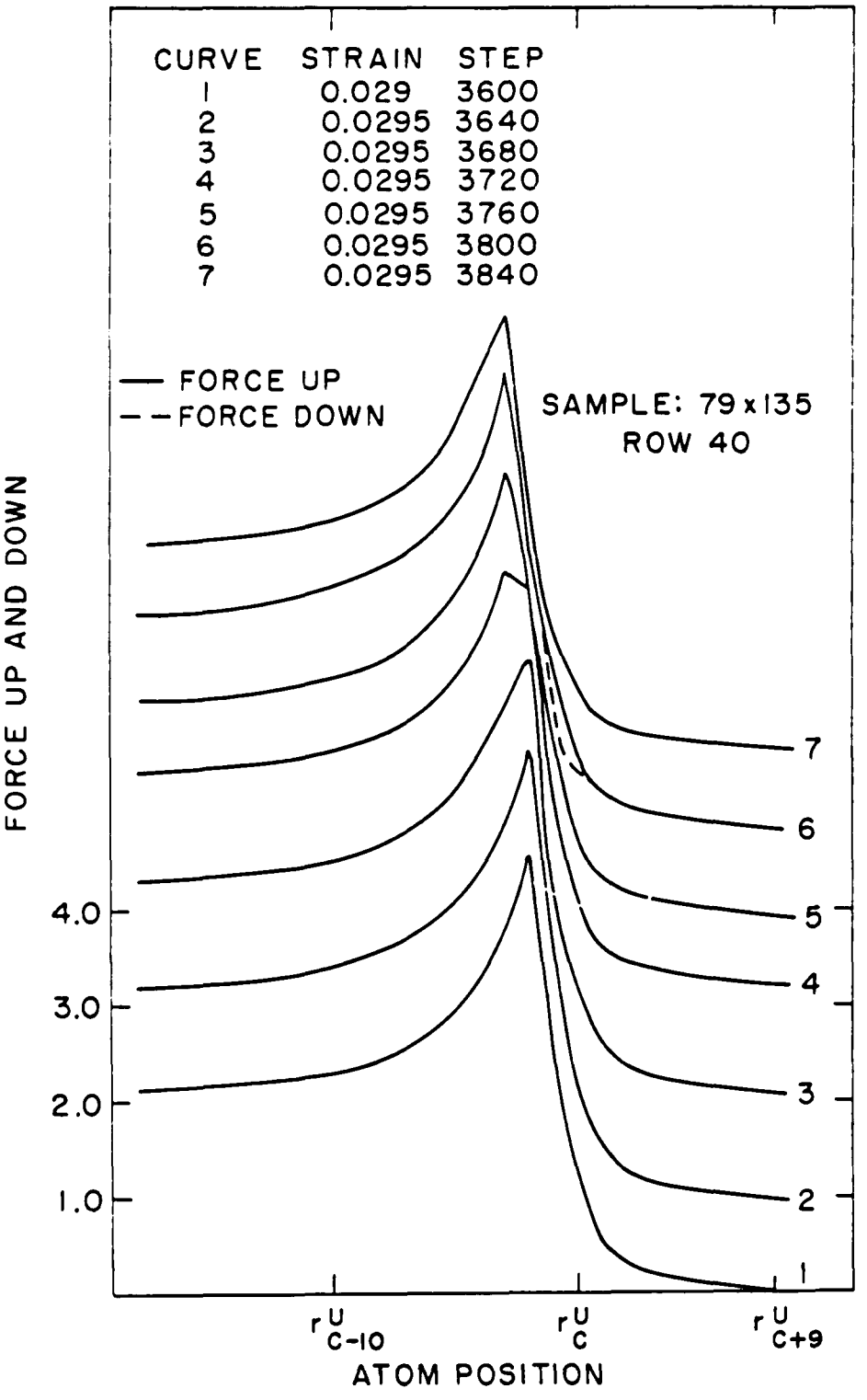


Figure 6.2.7 Plots of forces acting on atoms on row 40 of the largest sample against the atomic positions at different time steps as the crack propagates.

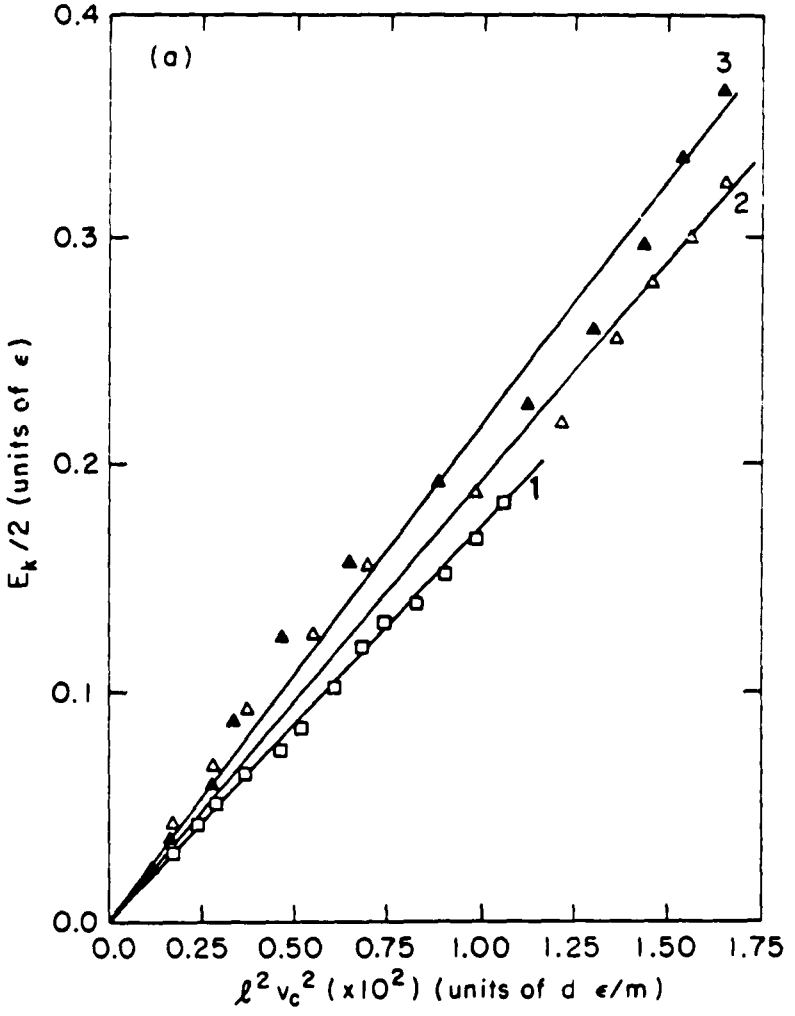


Figure 6.3.1 (a) Plots of $E_k/2$ against $l^2 v_c^2$ .

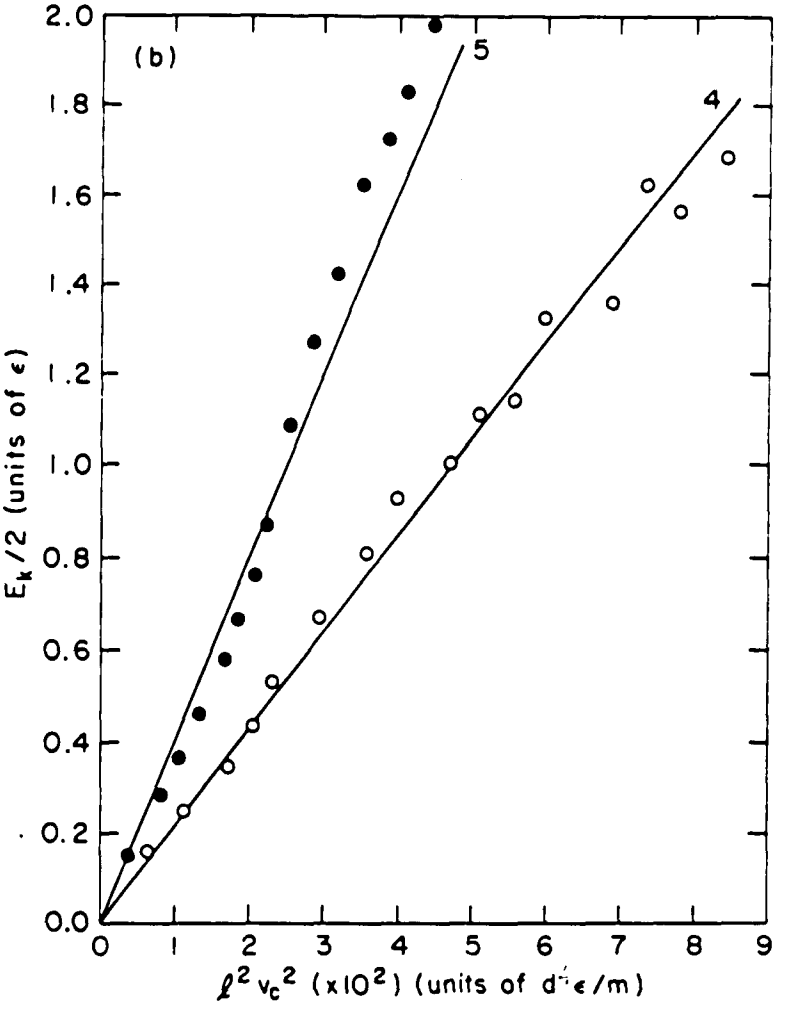


Figure 6.3.1 (b) Plots of $E_k/2$ against $l^2 v_c^2$ .

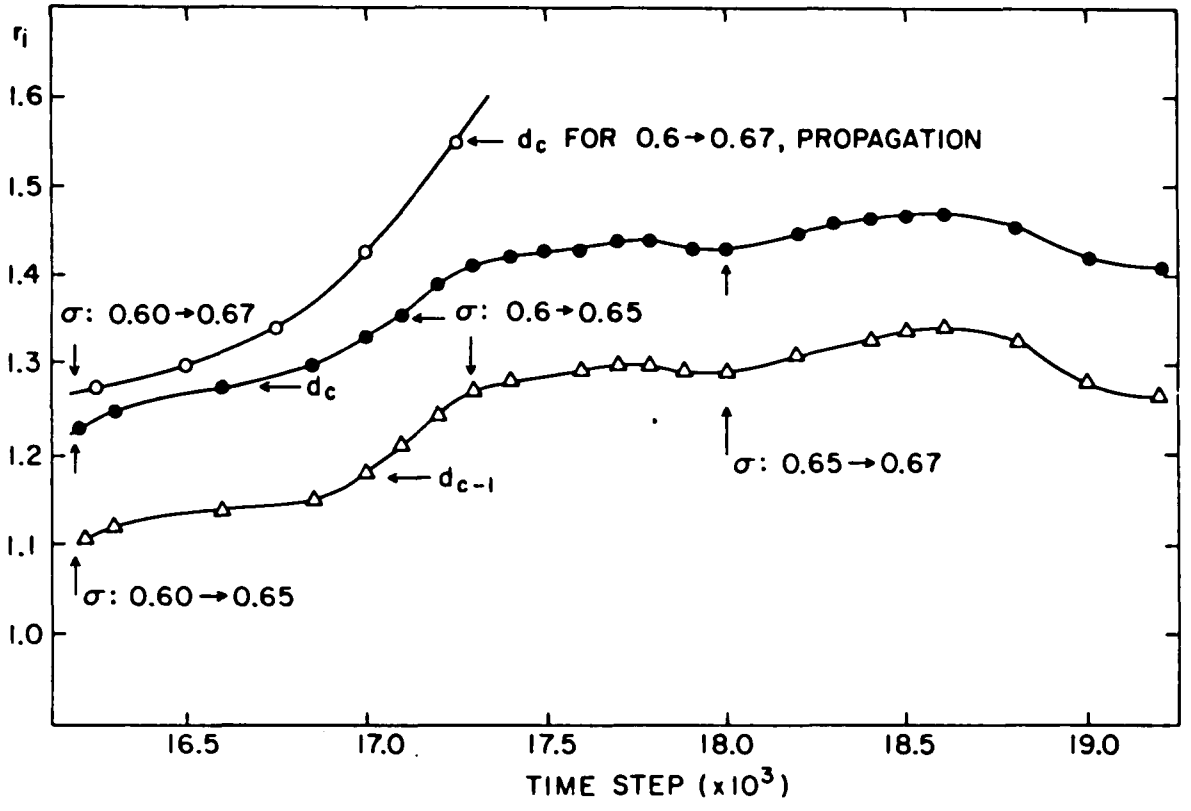


Figure 6.4.1 Healing and propagation of the crack upon various changes in the applied load.

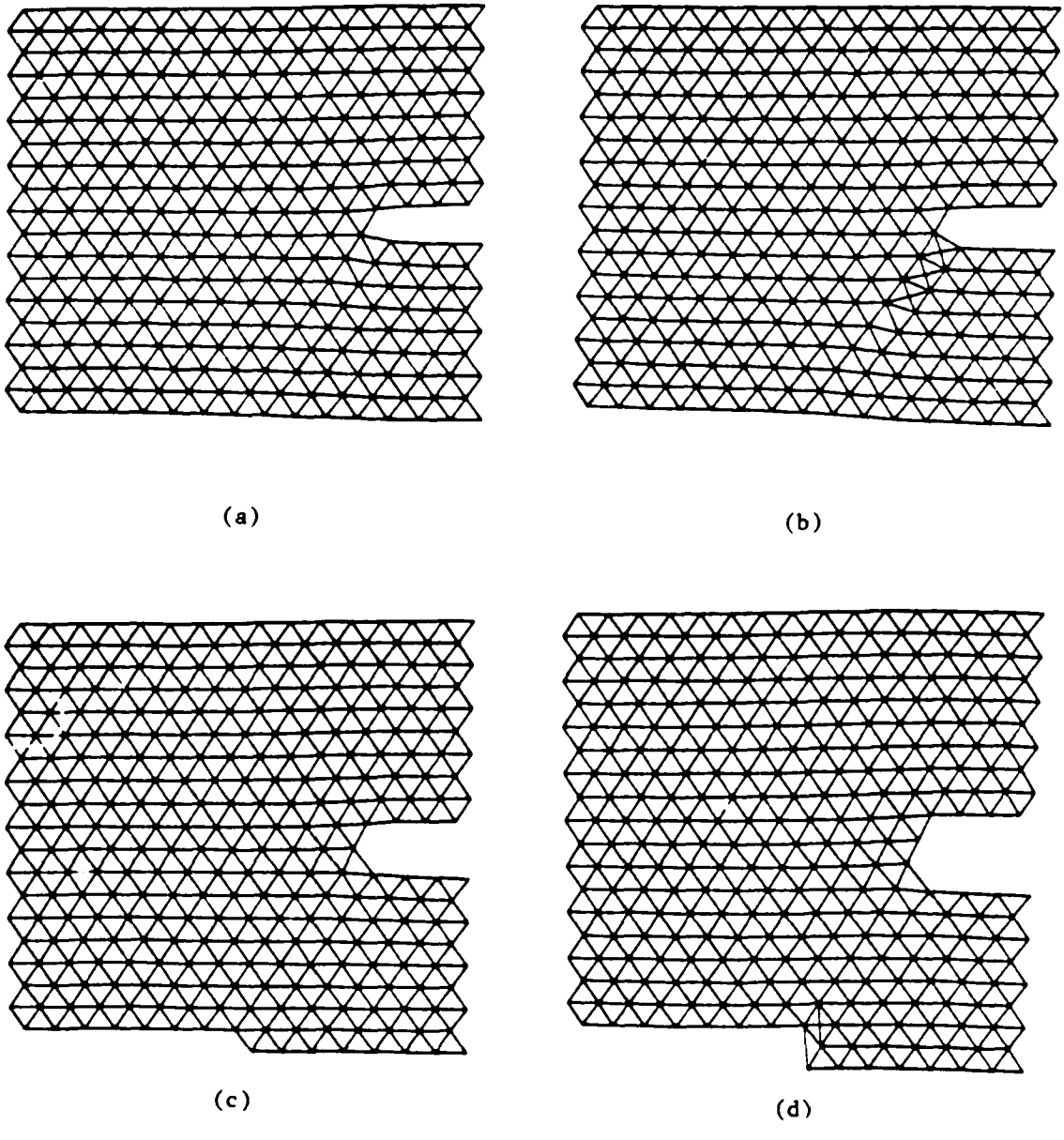


Figure 7.2.1 Run DFLF 1. Homogenous sample (no layer). Load raised from 1.90 to 2.09 at time step 1000. Time step: a) 1000; b) 1100; c) 1200 and d) 1650

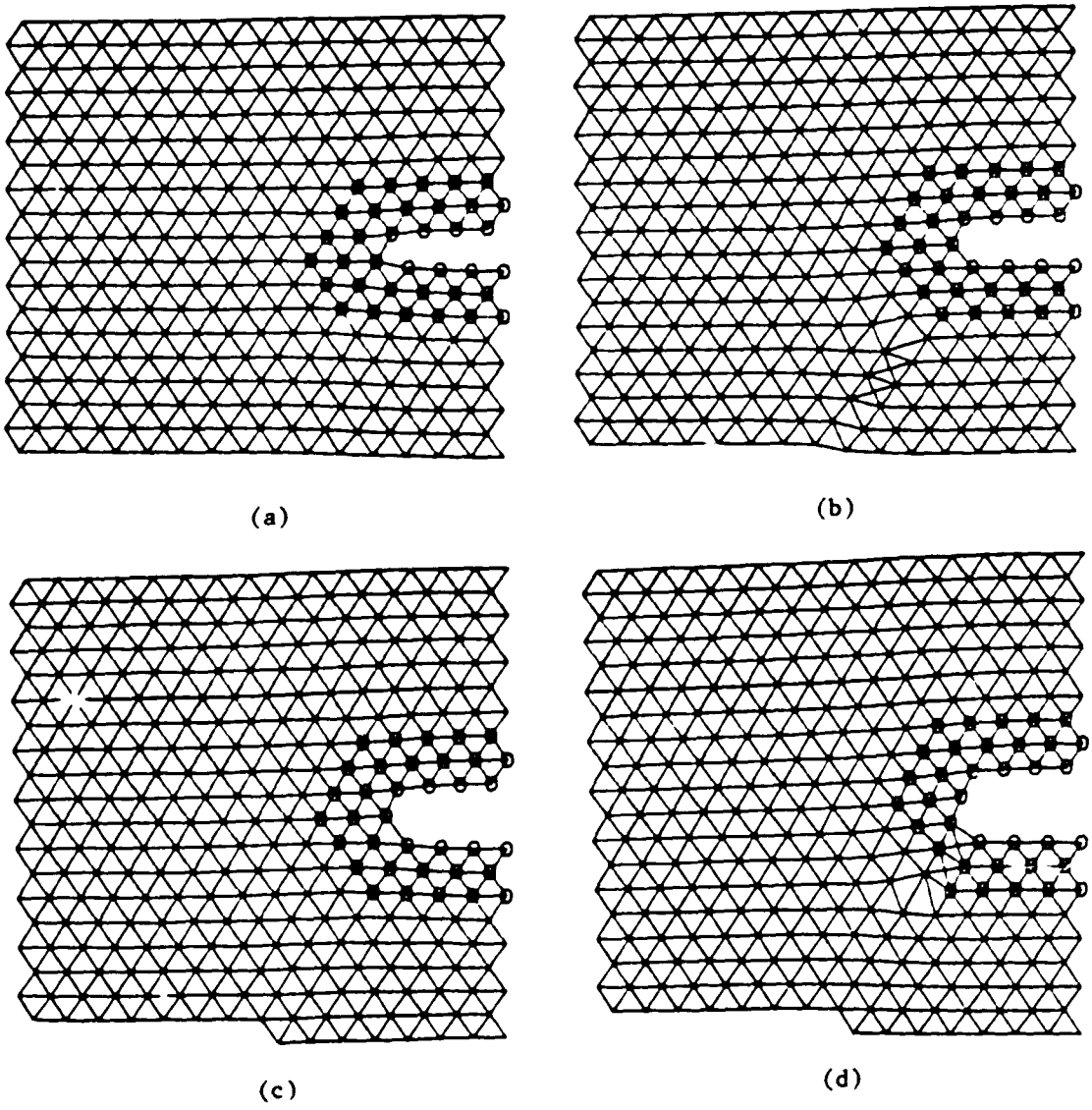


Figure 7.2.2 Run DFLF 2. Three layer film with FF = 2.0, FS = 1.5 . Load raised from 2.89 to 3.00 at time step 1000. Large circles represent the film atoms. Time steps: a) 1000; b) 1150; c) 1200; d) 1350

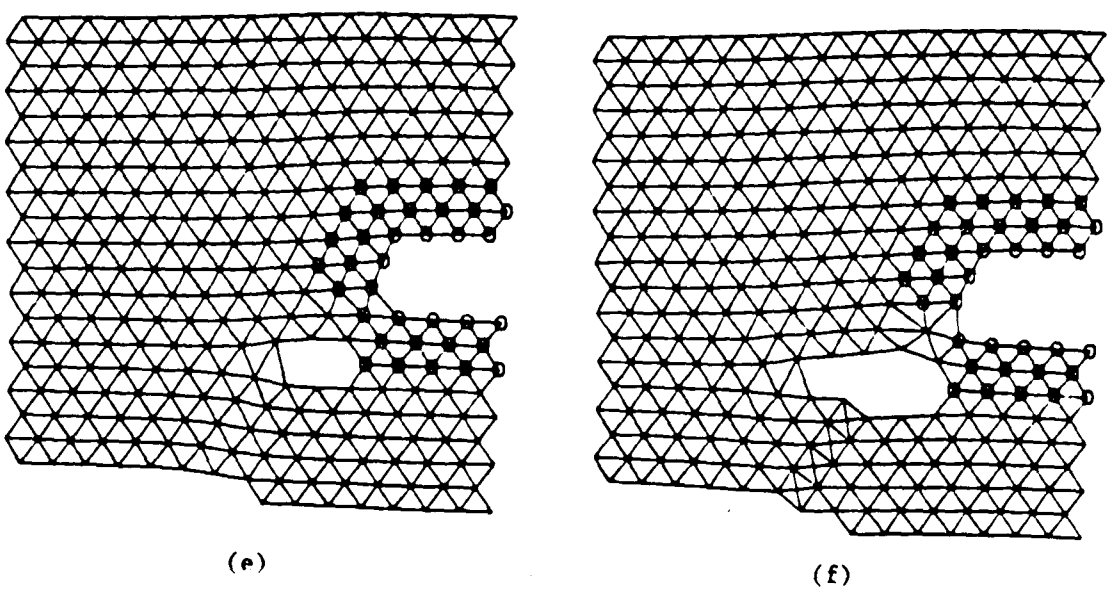

(e) (f)

Figure 7.2.2 Run DFLF 2. Three layer film with FF = 2.0, FS = 1.5 . Load raised from 2.89 to 3.00 at time step 1000. Large circles represent the film atoms. Time steps: e) 1400 and f) 1450.

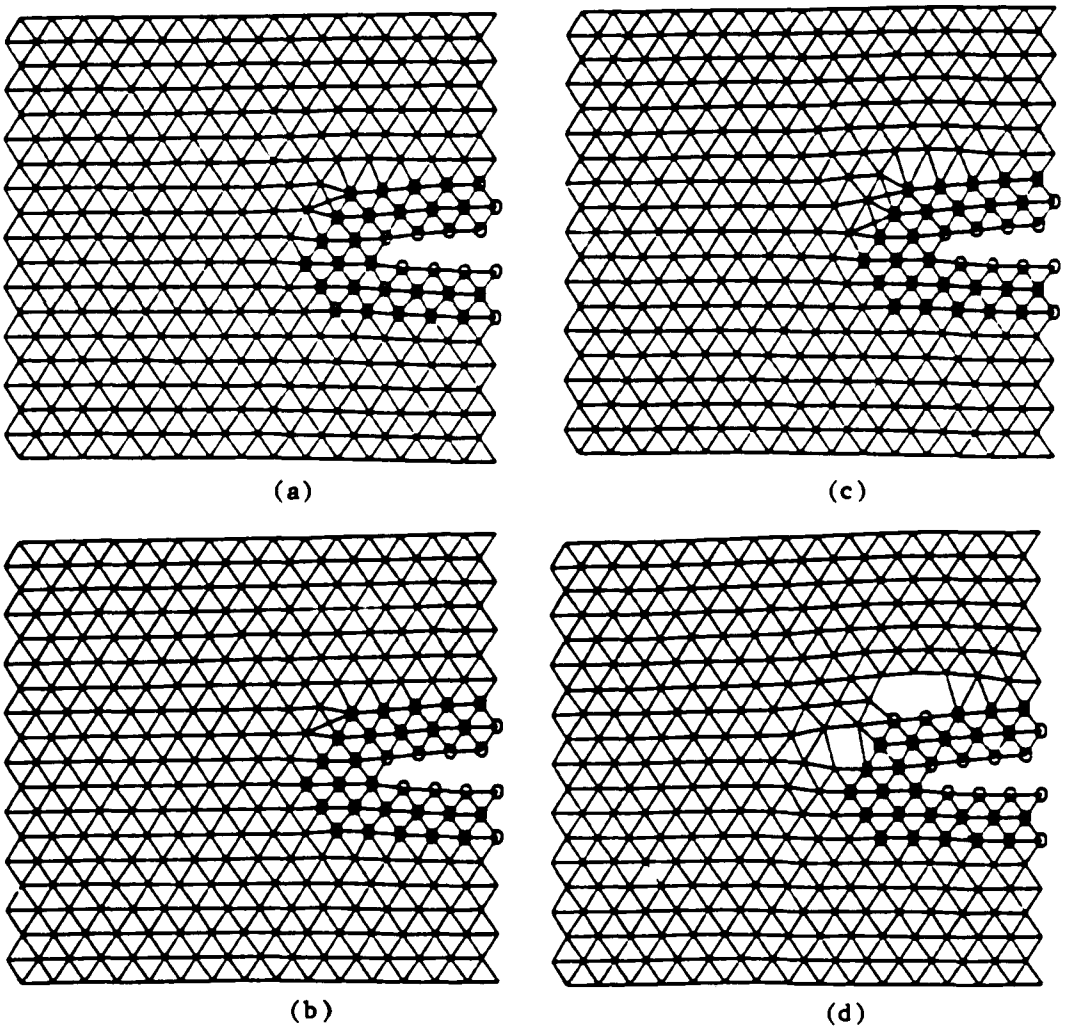


Figure 7.2.3 Run DFLF 3. Three layer film with FF = 5.0. Load raised from 3.80 to 3.99 at time step 1300. Large circles represent film atoms. Time steps: a) 1475; b) 1500; c) 1525 and d) 1550

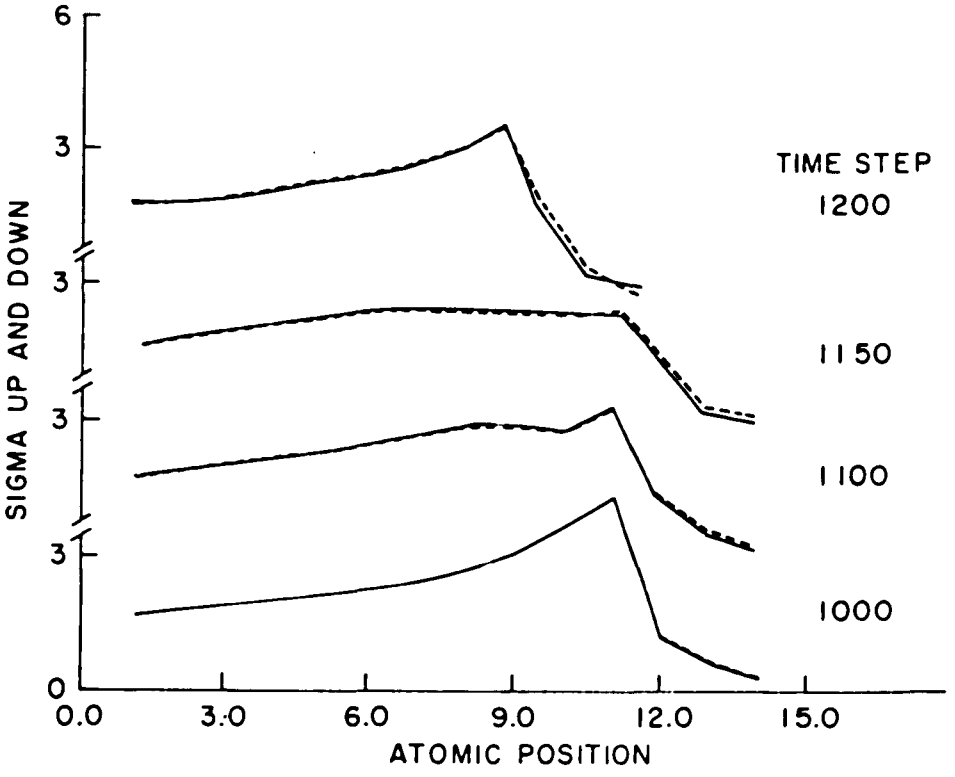


Figure 7.2.4 Local force profiles for run DFLF 1, the homogenous sample, on row 9 at the time steps indicated.

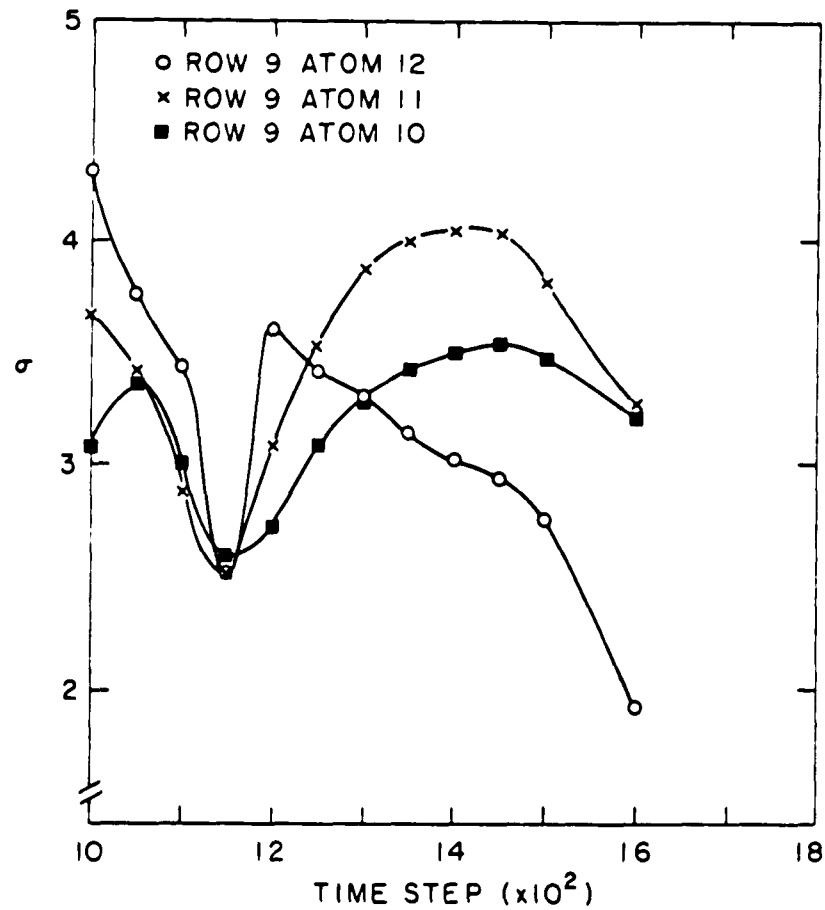


Figure 7.2.5 Time sequences of local forces for Run DFLF 1 on row 9 at the atom numbers listed.

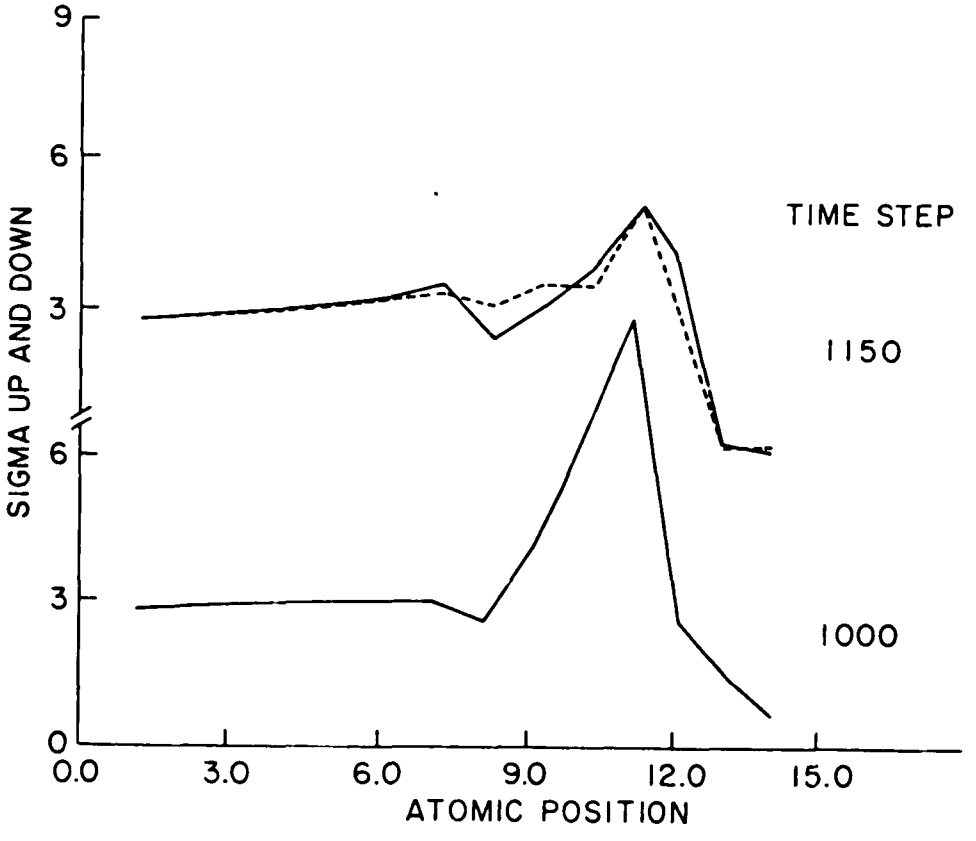


Figure 7.2.6 Local force profiles for Run DFLF 2, the sample with a three layer film (FF = 2.0, FS = 1.5), on Row 9 at the time steps indicated.

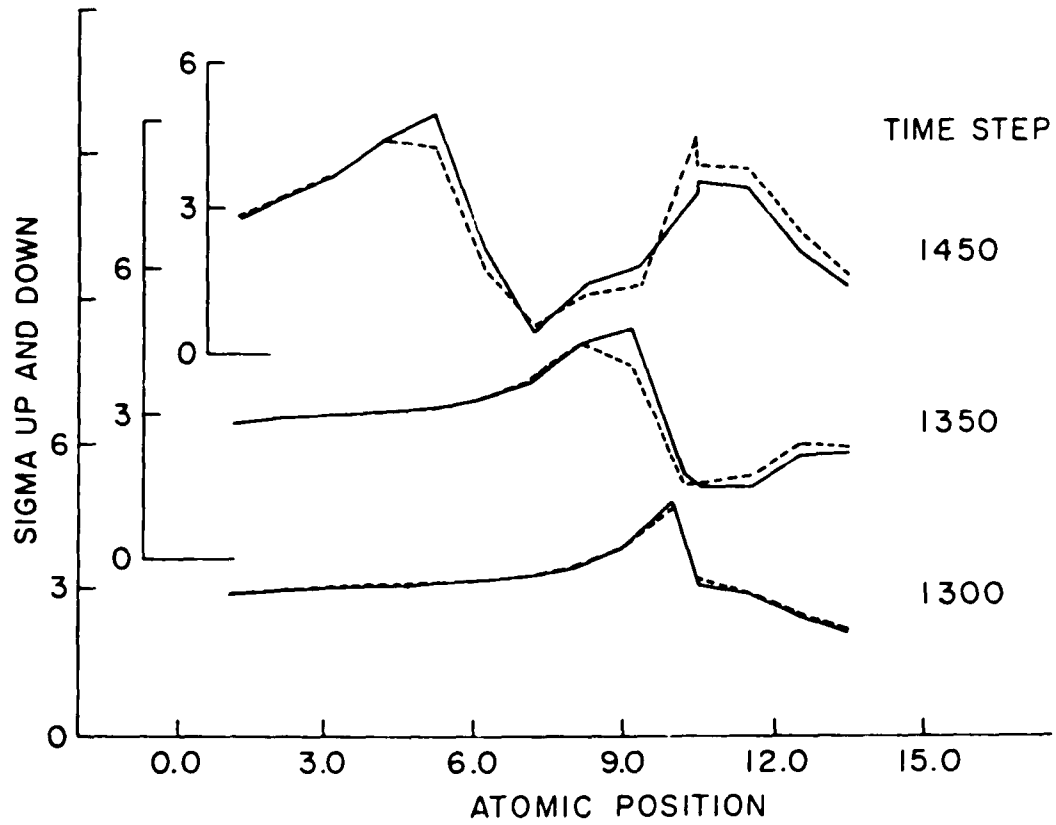


Figure 7.2.7 Local force profiles for Run DFLF 2 on row 6 at the time steps indicated.

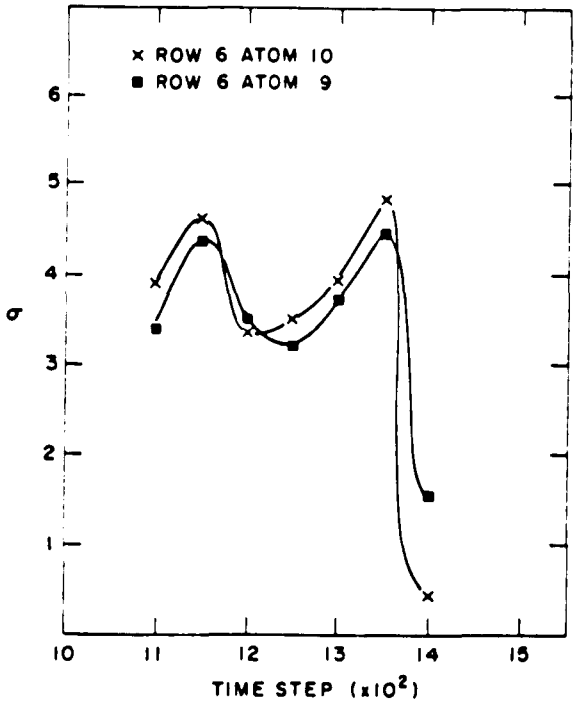


Figure 7.2.8 Time sequence of local forces for Run DFLF 2 on row 6 at the atom numbers listed.

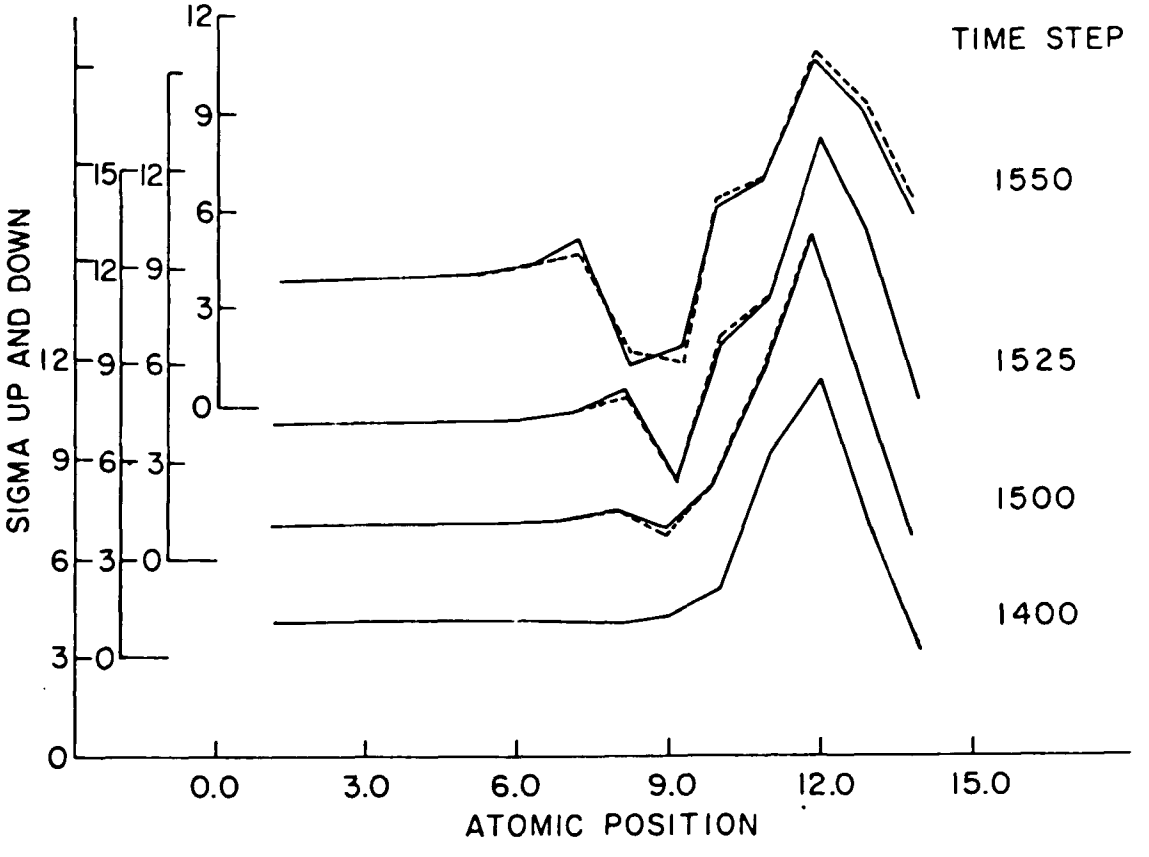


Figure 7.2.9 Local force profiles for Run DFLF3, the sample with a three layer film (FF = 5.0), on row 11 at the time steps indicated.

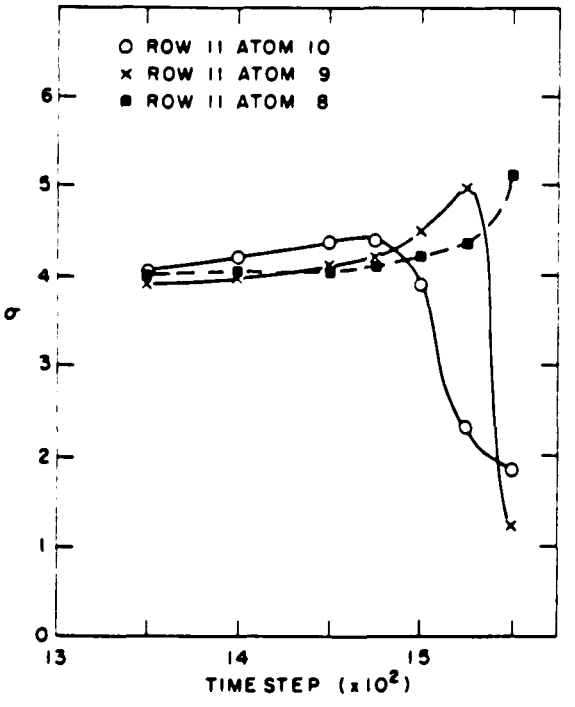


Figure 7.2.10 Time sequences of local forces for Run DFLF 3 on row 11 at the atom numbers listed.

# APPENDIX

The procedure for relating interatomic forces to stresses follows from the definition of the local stress. The stress tensor can be defined (see J.J. Gilman, 1969, Chap. 2) as a force per unit area. If the force, $\Delta F$, through the surface surrounding a region is resolved into its three components, $\Delta F_i$, and the vector area, $\Delta a$, is resolved into the three components, $\Delta a_i$, then the stress tensor $\sigma_{ij}$ is given by

$$\Delta F_i / \Delta a_j = \sigma_{ij} \qquad \text{A-1}$$

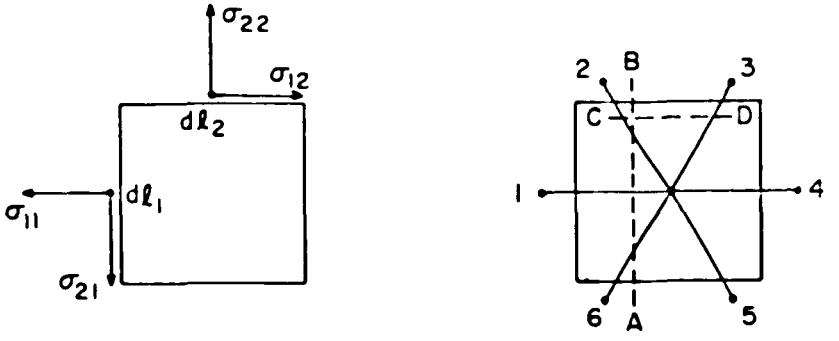


Figure Apndx. Calculation of the local stress for a system with a) four-fold and b) six-fold symmetry.

As we are concerned with a two-dimensional system we limit ourselves to i = 1,2 and j = 1,2 and also replace the vector element of area by a vector element of length, $\Delta \ell$. The stresses of interest are shown in Fig. Apndx. (a). While such a square cross section would be appropriate for a system with four-fold symmetry, it is not appropriate for a system of six-fold symmetry as can be seen by examining Fig. Apndx. b. In this figure the six near neighbors of atom 0 are shown with the directed bonds to atom 0 and the square of Fig. a centered on atom 0. If one calculates $\sigma_{ij}$ from (A-1) using the square region surrounding 0, with forces $\Delta F_i$ as the forces cutting $\Delta \ell_1$, and $\Delta \ell_2$, then

$$\sigma_{11} = \Delta F_1(r_{10})/\Delta \ell_1$$

$$\sigma_{22} = [\Delta F_2(r_{20}) + \Delta F_2(r_{30})]/\Delta \ell_2 \qquad \text{A-2}$$

For a system under uniform hydrostatic pressure P

$$\sigma_{11} = \sigma_{22} \propto P$$

but it can be seen that using definitios (A-2) we do not obtain this result. If we wish to use a definition consistent with the microscopic definition of pressure we must use the surfaces $\Delta \ell_1$ and $\Delta \ell_2$ which are the local limit of the macroscopic surfaces that gives $\sigma_{11}$ and $\sigma_{22}$ proportional to the pressure. It is readily shown that using the forces that cut lines AB and CD yield such a limiting result; namely

$$\sigma_{11} = \left\{\Delta F_1(r_{10}) + \tfrac{1}{2}[\Delta F_1(r_{20}) + \Delta F_1(r_{60})]\right\}/\Delta \ell_1 \qquad \text{A-3}$$

$$\sigma_{22} = [\Delta F_2(r_{20}) + \Delta F_2(r_{30})]/\Delta \ell_2 \qquad \text{A-4}$$

$$\sigma_{21} = \left\{\Delta F_2(r_{10}) + \tfrac{1}{2}[\Delta F_2(r_{20}) + \Delta F_2(r_{60})]\right\}/\Delta \ell_2 \qquad \text{A-5}$$

and

$$\sigma_{21} = [\Delta F_1(r_{20}) + \Delta F_1(r_{30})]/\Delta \ell_2 \qquad \text{A-6}$$

where $\Delta \ell_2 = d$ and $\Delta \ell_1 = \sqrt{3}d/2$

The factor 1/2 [ ] terms that appear in Eq. (A-3) and (A-5) arise from the way that the horizontal bond terms of the $\Delta F(r_{10})$ For example, sigma up can be written as type and the diagonal bond terms of the $\Delta F(r_{60})$ type repeat themselves as the length AC is laid and overlaid to cover the whole edge in the y direction. If AC is slightly less than the distance $r_{26} = 2(\sqrt{3}/2\,d)$ and A is just below 6, then each time the distance AC is repeated 2 terms of the horizontal type and two diagonal terms appear. Thus, the stress per $\sqrt{3}/2\,d$ (1/2 the distance $r_{26}$) introduces one horizontal term and one diagonal term. For symmetry this has been written centered around atom 0, as a horizontal term plus one half of the two diagonals. Using this definition, at equilibrium under hydrostatic pressure, $\sigma_{11} = \sigma_{22}$ and $\sigma_{21} = \sigma_{12}$.

The apparent lack of symmetry in the definitions (A-3) through (A-6) is a result of the assymetry of the 1 and 2 directions relative to the 6-fold symmetry of the lattice. The present definitions are for near-neighbor interactions. To extend the definitions to further neighbors, all forces interacting lines AB and CD are added to the appropriate stresses.

In the calculations reported here we have monitored sigma up and sigma down. Sigma up and sigma down can be related to $\sigma_{22}$ for cases of small deformations.
For example, sigma up can be written as

$$\sigma^{up} = [\Delta F_2(r_{20}) + \Delta F_2(r_{30})]/\Delta \ell_2 + \left\{\frac{\Delta F_2(r_{10})}{\Delta \ell_1}\right\}_{y_{10}>0} + \left\{\frac{\Delta F_2(r_{40})}{\Delta \ell_1}\right\}_{y_{40}>0} \quad \text{A-7}$$

Where $\{\ \}_{y_{j0}>0}$ means the term contributes to sigma up if the j-th atom lies above the 0-th atom. In small deformations $y_{j0} \sim 0$ and the $\{\ \}$ terms may be neglected and sigma up $\approx \sigma_{22}$ and similarly for the sima down term. For tensile stress and fracture in the mode-I, sigma up and sigma down are the important stresses and are mainly the stresses studied and reported previously.

When the distortions become large and local stresses confined to regions of the order of a cell size are desired, there are problems in going from the local forces to a unique stress definition. While the forces will vary smoothly and small displacements are made depending on the definition of stress, abrupt changes in stress may occur as bonds pass in and out of a surface. Thus, for studying effects in small regions near the crack tip the force definition sigma up and sigma down would seem preferable.

# BIBLIOGRAPHY

Ashurst, W.T. and Hoover, W.G. "Microscopic fracture studied in the two-dimensional triangular lattice" Phys. Rev. B 14. 1465-1473 (1976).

Alder, B.J. and T.E. Wainwright, J. Chem. Phys. 33, 1439-1451 (1960).

Barenblatt, G.J. "The mathematical theory of equilibrium cracks in brittle fracture" Adv. Appl. Math. 7, 55- (1962).

Baker B. R. "Dynamic stresses created by a moving crack" J. Appl. Mech. 29,449-458 (1962).

Beebe, W. M. Ph. D. Dissertation, California Institute of Technology, Pasadena (1966)

Beeler, I. K. and Kulcinski, G. L. In Interatomic Potentials And The Simulation Of Lattice Defects (eds. Gehlen et al), Plenum, New York (1971).

Berry, J.P. "Some Kinetic considerations of the Griffith criterion for fracture I - Equation of motion at constant force" J. Mech. Phys. Solids 8, 194-206 (1960).

Born, M. and Huang, K. The Dynamical Theory of Crystal Lattice, Oxford University Press, London (1954).

Bozso, F., Ertl, G., Grunze, M., and Weiss, M. "Chemisorption of Hydrogen on iron surfaces", App. of Surface Science 1, 103 (1977).

Broberg, K. B. "The propagation of a brittle crack", Ark. Fys. 18, 159-192 (1960). Dugdale, D. S. "Yielding of steel sheets containing slits" J. Mech. Phys. Solid. 8, 100-104 (1960)

Dienes, G.J. and Paskin, A. "Computer Modeling of Cracks" in Proc. of NATO Advanced Study Institute of Atomistics of Fracture (May 22-31, 1981, Corsica, France) (in press).

Dowben, P.A. and Jones, R.G. "Halogen adsorption on Fe(100)", Surf. Sci. 84, 449 (1979).

Eringen, A.C. "Continuum mechanics at the atomic scale" Crystal Lattice Defects 7, 109-130 (1977).

Esbjorn, P. and Jensen, E.J. "Computer studies of dislocation properties using two-dimensional model systems" J. Phys. Chem. Solids 37, 1081-1091 (1976).

Esterling, D.M. "Lattice theory of three-dimensional cracks" J. Appl. Phys. 47, 486-493 (1976).

Esterling, D.M. "Lattice statics approach to fracture and plasticity" Comments on Solid State Physics 9(4), 105-113 (1979).

Frandsen, J.D. and H.L. Marcus,"Environmentally Assisted fatigue crack propagation in steel",Metall. Trans. 8A, 265 (1977).

Fuller, E.R., Jr., Lawn, B.R. and Thomson, R.M. "Atomic modelling of chemical interactions at crack tips" Acta Met. 28, 1407-1414 (1980).

Fuller, E.R., Jr. and Thomson, R.M. "Lattice theories of fracture", Fracture Mechanics of Ceramics, R.C. Bradt et al. (editors), Plenum Publishing Corporation (1978) pp. 507-518.

Gehlen, P.C. et al. (editors) Interatomic Potentials and the Simulation of Lattice Defects, Plenum, New York (1972).

Gehlen, P.C. "Crack extension in a model of -iron" Scripta. Met.7, 1115-1118 (1973).

Genlen, P.C., Hahn, G.T. and Kanninen, M.F. "Crack extension by bond rapture in a model of BCC iron" Scripta. Met. 6, 1087-1092 (1972).

Gehlen, P. C. and Kanninen, M. F. In Inelastic Behavior Of Solids (eds. Kanninen et al) p. 587, McGraw-Hill, New York (1970)

Gilman, J. J. In Fracture (eds. Averback, B. L. et al) p. 193, Wiley, New York, (1959).

Gilman J. J. Micromechanics of flow in solids, McGraw-Hill Book Co., NY, 1969, Chap. 2

Goodier, J. N. and Field F. A. In Fracture of Solids (eds. Drucker et al) p. 103, Wiley, New York, (1963).

Griffith, A.A., "The phenomena of rapture and flow in solids" Phil. Trans. Roy. Soc. Lond. A221, 163-198 (1920).

Hahn, G. T. In Atomic Structure And Mechanical Properties Of Metals, Proceedings of the international School of Physics "Enrico Fermi" (ed. Gaglioti G.) North Holland Publishing Co, Amsterdam (1976)

Hernikoff, A. "Solution of problems of elasticity by the framework method", J. Appl. Mech. 8, A169-175 (1941).

Hsieh, C. and Thomson, R. "Lattice theory of fracture" J. Appl. Phys. 44, 2051-2063 (1973).

Hull, D. and Beardmore, P. and Valintine, A. "Crack propagation in single crystal of tungsten", Phil. Mag. 12, 1021-1041 (1965).

Inglis, C. E. "Stresses in a plate due to the presence of cracks and sharp corners" Trans. Instn. Naval. Archit. 55, 219 (1913)

Johnson, R.A. "Point defect calculation for an fcc lattice" Phys Rev. 145, 423-433 (1966).

Kanninen, M.F. and Gehlen, P.C. Interatomic potentials and simulations of lattice defects, P.C. Gehlen, et al. (editors) Plenum Press, New York (1972), p. 713.

Kelly, A., Tyson, W.R. and Cottrell, A.H. "Ductile and brittle crystals" Phil. Mag. 15, 567-586 (1967).

Knott, J. F. Fundamentals of Fracture Mechanics, The Butterworth group,London (1973).

Kramer, I.R. and Demer, L.J. Prog. Met. Sci. 9, 131 (1961).

Lawn, B.R. and Wilshaw, T.R. Fracture of Brittle Solids, Cambridge University Press, Cambridge (1975).

Liebowitz, H. (ed) Fracture, Academic Press, New York (1968).

Mott, N.F. "Brittle fracture in mild steel plates" Engineering 165, 16-19 (1948)

Paskin, A. and Rahman, A. "Effects of a long-range oscillatory potential on a radial distribution function and the constant of self-diffusion in liquid Na" Phys. Rev. Lett. 16, 300-302 (1966).

Paskin, A. and Dienes, G.J. "Molecular dynamic simulations of shock waves in solids" J. Phys. C 10, 1563-1566 (1977).

Paskin, A. Gonar, A., and Dienes, G.J. "Simulations of shock waves in solids" J. Phys. C 10, L5363-L566 (1977).

Paskin, A. Gohar A. and Dienes, G.J. "Kinetic energy and temperature profiles of shockwaves in solids" J. Phys. C 11, L857-L861 (1978).

Paskin, A., Gohar, A. and Dienes, G.J. "Simulation of shock waves in solids" J. Phys. Chem. Solids 39, 1307-1311 (1978).

Paskin, A., Gohar, A., and Dienes, G.J. "Computer simulation of crack propagation" Phys. Rev. Lett. 44, 940-943 (1980).

Paskin, A., Som, Dilip K. and Dienes, G. J. "Computer simulation of crack propagation: Lattice trapping" J. Phys. C 14, L171- L176 (1981)

Paskin, A., Sieradzki, K., Som, D. K. and Dienes, G. J. "Environmentally induced crack nucleation and brittle fracture" Acta. Metall.( in press).

Popelar, C.H. and Gehlen, P.C. "Modeling of dynamic crack propagation: II. Validation of two-dimensional analysis" Int. Journ. Fracture 15, 159-177 (1979).

Puroshothaman, S., Richards, R.J., Tien, J.K., and Frandsen, Met. "Kinetics of Environmental fatigue crack growth in Nickel-Copper alloy: Part I", Trans. 9A, 1101 (1978).

Rahman, A. "Correlation in the Motion of Atoms in Liquid Argon," 136 A 405-A 411 (1964).

Rice, J.R. "Thermodynamics of the quasi-static growth of Griffith cracks" J. Mech. Phys. Solids 26, 61-78 (1978).

Rice, J.R. and Thomson, R. "Ductile versus brittle behavior of crystals" Phil. Mag. 29, 73-97 (1974).

Roberts, D. K. and Wells, A. A. "The velocity of brittle fracture", Engineering 24,820 (1954).

Rolfe, S. and Barsom, J. In Fracture And Fatigue Control In Structures, Prentice Hall Inc., Engelwood Cliffs, New Jersey (1977).

Sanders, J. L. " On the Griffith-Irwin fracture theory" J. Appl. Mech. 27, 352-353 (1960).

Schand, E. B. J. Am. Ceram. Soc. 44, 71 and 451 (1961)

Schardin, H. In Fracture (eds B.L. Averbach, D,K. Felbeck, G.T. Hahn and D.A. Thomas), Wiley, New York (1959), p. 297.

Shchukin, E.D. and Yushechenkc, V.S. "Molecular Dynamic Simulation of Mechanical Behavior" J. Mat Sci. 16, 313-330 (1981).

Sieradzki, K."On the embrittlement of steels by hydrogen sulfide", Scripta Met. 15,171 (1981)

Sieradzki, K. "The effect of thin film formation at crack tips on fracture", Acta. Met. 30,973 (1982).

Sinclair, J.E. "The influence of the interatomic force law and of kinks on the propagation of brittle cracks" Phil. Mag. 31, 647-671 (1975).

Sinclair, J.E. and Fletcher, R. "A new method of saddle-point location for calculation of defect migration energies" J. Phys. C 7, 864-870 (1974).

Sinclair, J.E. and Lawn, B.R. "An atomistic study of cracks in diamond-structure crystals" Proc. Roy. Soc. Lond. A 329, 83-103 (1972).

Smith, E. "The conditions for a crack to be lattice trapped" Int. Jour. of Fracture 15, R87-R91 (1979).

Sneddon, I. N. In Fourier Transforms, Mc Graw-Hill, New York (1951).

Sneddon, I. N. and Lowengrub, M., Crack Problems In The Classical Theory Of Elasticity, New York (1969).

Thomson, R., Hsieh, C. and Rana, V. "Lattice trapping of fracture cracks" J. Appl. Phys. 42, 3154-3160 (1971).

Thomson, R.M. "Theory of chemically assisted fracture", J. Mater. Sci. 15, 1014 (1980).

Tyson, W.R. "Atomistic simulation of the ductile/brittle transition" Fracture 1977, Vol. 2, ICF4, Waterloo, Canada, June 19-24, 1977, pp. 159-164.

Van Elast, H. C. "The intermittent propagation of brittle fracture" Trans. AMIE. 230, 460-469 (1964).

Verlet, L. "Computer Experiments on Classical Fluids," Phs. Rev. 159, 98-103 (1967).

Weertman, J. "Fracture mechanics: A unified view for Griffith-Irwin-Orowan cracks" Acta Met. 26, 1731-1738 (1978).

Weiner, J.H. and Pear, W. "Crack and dislocation propagation in an idealized crystal model" J. Appl. Phys. 46, 2398-2405 (1975).

Welch, D.O., Dienes, G.J. and Paskin, A. "A molecular dynamical study of the equation of state of solids at high temperature and pressure" J. Phys. Chem. Solids 39, 589-603 (1978).

Westergaard, H.M. "Bearing pressures and cracks" J. Appl. Mech. 6 (2) A49-A53 (1939).

Yoffe, E.H. "The moving Griffith crack" Phil. Mag. 42, 739-750 (1951).